ENGINEERING DOCUMENT CHANGE CONTROL

Change Identification

21. Release:

SEP 04 2003
DATE:
STA: 15
HANFORD RELEASE
ID: 22

1. Category:
☐ Direct Revision ☐ Supplemental Change ☐ Page Change
☐ *Supersedure* ☐ *Cancel/Void* ☒ *New*

2. Classification of Change, or if New, CB?
☐ Major ☐ Minor ☒ Conf Baseline (CB)

3. Date: 9/3/03

4. Originator's Name, Organization, MSIN, and Telephone No.:
W. S. Josephson, DFSNW, H8-44, 373-9633

5. USQ Required? ☐ Yes ☒ No USQ No.: _____ CX No.: _____

6. Technical Authority:
W. S. Josephson, 373-9633

7. Project/Program (WMP, FFTF, etc.): WMP

8. Area: 200E

9. Building: WESF

10. Reviewer Designator: N/A

11. Plan:
WMP-16940, Revision 0, is a new document that provides thermal analysis for the Capsule Dry Storage Project.

12. Criteria:
WMP-16940, Revision 0, is a new document that provides thermal analysis for the Capsule Dry Storage Project. Criteria for the thermal analysis is to (1) summarize the pertinent thermal design requirements sent to vendors, (2) summarize and address the assumptions that underlie those design requirements, (3) demonstrate that an acceptable design exists that satisfies the requirements, and (4) identify key design features and phenomena that promote or impede design success, (5) support other CAP analyses such as corrosion and integrity evaluations, and (6) support the assessment of proposed designs.

13. Change or Document Description:
WMP-16940, Revision 0, is a new document.

14. Documents Issued or Changed by this EDC:

Document	Page	Revision	Document Title or Comments
WMP-16940	All	0	Thermal Analysis of a Dry Storage Concept for Capsule Dry Storage Project

15. Technical Justification (Need):
WMP-16940, Revision 0, is a new document that provides thermal analysis for the Capsule Dry Storage Project. The cesium and strontium capsules stored in pools at WESF will be moved to dry storage on the Hanford Site as an interim measure to reduce risk.

Evaluation and Coordination

16. Change or Document Impact:
New document.

17. Affected Documents:

Document Number	Page	Revision	Person Notified/Comments
N/A	N/A	N/A	N/A

ENGINEERING DOCUMENT CHANGE CONTROL (continued)

Verification

18. Verification:
PEER REVIEW

Per telecon W/ Susan Bussman N.F 9-4-03

19. Approvals/Reviews:

Initials, Last Name, Date, MSIN	Initials, Last Name, Date, MSIN
Technical Authority: 9/3/03 WS Josephson, 9/3/03, H8-44	Technical Authority Manager: JA Swenson, 9/3/03, H8-14
Reviewer (Title): Acting Director, Planning & Projects LL Fritz, 9/3/03, H8-44 LL Fritz 9.4.03	Reviewer (Title):

Solution

20. Change Description (Solution) - Continuation Sheet:
N/A

DISTRIBUTION SHEET

To	From	Page 1 of 1
Distribution	W. S. Josephson	Date 09/03/2003
Project Title/Work Order		EDT No. N/A
WMP-16940, Revision 0, Thermal Analysis of a Dry Storage Concept for Capsule Dry Storage Project		ECN No. N/A

Name	MSIN	Text With All Attach.	Text Only	Attach./ Appendix Only	EDT/ECN Only
S. Bath	H8-44	x			
S. E. Bussman	H8-44	x			
L. I. Covey	S6-82	x			
L. L. Fritz	H8-44	x			
K. L. Hladek	H8-44	x			
C. R. Hoover	H8-44	x			
W. S. Josephson	H8-44	x			
D. R. Lucas	H8-44	x			
J. L. Pennock	S6-72	x			
E. D. Robbins	T3-28	x			
P. T. Saueressig	S6-81	x			
R. A. Sexton	H8-44	x			
F. M. Simmons	S6-81	x			
K. E. Smith	H8-44	x			
J. A. Swenson	H8-44	x			
J. R. Weidert	T3-09	x			
D. E. McKenney	H8-44	x			
K. M. Quigley	H8-44	x			
S. L. Kooiker	H8-20	x			
Central Files H	B1-07	x			

WMP-16940
Revision 0

Thermal Analysis of a Dry Storage Concept for Capsule Dry Storage Project

Prepared for the U.S. Department of Energy
Assistant Secretary for Environmental Management

Fluor Hanford
P.O. Box 1000
Richland, Washington

Contractor for the U.S. Department of Energy
Richland Operations Office under Contract DE-AC06-96RL13200

WMP-16940
Revision 0

Thermal Analysis of a Dry Storage Concept for Capsule Dry Storage Project

FJ Heard, DFSNW
KR Roberson, DFSNW
JE Scott, DFSNW

MG Plys, Fauske & Associates, Inc.
SJ Lee, Fauske & Associates, Inc.
B Malinovic, Fauske & Associates, Inc.

September 2003

Prepared for the U.S. Department of Energy
Assistant Secretary for Environmental Management

Fluor Hanford
P.O. Box 1000
Richland, Washington

Contractor for the U.S. Department of Energy
Richland Operations Office under Contract DE-AC06-96RL13200

Chris Hallingstad 9/4/03
Clearance Approval Date

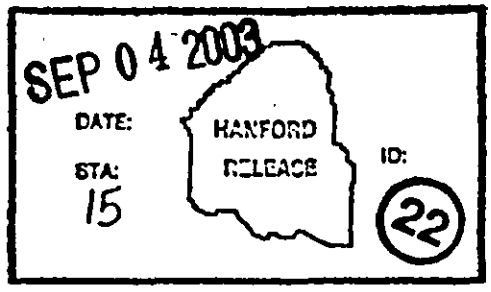

Release Approval (stamp)

Approved for Public Release
(Upon receipt of Clearance approval)
Further Dissemination Unlimited

For use with Technical Documents (when appropriate)	
EDC- 03-17860	FMP-
EDT-	ECN-
Project No.:	Division: WMP
Document Type:	Page Count: 184

For use with Speeches, Articles, or Presentations (when appropriate)							
Abstract		Summary		Full Paper		Visual Aid	
Conference Name:							
Conference Date:							
Conference Location:							
Conference Sponsor:							
Published in:							
Publication Date:							

THERMAL ANALYSIS OF A DRY STORAGE CONCEPT FOR CAPSULE DRY STORAGE PROJECT

September 2003

F. J. Heard
K. R. Roberson
J. E. Scott
Duratek Federal Services, Inc., Northwest Operations

and

M. G. Plys
S. J. Lee
B. Malinovic

Fauske and Associates, Inc.

ACKNOWLEDGMENT

The authors would like to acknowledge the contributions of Dr. Donald R. Olander. In his role as peer reviewer, Dr. Olander identified and supplied information that was useful in assuring proper coverage for the scope of the document. His work was appreciated and was very helpful, especially when determining the extent of the parametric analyses, as discussed in Section 4.4. In performing his review, Dr. Olander contributed Appendix B, "Energy Absorbed by a Salt Log from an Adjacent Log," and Appendix C, "Radial Distribution of the Gamma Heat Source in CsCl."

EXECUTIVE SUMMARY

A viable conceptual design for dry storage of cesium chloride or strontium fluoride capsules is noted. The conceptual design is capable of meeting performance specifications for the salt-metal interface temperature for nominal operations, process events including process upset events, and postulated accident conditions, with the potential exception of the high-power strontium capsule during processing and process upset events. All assumptions and related design features, while appropriate for conceptual designs, must be technically justified for the final design.

Significant reductions in the salt-metal interface temperature were obtained through the application of external fins, helium backfill, and axial conduction. The potential exists to use loading strategy to maintain the total overpack decay power less than 2,540 W. This will have to be assessed and technically justified for any final design. However, loading limits/strategies may include, but are not limited to, mixing high- and low-power capsules, limiting the total number of capsules within an overpack, or simply preventing the placement of high-power capsules adjacent to one another.

It is recommended that the final design expand on the analyses documented within this report and provide additional technical support to process Type W overpack and high-power strontium fluoride capsules. It is also recommended that the final design address the potential for local hot spots due to heterogeneities in the salt, Type W capsules, and surrounding structure.

Finally, it is recommended that the original capsule fabrication documentation be reviewed to verify the validity of the capsule descriptions and to validate the data in the capsule database that is pertinent to the dry storage project and used for the thermal analyses within this report.

TABLE OF CONTENTS

LIST OF FIGURES

LIST OF TABLES

LIST OF TERMS

^{137}Ba	barium-137
^{137}Cs	cesium-137
^{137m}Ba	barium-137 metastable
1-D	one-dimensional
2-D	two-dimensional
3-D	three-dimensional
^{90}Sr	strontium-90
AEF	area enhancement factor
ANS	American Nuclear Society
BUSS	Beneficial Uses Shipping System
CAP	Capsule Advisory Panel
CDSP	Capsule Dry Storage Project
Cs	cesium
CSB	Canister Storage Building
CsCl	cesium chloride
DFSNW	Duratek Federal Services Northwest
DOE	U.S. Department of Energy
FAI	Fauske & Associates, Inc.
HEPA	high-efficiency particulate air
HLW	high-level waste
HVAC	heating, ventilation, and air conditioning
IC	inner capsule
LAW	low activity waste
LOF	loss-of-flow
LOV	loss-of-ventilation
MCNP	Monte Carlo Neutron Photon (computer program)
MCO	multi-canister overpack
NMSH	Nuclear Material Systems Handbook
OC	outer capsule
PFP	Plutonium Finishing Plant
QA	Quality Assurance
SNFP	Spent Nuclear Fuel Project
Sr	strontium
SrF_2	strontium fluoride
SS	stainless steel
W	Type W overpack
WESF	Waste Encapsulation and Storage Facility
WRAP	Waste Receiving and Packaging
WTP	Waste Treatment Plant

1.0 INTRODUCTION AND BACKGROUND

There are 1,936 cesium (Cs) and strontium (Sr) capsules stored in pools at the Waste Encapsulation and Storage Facility (WESF). These capsules will be moved to dry storage on the Hanford Site as an interim measure to reduce risk. The Cs/Sr Capsule Dry Storage Project is conducted under the assumption that the capsules will eventually be moved to the repository at Yucca Mountain, and the design criteria include requirements that will facilitate acceptance at the repository. The storage system must also permit retrieval of capsules in the event that vitrification of the capsule contents is pursued.

1.1 PURPOSE

The Capsule Advisory Panel (CAP) was created by the Project Manager for the Hanford Site Capsule Dry Storage Project (CDSP). The purpose of the CAP is to provide specific technical input to the CDSP; to identify design requirements; to ensure design requirements for the project are conservative and defensible; to identify and resolve emerging, critical technical issues, as requested; and to support technical reviews performed by regulatory organizations, as requested. The CAP will develop supporting and summary documents that can be used as part of the technical and safety bases for the CDSP.

The purpose of capsule dry storage thermal analysis is to:

1. Summarize the pertinent thermal design requirements sent to vendors,
2. Summarize and address the assumptions that underlie those design requirements,
3. Demonstrate that an acceptable design exists that satisfies the requirements,
4. Identify key design features and phenomena that promote or impede design success,
5. Support other CAP analyses such as corrosion and integrity evaluations, and
6. Support the assessment of proposed designs.

It is not the purpose of this report to optimize or fully analyze variations of postulated acceptable designs. The present evaluation will indicate the impact of various possible design features, but not systematically pursue design improvements obtainable through analysis refinements and/or relaxation of conservatisms. However, possible design improvements will be summarized for future application. All assumptions and related design features, while appropriate for conceptual designs, must be technically justified for the final design.

The pertinent thermal design requirements and underlying assumptions are summarized in Section 1.3. The majority of the thermal analyses, as described in Sections 4.2 and 4.3, focus on an acceptable conceptual design arrived at by refinement of a preliminary but unacceptable design. The results of the subject thermal analyses, as presented in Section 4.0, satisfy items 3 and 4 above.

The analysis results (steady-state and transient temperatures) summarized within Sections 4.0, 5.0, and 6.0 provide essential information required for the support of other CAP analyses. This information, together with the identification of key design features and phenomena, supports the assessment of vendor-proposed designs.

1.2 SCOPE AND MODELING APPROACH

The thermal behavior of a conceptual design configuration consisting of a dry storage module with capsule overpacks will be modeled to predict steady-state and transient temperature distributions within the dry storage module, overpack, and capsules. The temperature distribution across the conceptual design configuration, including the maximum salt temperature, the salt-metal interface temperature, the overpack structure, and external surface temperatures will be predicted. These results will be used to assess the potential for corrosion of the capsules and overpacks while in dry storage, as well as the potential for material property changes (e.g., phase changes) that could impact long-term integrity of the capsules and the dry storage system. The transient analyses will focus on determining the temperature profile of the capsules within an overpack within a dry storage module during several postulated events (i.e., range fire and loss-of-ventilation [LOV] due to plugging of either the inlet or outlet vents).

The HADCRT computer code and the general-purpose mathematics solver MathCAD[1] will be used to perform a series of independent analyses. Comparisons will be made between the HADCRT and MathCAD results to provide an appropriate amount of technical review. The MathCAD and HADCRT thermal models were independently checked using FlexPDE[2] (Heard 2003).

The HADCRT computer code, as described in Appendix A, is an integrated model for analysis of nuclear fuel cycle facilities and chemical processing plants capable of simulating operations and off-normal conditions at Hanford Site facilities and for U.S. Department of Energy (DOE) installations in general. It is a graded-approach tool whose models are chosen to contain an appropriate level of detail for licensing, yet retain fast running times despite its broad scope. HADCRT was created and is maintained under the Fauske & Associates, Inc. (FAI) Quality Assurance (QA) program, audited, and accepted by Hanford Site contractors.

1.3 DESIGN CRITERIA AND ANALYSIS ASSUMPTIONS

The CDSP is conducted under the assumption that the capsules will eventually be moved to the national repository at Yucca Mountain. The design criteria include some requirements, e.g., size of overpacks and maximum thermal load per overpack that will facilitate repository acceptance. The storage system must also permit retrieval of capsules in the event that vitrification of the capsule contents is pursued.

---

[1] MathCAD is a trademark of MathSoft Engineering & Education, Cambridge, Massachusetts.

[2] FlexPDE is a trademark of PDE Solutions, Inc., Antioch, California. Flex PDE is a scripted finite element model builder and numerical solver.

The following system design requirements have been supplied for use to prospective vendors:

1. The overpack shall be limited to an outer diameter no greater than 55.9 cm (22 in.),
2. The overpack shall be limited to a maximum length of 2.03 m (80 in.),
3. The overpack shall be limited to a maximum decay heat of 2,540 W, and
4. The salt-metal interface temperature within a capsule shall not exceed the specified maximum temperatures, as presented in Table 1-1.

The following assumptions are made for the thermal analyses:

1. Each overpack will contain 16 Cs capsules at 160 W per capsule based on average power decayed to June 3, 2003.
2. Specific power (W/m^3) within the cesium and strontium salts was derived assuming a salt height of 0.4318 m (17 in.).
3. Heat loading will be based on blending high and low decay heat capsules within a given overpack.
4. The dry storage module will contain multiple overpacks, but will be limited to a total heat load of 24 kW.
5. Ultimate heat rejection during dry storage shall be by passive means.
6. An overpack must not mix Cs with Sr capsules, or with Type W overpack capsules. Separate overpacks will be used for the Cs, Sr, and Type W capsules.
7. The capsules are sufficiently straight to fit within a 7.033 cm (2.875-in) tube and the Type W capsules will fit within a 8.89 cm (3.50-in.) tube. (Special overpacks will be required for use with the Type W overpack capsules.)
8. The annulus between the inner and outer capsule contains a mixture of various gases, which has a thermal conductivity similar to dry air.
9. Diurnal and seasonal temperature variations shall be accounted for when confirming peak salt and salt-metal interface temperatures. Hanford Site-specific environmental conditions were used as the inlet boundary conditions for the dry storage module.
10. A 50-year design lifetime for the overpack and dry storage module and a similar period of performance for the capsules.

1.4 PERFORMANCE SPECIFICATIONS

The system for movement and dry storage of the capsules must be designed so that the following maximum temperatures at the salt-metal interface are not exceeded (HNF-16138, *Performance Specification for Capsule dry Storage Project Design and Fabrication).*

Table 1-1 presents the performance specifications for maximum salt-metal interface temperatures during accident conditions, processing (including process upsets), and interim storage under summer conditions.

The salt-metal interface (metal side) temperature was selected as the controlling location, because this temperature governs any chemical reactions for corrosion with the inner capsule. It is possible that there is not complete physical contact between salt and the capsule inner wall interior due to shrinkage of salt (in the case of Cs salt) or voids (in the case of Sr salt). In this case, it the temperature refers to the temperature of the capsule inner wall interior surface.

Table 1-1. Performance Specifications for Salt-Metal Interface Temperature.

	Strontium capsules	Cesium capsules
Accident Conditions	800 °C	600 °C
Processing, including process upsets	540 °C	450 °C
Interim storage configuration under summer storage conditions	540 °C	317 °C

2.0 SUMMARY, FINDINGS, AND RECOMMENDATIONS

The CAP has addressed the acceptability of key requirements of HNF-16138, and reviewed the technical basis for the CDSP. The following is a summary of the findings and recommendations related to this topical report. See WMP-17265, *Capsule Advisory Panel Topical Summary Report,* for a complete summary listing of findings and recommendations from all topical reports, including links to the topical reports for each of the findings and recommendations.

It is not the purpose of this thermal analysis to optimize a design or to fully analyze all possible variations of an acceptable design. The present evaluation indicates the impact of various possible design features, but does not systematically pursue design improvements, additional margin obtainable through analysis refinements, and relaxation of conservatisms. These are simply assumed, and known by experience, to be feasible and attainable by a suitable vendor.

2.1 SUMMARY

The thermal analysis for the Cs and Sr capsules considered normal operations, process operations, and selected accident scenarios. A conceptual design, as documented within this report, is capable of meeting the CDSP performance criteria; with the potential exception of the high-power Sr capsules during process upset events.

The analyses predicted the temperature distribution within an overpack container for the following conditions:

1. A dry storage module for normal ambient conditions including diurnal temperature variations

2. A WESF cell during process operations (proof-of-dryness)

3. A dry storage module for postulated accidents including flow blockage and an engulfing fire.

The analysis began at a very fundamental level, with a simplified one- (1-D) and two-dimensional (2-D) assessment of the overpack container at the midplane, in order to provide the design guidance as discussed above.

The midplane model neglected axial heat flow because the dominant heat flow path is radial. Midplane model results guided evolution of the preliminary conceptual design toward the revised conceptual design. Midplane models are capable of assessing first-order influences of design features excepting of course those pertinent to axial heat flow. A very versatile analytical 1-D midplane model was formulated to explore sensitivity to design features.

The 2-D midplane model was extended to three dimensions (3-D) by concatenating three 2-D plane models for the overpack, base plate, and shield plug; together these created a 3-D representation of an overpack.

To simulate dry storage, the overpack was filled with helium and linked to a 3-D model of the dry storage module containing the heat load associated with ten overpacks. The dry storage module model consisted of a lower region containing nine overpack containers and an upper region containing one overpack. The upper overpack was modeled in detail. Boundary conditions are consistent with the gas exit temperature from the dry storage module. The dry storage module model included inlet and outlet flow junctions for natural circulation with the environment. In this model, the buoyancy-driven flow through the dry storage module is mechanistically calculated.

To simulate the WESF proof-of-dryness test, under vacuum conditions, the gap resistances were adjusted internal to the overpack model, and the overpack was exposed to a constant environment temperature consistent with measurements obtained for "G-all" during loading of a Beneficial Uses Shipping System (BUSS) cask.

Nominal conditions of dry storage were also simulated for an environment with both diurnal temperature variation and solar heating on the dry storage module top and side surfaces representative of a consecutive string of hot Hanford Site days. These cases established basic agreement with midplane results and showed that salt temperature variation is dampened compared to that of the environment.

Off-normal conditions in dry storage were simulated by simple variation of the normal input models. Loss of flow was modeled by simply blocking the inlet flow junctions for 24 hours. An engulfing fire was modeled by setting the ambient temperature to the fire temperature, 800 °C, and injecting fire gases at this temperature into the module interior and low elevation; fire duration is 30 minutes and the long-term cool down was tracked.

An estimate of the Type W overpack salt-metal and centerline temperatures was made. However, no transient analyses were performed for the Type W overpacks, because it is also obvious that decreasing the number of such capsules in an overpack will decrease any temperature of interest, even though the Type W overpack introduces an extra gap resistance. Simply put, the temperature increment associated with an extra gap resistance can be easily compensated by a reduction in overpack power. However, since there are only 23 Type W overpacks, only a few specially made inserts will be required and will not influence design strategy.

Steady-state analyses were performed for the Sr capsules. No transient analyses were performed for the Sr capsules, because it is obvious that by reducing the number of capsules from the 16 assumed in Cs cases in order to meet the requirement of maximum power per overpack, and perhaps by a strategy to mix high- and low-power capsules, temperatures within these capsules will be acceptable. The most important part of this conclusion is simply that Sr salt will be well below its melting point, and there is no phase change issue associated with this salt.

2.2 FINDINGS AND RECOMMENDATIONS

The CAP was chartered to assess the acceptability of key design requirements for the CDSP to ensure they are conservative and defensible. The results of this assessment are listed below for this topical report.

2.2.1 Heat Rejection

A suitable dry storage system must be capable of passively dissipating the heat generated by decay of the concentrated CsCl and SrF_2, as well as radioactive decay products in the capsules. Temperatures of the capsules will be elevated over those seen in water pool storage, and must be maintained at levels that ensure safe, interim storage. Limiting temperatures were specified in HNF-16138 for normal, processing, and accident conditions for both CsCl and SrF_2 capsules.

Thermal modeling was performed to assess the feasibility of designing a dry storage system that could meet the prescribed limits.

2.2.1.1 317 °C Maximum Temperature of Cesium Capsules at the Salt-Metal Interface During Dry Storage.

Feasible design concepts for dry storage systems exist to limit the salt-metal interface temperature to no more than 317 °C. These results were obtained with a conceptual overpack design containing a sufficient number of capsules to attain the 2,540 W total decay heat limit established by the CDSP. If the capsule wall is maintained at 317 °C, the resulting capsule centerline temperature will be about 371 °C.

2.2.1.2 450 °C Maximum Temperature of Cesium Capsules at the Salt-Metal Interface During Processing.

Processing conditions, such as a vacuum test for capsule dryness, will increase the capsule temperatures for a duration of a few hours to a few days. With a limit of 450 °C at the salt-metal interface, centerline temperatures in the CsCl capsules could potentially exceed 500 °C.

2.2.1.3 600 °C Maximum Temperature of Cesium Capsules at the Salt-Metal Interface Under Accident Conditions.

Accident conditions such as a fire could expose the capsules to higher temperatures for a short duration of a few to several hours. The temperatures associated with a prescribed 800 °C fire in the assumed dry storage system concept were analyzed. The resulting capsule centerline temperature exceeded the conservative 430 °C melting point for a period of a few hours, with the maximum temperature predicted to be approximately 520 °C. However, based on an accident condition temperature limit of 600 °C, the final design may achieve higher temperatures within the salt for longer durations. In addition, the actual design developed by the system subcontractor could result in higher internal temperatures based upon the allowable limit of 600 °C.

2.2.1.4 540 °C Maximum Temperature of Strontium Capsules at the Salt-Metal Interface During Normal Dry Storage.

With SrF_2 capsules operating at 540 °C at the salt-metal interface, centerline temperatures could approach 600 °C.

2.2.1.5 540 °C Maximum Temperature of Strontium Capsules at the Salt-Metal Interface During Processing Conditions.

Because this temperature is the same as the normal operating temperature, the capsule response to these conditions would be identical to that noted in Section 2.1.1.4. However, scoping analyses indicate that maintaining this temperature during a vacuum test for dryness of SrF_2 capsules may not be achievable for high-power SrF_2 capsules without supplemental cooling.

Temperatures of approximately 700 °C are predicted using the conceptual model without some form of active cooling of the overpack during such an event.

2.2.1.6 800 °C Maximum Temperature of Strontium Capsules at the Salt-Metal Interface Under Accident Conditions.

A maximum temperature increase of approximately 200 °C from nominal conditions is estimated for a postulated fire and would result in Sr capsule salt-metal interface and centerline temperatures of approximately 702 °C and 771 °C, respectively. The salt-metal interface performance specification of 800 °C is attainable for accident conditions.

2.2.2 Containment

This report does not address this topic.

2.2.3 Recovery Capability

This report does not address this topic.

2.2.4 Design Life

Design features and requirements were selected based on a 50-year lifetime for the dry storage system. Key elements of the design requirements were analyzed to assess the viability of achieving the 50-year lifetime based on these requirements.

2.2.4.1 Corrosion Allowance for 316L Stainless Steel Overpack Interior.

HNF-16138 specifies that the overpack be made of 316L stainless steel (SS) with an internal corrosion allowance of 0.318 cm (0.125 in.) to protect against potential capsule leaks. An assessment was performed to determine the acceptability of the specified material and the suitability of the specified corrosion allowance.

Predicted overpack temperatures supported corrosion analyses of the overpack inner wall based on the assumed leakage of CsCl or SrF_2 from the capsules. Temperatures for the overpack are

predicted to be in the range of 200-225 °C during normal operations, and will reduce with decay of the Cs and Sr.

2.2.4.2 External Corrosion

Though well suited for containment of the CsCl and SrF_2 salts, 316L SS is susceptible to stress corrosion cracking if exposed to water without proper purity control. A scoping assessment of exterior corrosion potential of the overpack was performed.

Based on a 316L SS overpack, WMP-16937, *Corrosion Report for the Capsule Dry Storage Project,* identifies the possibility of stress corrosion cracking on the exterior of overpacks if condensation or moisture were present. Temperatures on the exterior of the overpacks could drop to the point where moisture could collect on the stainless steel.

2.2.4.3 Metal Aging

Structural metals exposed to elevated temperatures are potentially susceptible to changes in properties that can challenge their long-term suitability. Since dry storage will elevate the capsule temperature well above those experienced in water pool storage, an assessment of the effects of metal aging was performed.

WMP-16938, *Capsule Characterization Report for Capsule Dry Storage Project*, and WMP-16939, *Capsule Integrity Report for Capsule Dry Storage Project*, considered the significance of aging of the capsule and overpack materials. These reports show the effect of aging during the 50-year design life at capsule dry storage operating and processing temperatures, including loss of ductility, is insufficient to affect capsule performance. The thermal analyses predicted these temperatures to be in the range of 200-300 °C for the outer walls of the CsCl and SrF_2 capsules and the materials of the overpack. Accident conditions could raise these temperatures to as high as 600 °C or higher at the capsule walls for periods of a few hours to a few days. The effects of these higher temperatures on metal aging and recovery actions are discussed in WMP-17265, WMP-16938, and WMP-16939.

2.3 OTHER CONSIDERATIONS

Other aspects of the CDSP were assessed to ensure the viability of the approach. These primarily focused on characterizing the capsules to assess their suitability for dry storage and evaluation of some special capsule families.

2.3.1 Capsule Characterization

Capsule characterization is the analysis and tests necessary to demonstrate that the capsule conditions are suitable for dry storage.

2.3.1.1 Capsule Integrity.

This report does not address this topic.

2.3.1.2 Calorimetry.

The power level of most capsules was measured when the capsules were fabricated. These power levels must be known to safely and efficiently load capsules into an overpack without exceeding the 2,540 watts (W) limit.

WMP-16938 included a review of evaluations performed of WESF calorimetry. This review bounds the uncertainty of capsule decay heats at +/- 10%, and supports the use of existing data without new calorimetry. This level of uncertainty is deemed to be acceptable for design analysis and for planning for capsule loading.

2.3.1.3 Capsule Fit into Overpack.

This report does not address this topic.

2.3.2 Strontium Waste Capsules

This report does not address this topic.

2.3.3 Type W Overpack Capsules

A small number of capsules with suspect integrity, as well as materials from capsule destructive examinations and test programs, were sealed inside welded containers (Type W overpacks) for additional assurance against leakage. A total of 23 Type W overpacks were fabricated and are currently stored in WESF.

The Type W overpack capsules have an additional annulus that affects the thermal analysis and thus the design. A suggested design solution to accommodate these in the dry storage system is to limit the number of Type W capsules loaded in an overpack to approximately eight (8), which will maintain the salt temperature at comparable levels to those of a normal capsule. Because the Type W overpacks are a larger diameter due to the additional capsule wall, fewer capsules may fit into an overpack anyway.

2.3.4 Consequences of Capsule Leakage

This report does not address this topic.

2.4 KEY RECOMMENDATIONS

The development of the conceptual thermal model for a dry storage system identified some key features that must be considered in the design. In addition, simplifying assumptions were made in the conceptual analysis that will have to be addressed in the detailed design.

Specific recommendations for detailed design include the following.

- Significant reductions in the salt-metal interface and centerline salt temperatures were achieved through the application of external fins, helium backfill, and axial conduction.

Additional reductions can be achieved for the conceptual design by employing one or more of the following items:

- Accurately determine both the fraction of energy deposited within the CsCl salt and the radial power distribution across the salt.
- Increase the effective thermal conductivity for the gaps between the overpack and insert and/or between the insert and the outer capsule, or decrease the size of the middle gap.
- Modify the conceptual design assumed for this report to increase the contact area between the insert, the lower baseplate, and the upper shield plug. This will promote axial heat transport and increased heat rejection by using the combined surface areas of the overpack, baseplate, and shield plug. This was one of the concepts used by the BUSS cask to obtain adequate heat rejection when loaded with 16 Cs capsules.
- Modify the conceptual design to incorporate a full-length annular design that would allow convective cooling from both the external and interior surfaces of an overpack.

- The potential exists to use loading strategy to maintain the total overpack decay power less than 2,540 W. This will have to be assessed and technically justified for any final design. However, loading limits/strategies may include, but are not limited to, mixing high- and low-power capsules, limiting the total number of capsules within an overpack, or simply preventing the placement of high-power capsules adjacent to one another.
- The Sr capsule salt-metal interface temperature performance specification of 540 °C for processing events appears to be overly conservative and could be raised to at least 700 °C. The process event (proof-of-dryness) indicates that the 540 °C limit may only be achievable if active cooling is employed. The proposed limit of 700 °C is well below any temperature at which phase transition or melting could occur for Sr capsules. However, the effects on metal aging must be addressed.
- External temperature drop (overpack container wall to local environmental temperature) and temperature drops across internal gaps (between an insert and overpack wall, between capsule and structure, etc.) are by far the largest in the system, and are obvious candidates for design optimization. For this reason the revised conceptual design uses external fins and eliminates an internal gap.
- Using helium as a cover gas is far more effective than reducing the number of capsules in order to control the salt-metal interface temperature.
- Relatively high emissitivity values were assumed for the metal surfaces of the overpack to improve radiative heat transfer. If these values are carried forward to detailed design, fabrication of the overpacks must include the processes to achieve these higher values.
- Self-shadowing of fins has a significant affect on the salt-metal interface and centerline temperatures, especially for natural circulation systems where radiative heat transfer provides a large fraction of the energy rejected from the system. The surface emissivity and effective view factor from the fins must be technically justified and supported.

The sensitivity of the salt-metal interface and salt centerline temperature to various ancillary effects are comparatively small and include these:

- Decreasing gamma deposition in salt from a conservative value of 75% to a possibly more realistic estimate of 50% is the largest secondary effect, about 20 °C reduction in interface and 40 °C reduction in centerline values.
- Reducing the value of emissivity assumed for the fins by approximately 50%, to approximate fin shadowing, increased the salt-metal and centerline temperatures by 25 °C and 30 °C. This is the next largest secondary effect.
- Reducing salt thermal conductivity by 35% to account for barium build-in can increase centerline temperature by about 20 °C.
- Rendering gamma deposition non-uniform in salt increases centerline temperature by about 10 °C.
- Allowing a gap between salt and cladding inner surface increases centerline temperature by about 5 °C.
- Varying capsule type (except Type W) increased the salt-metal and centerline temperature by about 10 °C.

The following limitations are noted

- The subject thermal models are based on a single capsule, either CsCl or SrF_2, within an overpack assuming symmetric placement of equal-power capsules.
- Multiple adjacent (i.e., side-to-side) capsules around the insert were not modeled. The potential exists for local hot spots due to the possibility of two or more adjacent capsules with greater-than-average power. The potential exists to use loading strategy to maintain the total overpack decay power less than 2,540 W. This will have to be assessed and technically justified for any final design. Loading limits/strategies may include, but are not limited to these items: mixing high- and low-power capsules, limiting the total number of capsules within an overpack, or simply preventing the placement of high-power capsules adjacent to one another.
- The conceptual design did not specifically address Type W overpack capsules. However, the affect of the Type W overpacks on peak centerline and salt-metal interface temperatures can be estimated with the current thermal models (see Section 4.2.4).
- Only steady-state, 1-D midplane analyses were performed for the Type W and SrF_2 capsules.
- Contact resistance between the salt and inner capsule was neglected when a salt-metal gap was not modeled.
- Specific power (W/m^3) within the Cs and Sr salts was derived assuming a salt height of 0.4318 m (17 in.). Undoubtedly longer and shorter salt heights exist.

3.0 CONCEPTUAL DESIGN CONFIGURATION

3.1 CAPSULE AND OVERPACK CONTAINER

3.1.1 Capsule Information

Figure 3-1 presents an isometric breakout of a Cs capsule during assembly. Figures 3-2 and 3-3 and Table 3-1 present and summarize the dimensions associated with each type of CsCl capsule. Figures 3-4 and 3-5 and Table 3-2 present and summarize the corresponding dimensions associated with the single type of SrF_2 capsule.

The CsCl capsules were manufactured using three different combinations (wall thicknesses) of stainless steel tubing dimensions for the inner and outer capsules. The resulting capsules are referred to as Type 1, Type 2, and Type 3. The Type 3 capsules are the most numerous. Twenty-three Cs capsules were overpacked within a third capsule. These capsules are referred to as the Type W overpacks. All four types of CsCl capsules were constructed using 316L stainless steel tubing.

Only one type of SrF_2 capsule was manufactured using a high nickel alloy (Hastelloy[3] C-276) for the inner capsule and 316L SS for the outer capsule.

It was recently "discovered" that some of the Sr capsules were fabricated with both inner and outer walls of Hastelloy C-276 rather than a 316L SS outer capsule over a Hastelloy C-276 inner capsule. Documentation did not identify this design for the Sr capsules. This shortfall in the capsule documentation as well as some apparent discrepancies in the capsule database must be corrected. It is recommended that the original capsule fabrication documentation be reviewed to verify the validity of the capsule descriptions and to validate the data in the capsule database that is pertinent to the CDSP.

3.1.2 Preliminary Conceptual Design Configuration

Figures 3-6 and 3-7 present the elevation and plan views, respectively, of the preliminary conceptual design configuration, and contain three gaps: (1) the inner gap between the inner and outer capsule, (2) the middle gap between the outer capsule and insert, and (3) the outermost gap between the outer surface of the insert and the inner surface of the overpack. The preliminary conceptual design assumes a small 0.318 cm (0.125-in.) outer gap between the insert and overpack. The insert contains 16 holes (the insert is also referred to as the "gun barrel" or "ring"). Figures 3-6 and 3-7 were derived consistent with the overpack containing an insert for 16 Type 3 Cs capsules. Sixteen capsules per overpack was an arbitrary number chosen as a "first cut" to represent the maximum potential loading.

As shown in Figure 3-8, each bore within the insert is capable of accepting a single Type 1, 2, or 3 CsCl or SrF_2 capsule. Figure 3-8 represents the symmetric portion (i.e., wedge or pie-shaped

[3] Hastelloy is a trademark of Union Carbide and Carbon Corporation Corporation, New York, New York.

slice) of the insert and overpack corresponding to one-sixteenth (1/16) of the overall geometry. Note that Figures 3-6 through 3-8 are not to scale. The inner diameter of the capsule hole within the insert is 7.033 cm (2.875 in.). This is consistent with the BUSS cask that has been used previously to transport Cs capsules. The BUSS cask can accommodate distorted capsules that may have resulted due to thermal stresses and handling. The conceptual design will not accommodate Type W Cs capsules. A separate insert with larger holes (8.89 cm [3.5 in.]) will be developed for Type W capsules. See Tables 3-1 and 3-2 for a summary of the dimensions for each type of capsule.

The nominal radial gaps can be determined from Table 3-1 and Figure 3-8 for a Type 3 Cs or SrF_2 capsule within the preliminary conceptual design. For Cs capsules, a nominal gap size of 0.165 cm (0.065 in.) was derived for the first or innermost gap between the outer surface of the inner capsule and the inner surface of the outer capsule. A nominal gap size of 0.277 cm (0.109 in) was derived for the middle gap between the outer surface of the outer capsule and the inner surface of the insert. Finally, a nominal gap size of 0.318 cm (0.125 in.) was specified for the third and outermost gap between the outer surface of the insert and inner surface of the overpack.

Large temperature drops are expected to occur across the gaps. The temperature drop across each gap is dependent on the assumed total capsule power, gap size, location of the gap, and the thermal conductivity of backfill gas/mixture within each gap.

3.1.3 Revised Conceptual Design Configuration

As discussed in Section 3.1.2, the preliminary conceptual design contained three gaps. The revised conceptual design configuration, as discussed within this section, contains only two gaps. The third or outermost gap was eliminated by constructing the insert and overpack from a monolithic piece of stainless steel. Fins were also added to the external surface of the overpack.

Figures 3-9 and 3-10 present the elevation and plan views, respectively, of the revised conceptual configuration with a monolithic insert and overpack with external fins. The revised conceptual configuration is based on a monolithic insert and overpack with 16 holes. As shown in Figure 3-11, each hole within the insert is capable of accepting a single Type 1, 2 or 3 CsCl or SrF_2 capsule. Figure 3-11 represents the symmetric portion (i.e., wedge or pie-shaped slice) of the monolithic insert and overpack corresponding to one-sixteenth (1/16) of the overall geometry. Note that Figures 3-9 through 3-11 are not to scale. The inner diameter of the capsule hole within the insert is 7.033 cm (2.875 in.). This is consistent with the BUSS cask that has been used previously to transport Cs capsules. The BUSS cask can accommodate distorted capsules that may have resulted due to thermal stresses and handling. The conceptual design will not accommodate Type W Cs capsules. A separate insert with larger holes (8.89 cm [3.5 in.]) will be developed for Type W capsules. See Tables 3-1 and 3-2 for a summary of the dimensions for each type of capsule.

The revised conceptual design eliminated the third or outermost gap by assuming the insert and overpack would be constructed from a monolithic piece of stainless steel. The nominal radial gaps can be determined from Table 3-1 and Figure 3-11 for a Type 3 Cs or SrF_2 capsules within the baseline configuration. For Cs capsules, a nominal gap size of 0.165 cm (0.065 in.) was derived for the first or innermost gap between the outer surface of the inner capsule and the inner

surface of the outer capsule. A nominal gap size of 0.277 cm (0.109 in.) was derived for the middle gap between the outer surface of the outer capsule and the inner surface of the insert.

3.1.4 Decay Heat and Capsule Data

Cesium-137 (^{137}Cs) and strontium-90 (^{90}Sr) are radioactive isotopes. Cesium-137 has a half-life of approximately 30.07 years and decays by beta emission following one to two distinct decay modes. Strontium-90 has a half-life of approximately 28.78 years and decays by beta emission.

For Cs, the first decay mode corresponds to a direct decay to the ground state of barium-137 (^{137}Ba). The second decay mode corresponds to decay to an excited state of barium-137 metastable (^{137m}Ba), which in turn decays on a 2.55-minute half-life to the ground state of ^{137}Ba by a combination of gamma and internal-conversion electrons. Because of the gamma associated with the second decay mode, not all the energy released is deposited within the CsCl salt.

The Cs capsule is assumed to have a recoverable decay heat of 160 W, of which 120 W (75%) is assumed to be deposited within the CsCl, 15 W (9.375%) within the first capsule wall, 10 W (6.25%) within the second capsule wall, 10 W (6.25%) within the surrounding insert/structure, and 5 W (3.125%) within the overpack wall. The assumed fractional amount of the total decay heat deposited within the CsCl is higher than previous studies (*Characterization of Two WESF Capsules After Five years of Service* [Sasmor et al. 1988]) have indicated. However, none of the previous studies has had as many capsules in close proximity. It is expected that decay energy (gamma) from the adjacent capsules will increase the fraction of total energy deposited within the CsCl salt. However, a brief study, as documented within Appendix B ("Energy Absorbed by a Salt Log from an Adjacent Log"), indicates that a very small fraction of additional energy (approximately 0.4 W) is deposited within a capsule due to radiation from the adjacent (side-to-side) capsules.

The Cs capsule thermal models assume a uniform heat generation rate across the salt. This may not be appropriate, since a decay gamma created near the perimeter of the salt will have a higher probability of escaping the salt than a gamma created near the centerline. The actual power deposition may be a function of radius. This will result in a centerline peaked power distribution that will lead to increased centerline temperatures and lower salt-metal interface temperatures. A second study, as documented within Appendix C ("Radial distribution of the Gamma Heat Source in CsCl"), indicates that the absorption rates (which is the rate of heat generation) is not uniform across the Cs salt, but varies by a factor of approximately two. This will affect the peak centerline temperature of the salt, but not the salt-metal interface temperature.

However, as previously discussed, none of the previous studies has had as many capsules in close proximity. It is expected that decay energy (gamma) from the adjacent capsules will not only increase the fraction of total energy deposited within the CsCl salt, but may very well produce a more uniform power deposition profile. This remains to be determined. (As an indicator of how complete each vendor's basis is for the corresponding thermal analysis, a Monte Carlo Neutron Photon [MCNP] analysis could have been performed to determine the deposited power profile across the salt and remaining structure.) Additional analyses are recommended to confirm the distribution across the salt and the distribution of absorbed energy within the remaining structure.

It is expected that the salt-metal interface temperature will be somewhat sensitive to the overall fraction of energy deposited within and the distribution across the CsCl. (Parametric analyses were performed assuming 50% of the decay heat was deposited within the salt and the heat generation rate was peaked along the centerline of the salt. The results of this analysis are discussed within Section 4.4.).

The strontium capsule was assumed to have 100% of the recoverable decay power deposited within the salt.

Verification of the capsule calorimetric data used for the thermal analysis was completed (WMP 16938). For individual capsules, the calorimetric data has been determined to have a statistical accuracy of plus or minus 10%. Given a large enough sample and the statistical nature of the calorimetric data, the uncertainties associated with the power of a loaded overpack will tend to reflect average conditions. It is believed that the assumption of 75% of the total decay heat deposited within the salt will accommodate the uncertainties associated with the calorimetric data. .

Capsule powers were decayed to July 1, 2003, assuming a half-life ($t_{1/2}$) of 30.07 years for Cs capsules and 28.78 years for Sr capsules. Power was computed from Equation 3.1-1:

$$P = P_0 \exp\left(\frac{-0.6931\,\Delta t}{t_{1/2}}\right) \qquad \text{Equation 3.1-1}$$

Where P_0 is the initial power and Δt is the number of years between July 1, 2003, and the calorimetric date. Table 3-3 summarizes the statistics that were derived given the Cs and Sr capsule populations. Figures 3-12 and 3-13 present the power histograms and cumulative distributions for the Cs and Sr capsules, respectively.

3.1.5 Material Properties

The thermo-physical material properties (thermal conductivity, specific heat density, and surface emissivities) for CsCl, SrF_2, 316L stainless steel, Hastelloy C-276, and various pure gases used for the subject thermal analyses are attached as Appendix F and are documented in WMP-16878, *WESF Capsule Databook.*

3.1.6 Environmental Conditions

Environmental conditions will affect the design and performance of the preliminary conceptual overpack and dry storage system. Site-specific environmental conditions, maximum day hourly temperatures, nominal maximum and minimum temperatures for a year (seasonal), and solar insolation values for flat and curved surfaces, were obtained from WMP-16878. For completeness, the hourly solar insolation values for curved surfaces are presented in Table 5-1 and the nominal maximum and minimum seasonal temperatures are presented in Figure 5-9.

3.2 CONCEPTUAL DRY STORAGE MODULE DESIGN

Figure 3-14 presents the conceptual design of a dry storage module with an internal heat load (Q_{total}) corresponding to the decay heat associated with an overpack loading. Figure 3-14 depicts the conceptual dry storage module with overpacks, with natural circulation flow induced by the density difference between the interior gas and the ambient environment. For simplicity, dry storage module walls are modeled as one vertical planar wall; this proved to be sufficient for the time being because conduction is not the dominant means of heat removal. Solar insolation is depicted in the figure as a boundary condition on the wall outer surface. Solar insolation is neglected in the initial calculation and treated as part of the parametric calculations later on. Table 3-4 presents the dimensions and derived quantities assumed for the conceptual dry storage module.

3.3 ADDITIONAL DESIGN CONSIDERATIONS

A small number of Cs capsules with suspect integrity, as well as materials from capsule destructive examinations and test programs, were sealed inside an additional welded container for additional assurance against leakage. These capsules are referred to as Type W overpacks. The Type W overpack capsules have an additional annulus/gap and capsule wall that impacts thermal analysis and thus the design.

The preliminary and revised conceptual designs, as presented in Figures 3-6 through 3-11, do not accommodate Type W overpack capsules. However, since there are only 23 Type W overpacks, only a few specially made inserts will be required.

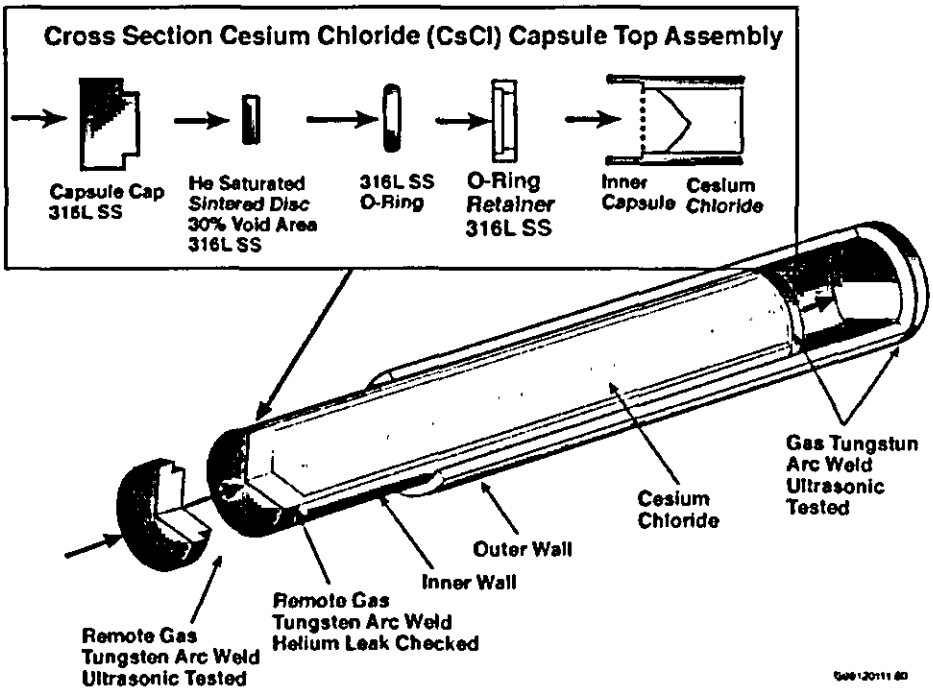

Figure 3-1. Isometric View of Cesium Chloride Capsule During Assembly.

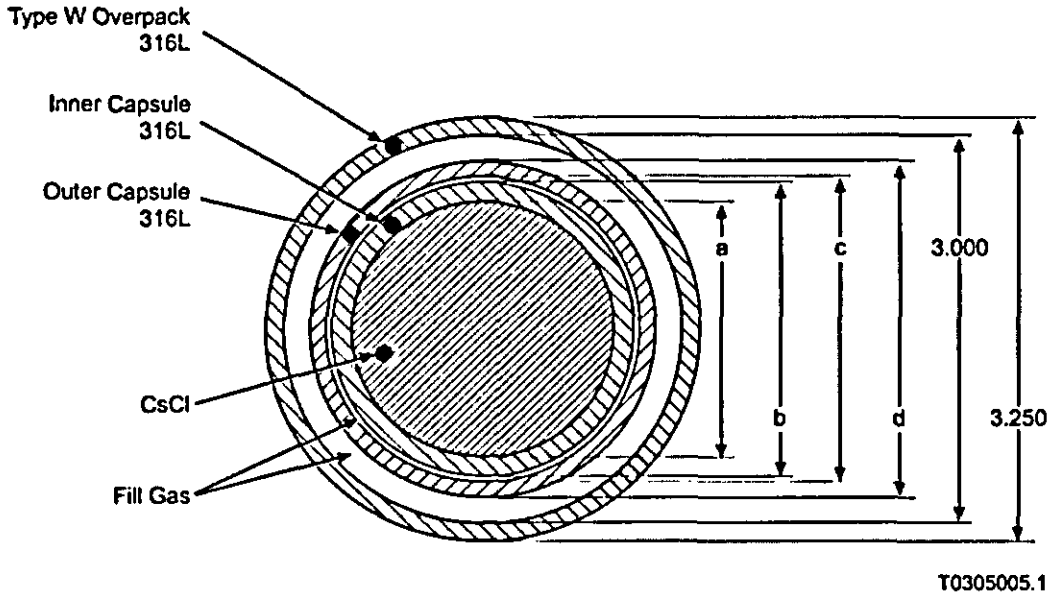

Figure 3-2. Cross-Section of Cesium Chloride Capsule.
(See Table 3-1 for a summary listing for all capsule types.)

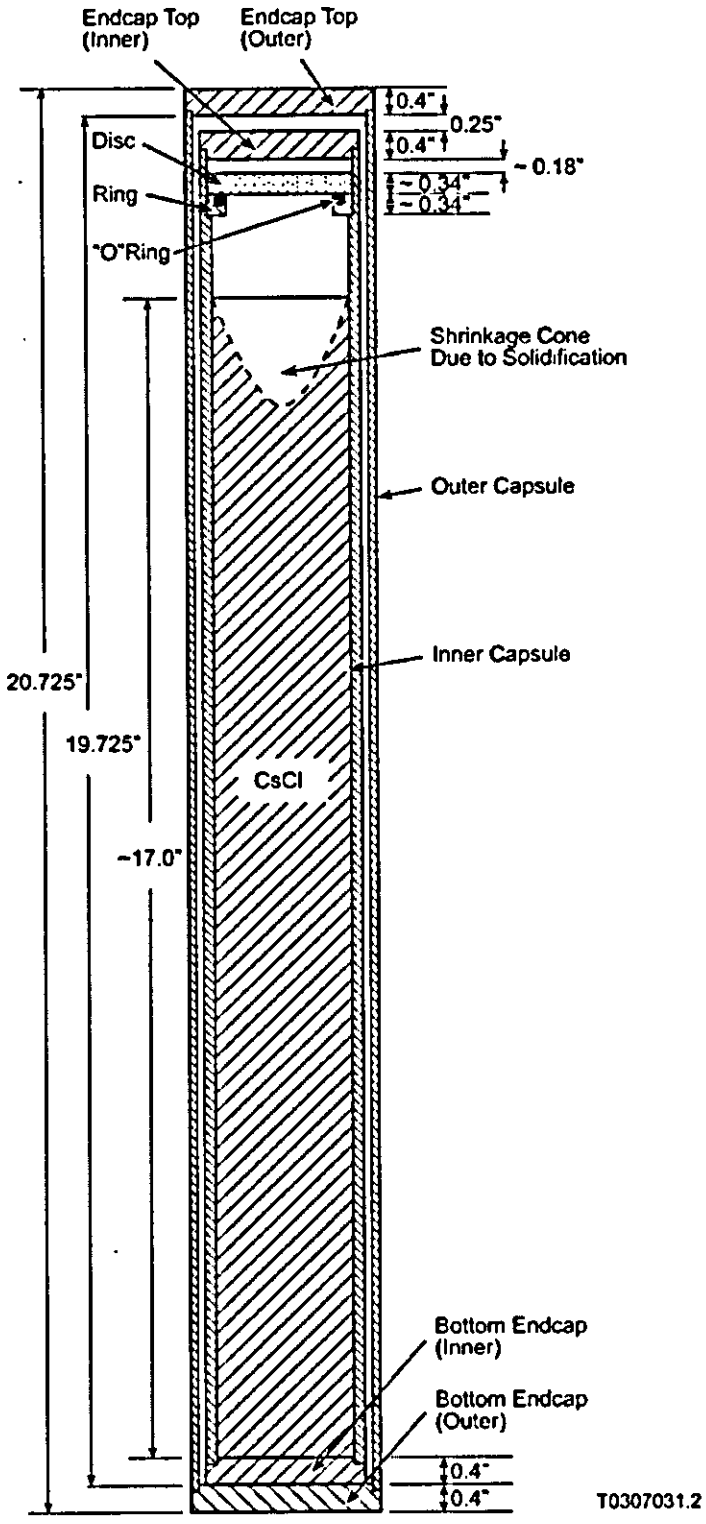

Figure 3-3. Elevation View of Representative Cesium Chloride Capsule.

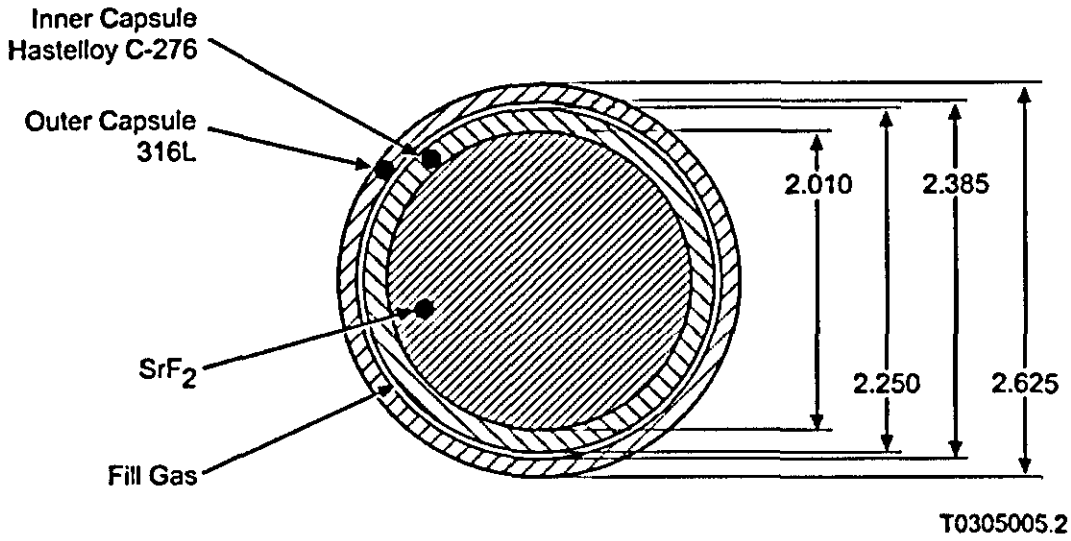

Figure 3-4. Cross Section of Strontium Fluoride Capsule.
(See Table 3-2 for additional strontium capsule dimensions.)

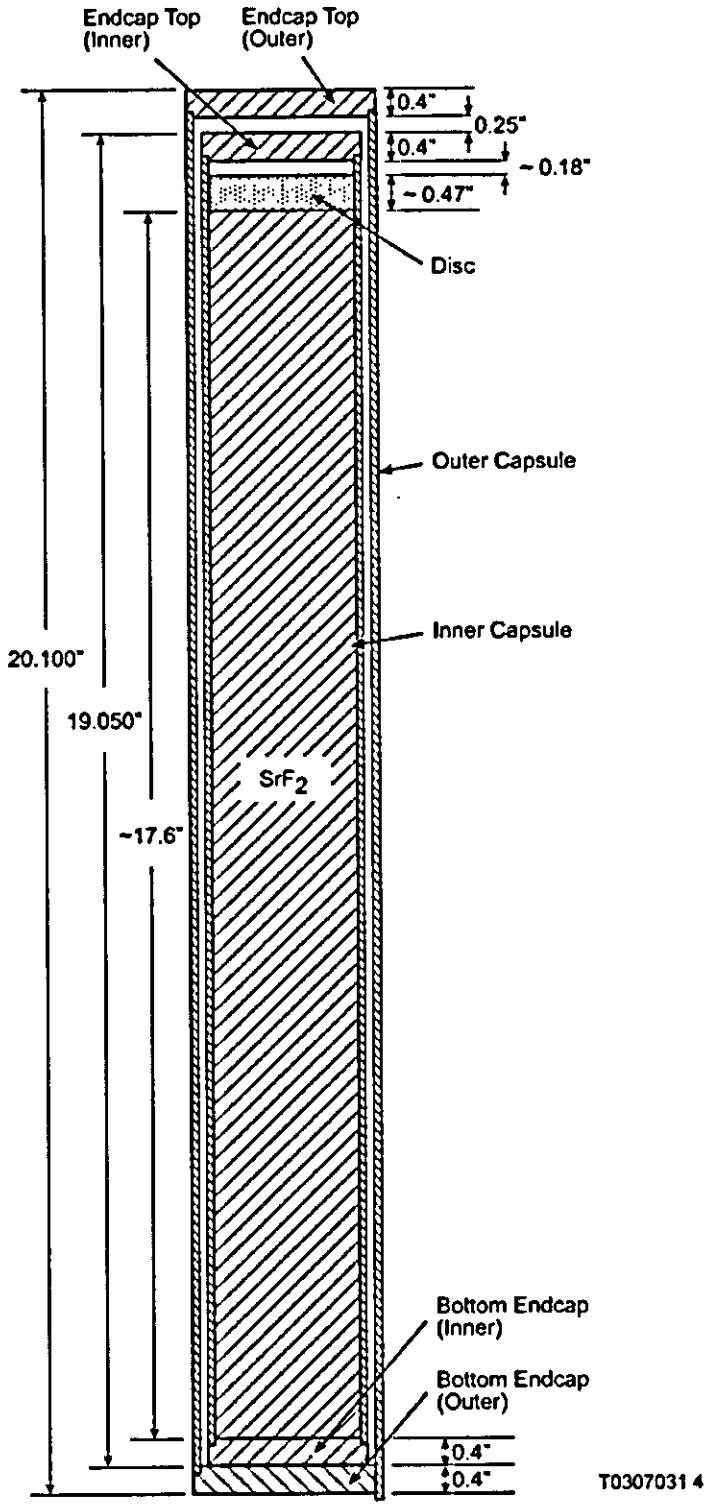

Figure 3-5. Elevation View of Representative Strontium Fluoride Capsule.

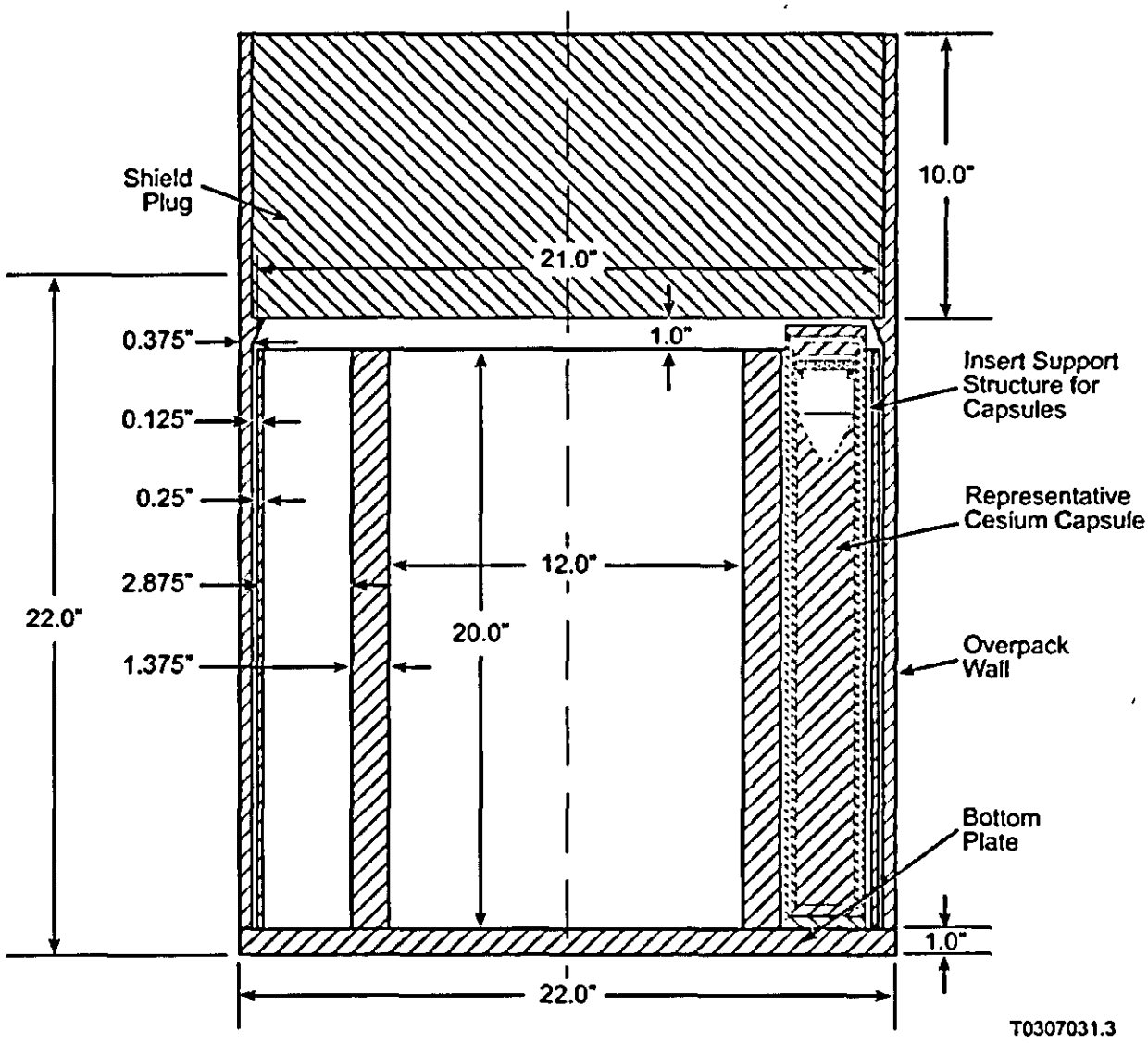

Figure 3-6. Elevation View of Preliminary Conceptual Design for Insert and Overpack (Separate Insert and Overpack without Fins).

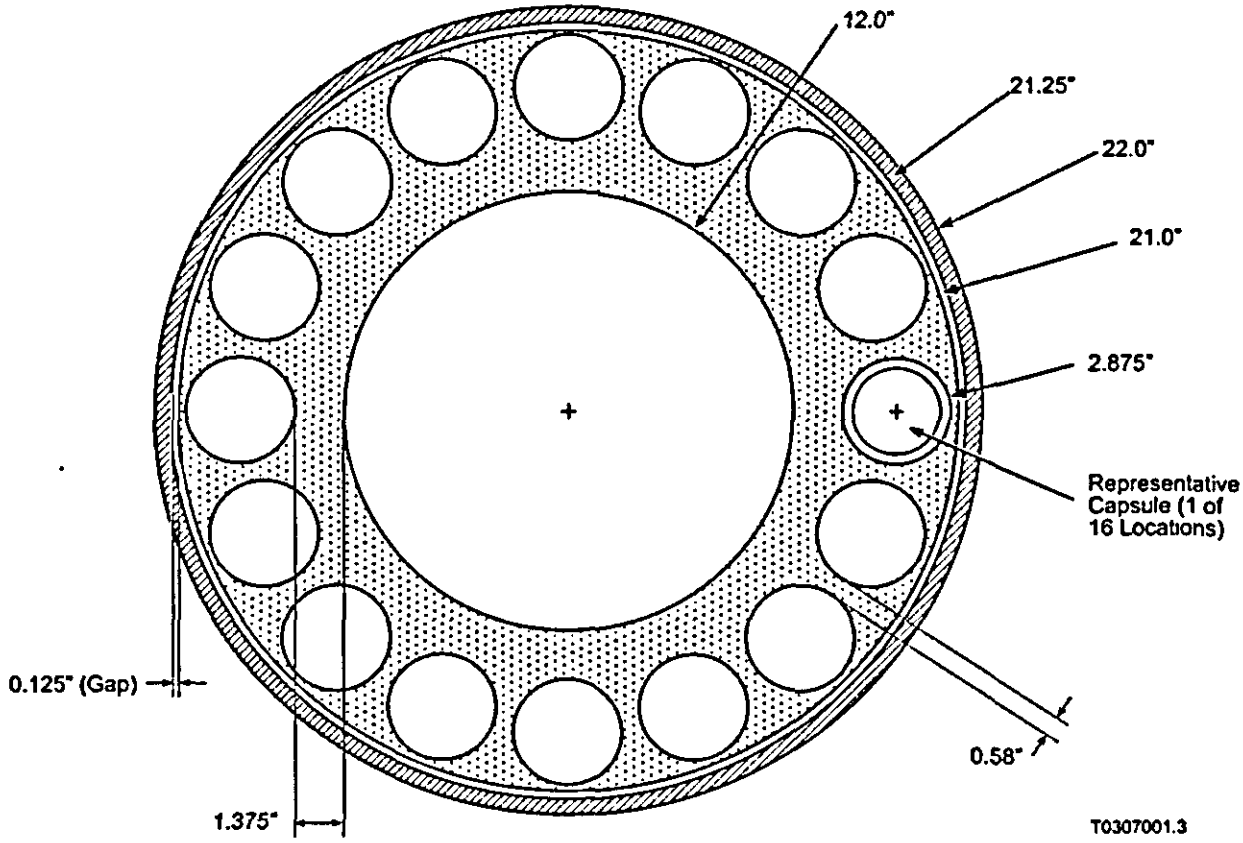

Figure 3-7. Plan View of Preliminary Insert and Overpack Design for 16 Type 3 Cesium Capsules (Separate Insert and Overpack without Fins).

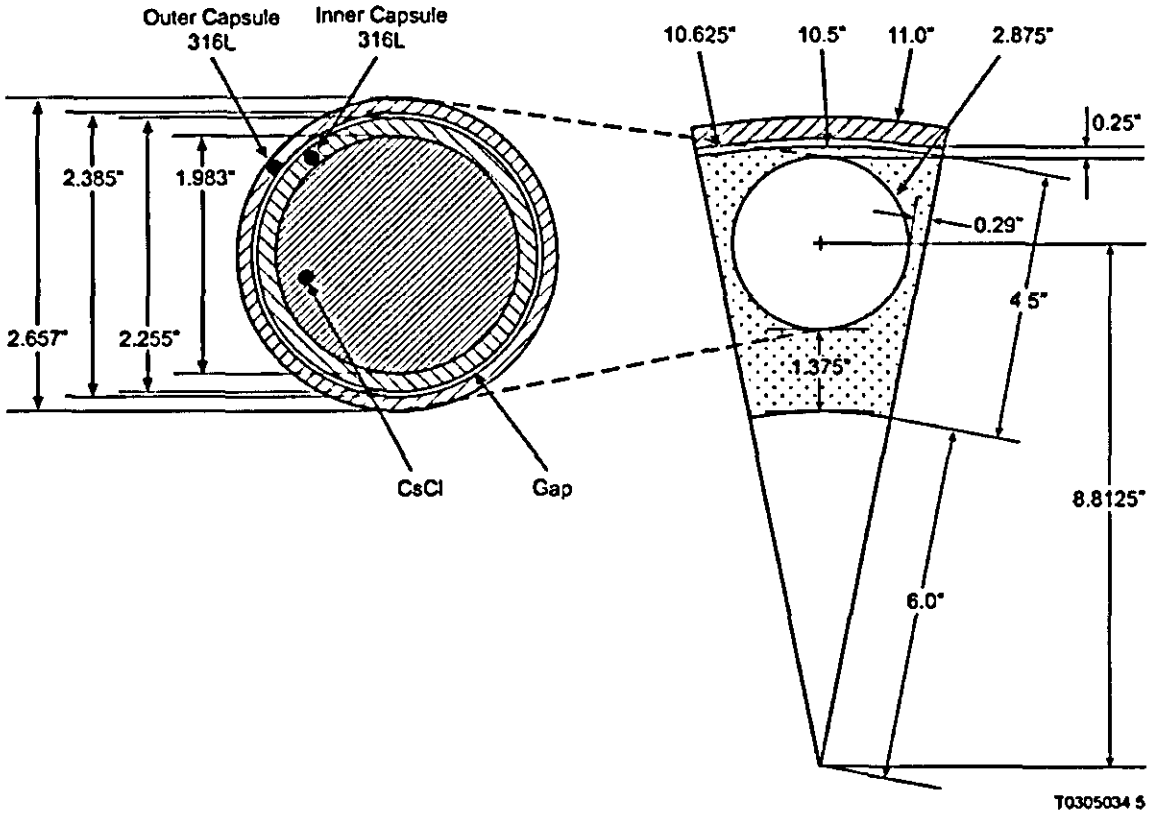

Figure 3-8. Preliminary Conceptual Design - Location of Type 3 Cesium Chloride or Strontium Fluoride Capsules (Separate Insert and Overpack without Fins).

(See Table 3-1 and 3-2 for dimensions associated with each type of capsule.)

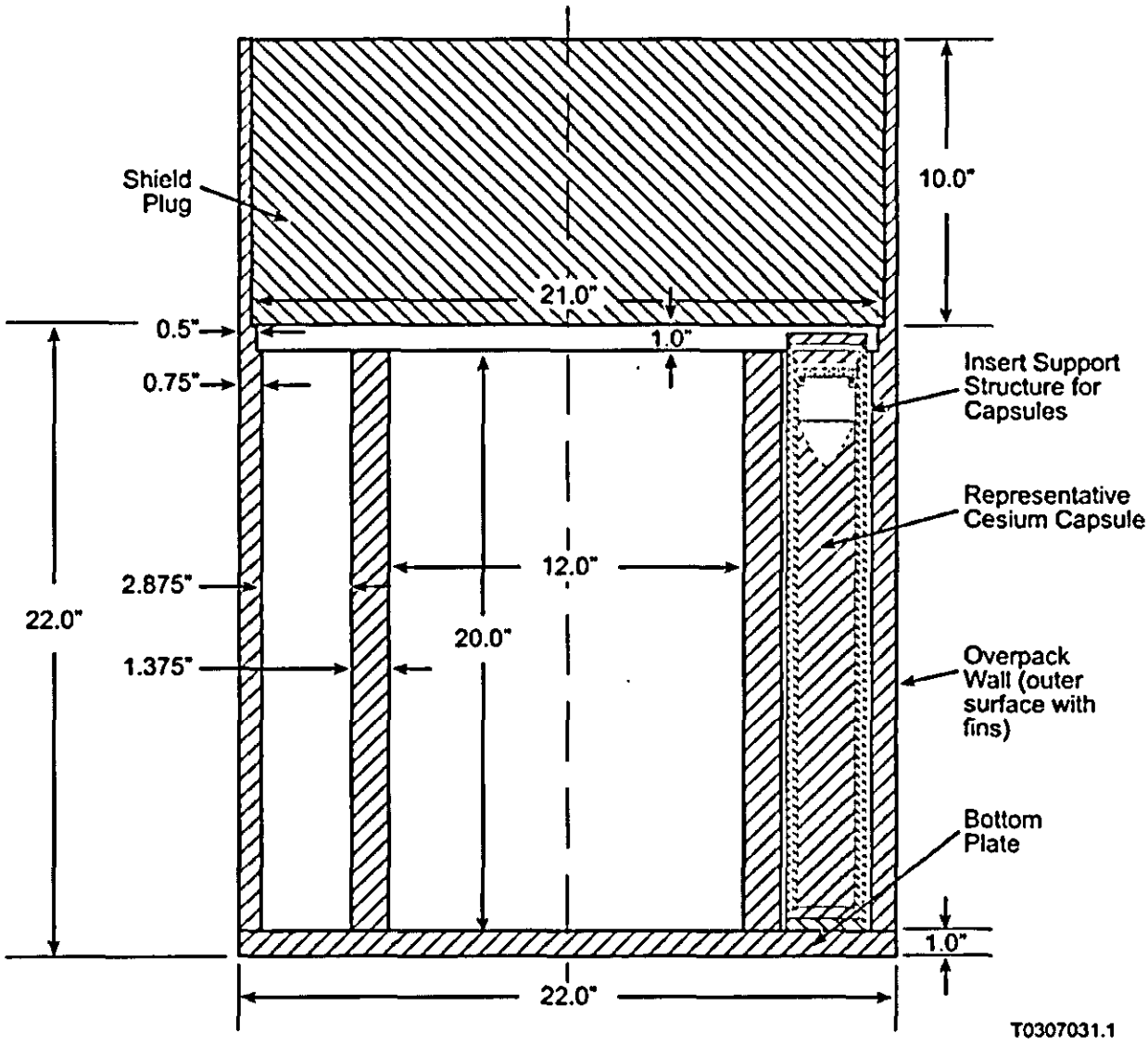

Figure 3-9. Elevation View of Revised Conceptual Design for Monolithic Insert and Overpack with Fins.

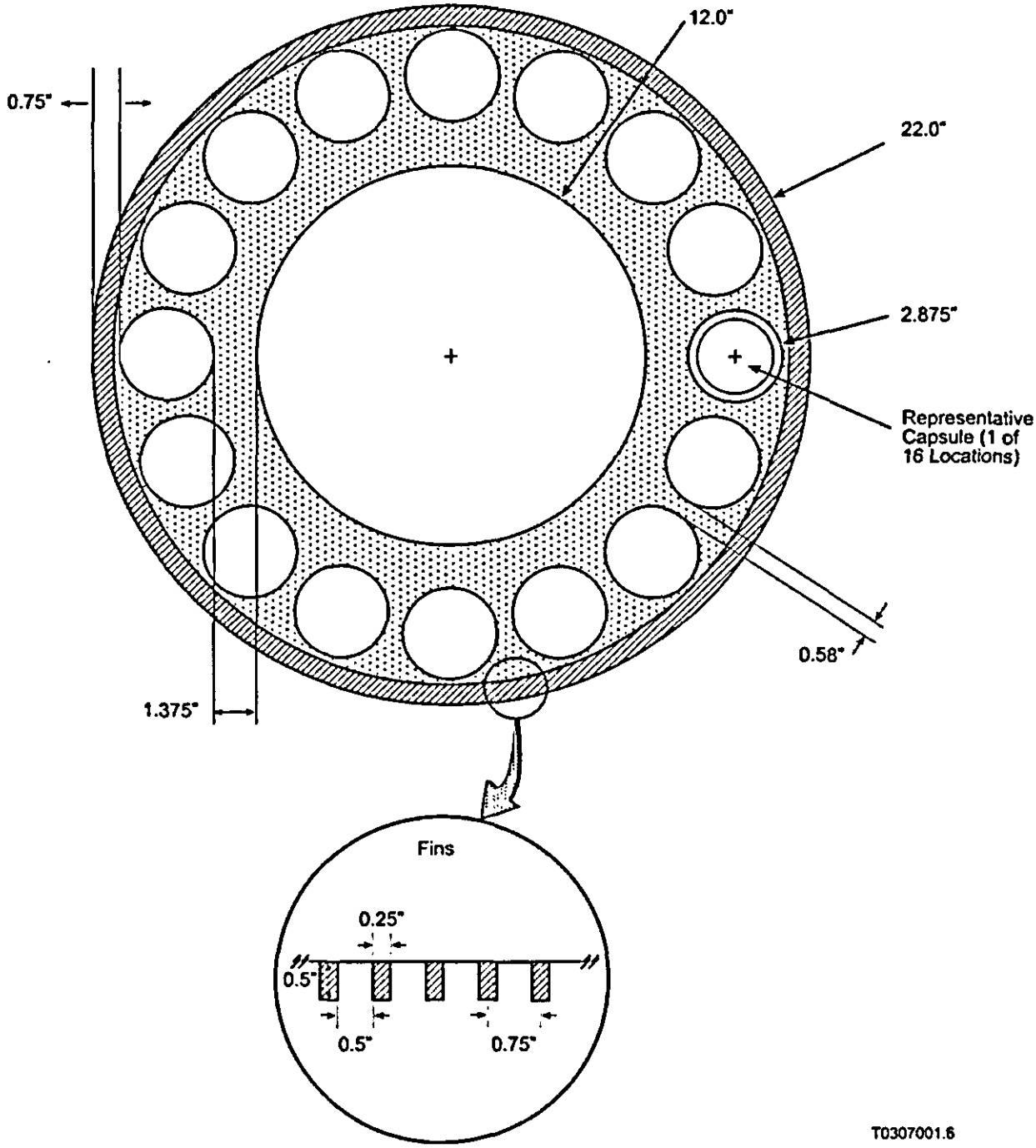

Figure 3-10. Plan View of Revised Conceptual Design for Monolithic Insert and Overpack with Fins.

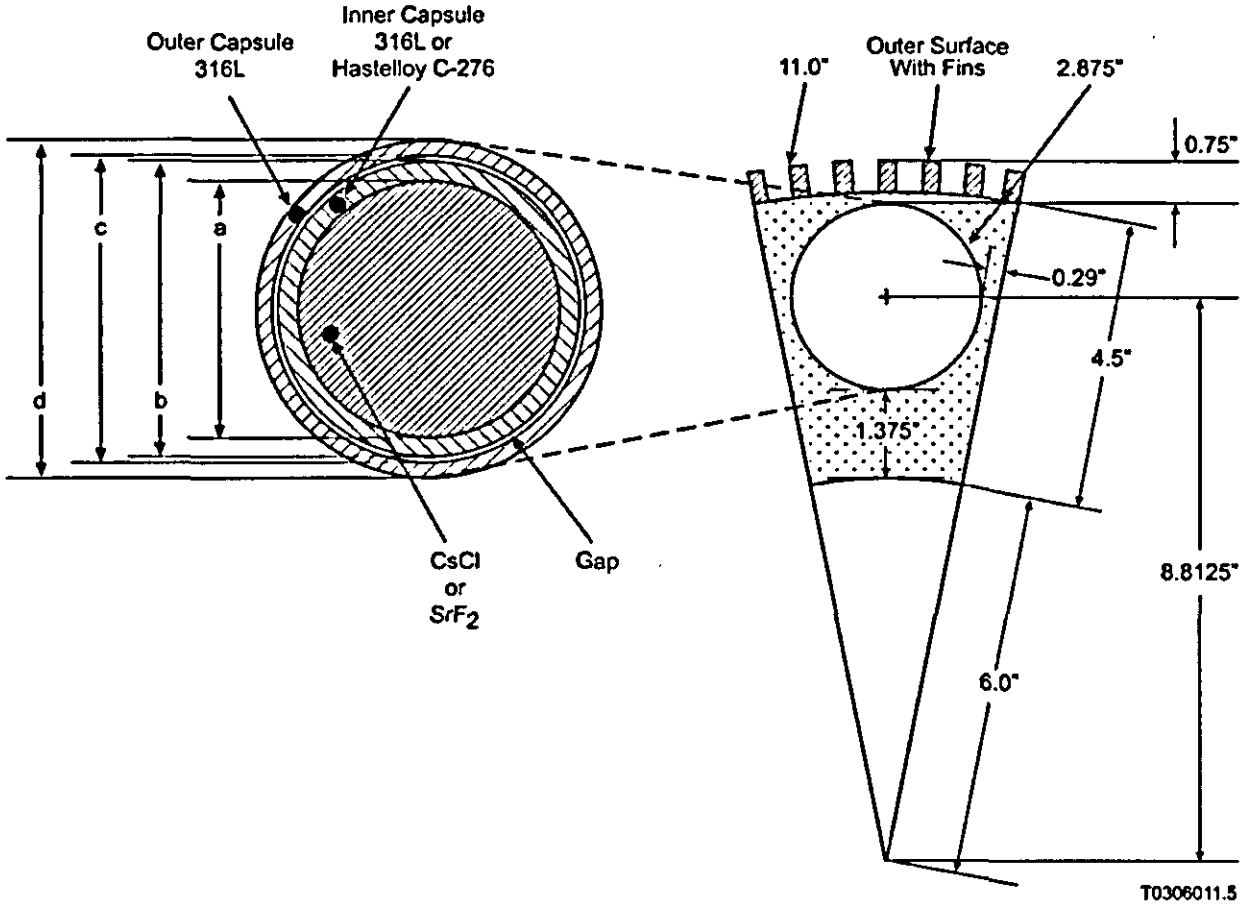

Figure 3-11. Revised Preliminary Conceptual Design Showing Location of Type 3 Cesium Chloride or Strontium Fluoride Capsule (Monolithic Insert and Overpack with Fins).

(See Table 3-1 and 3-2 for dimensions associated with each type of capsule.)

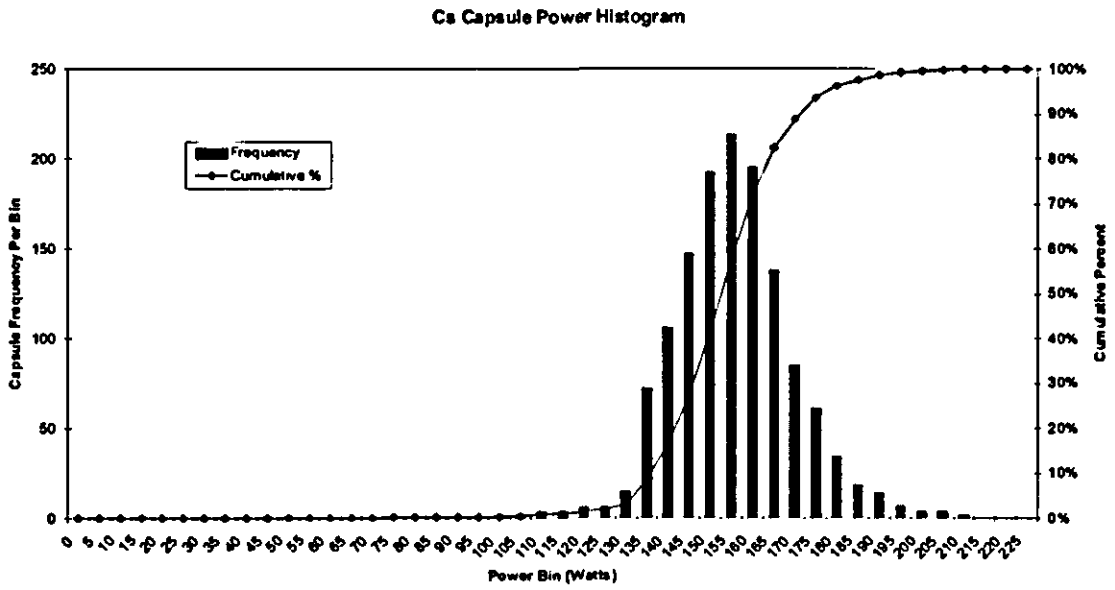

Figure 3-12. Cesium Capsule Power Histogram and Cumulative Fraction (Based on Decay to July 1, 2003).

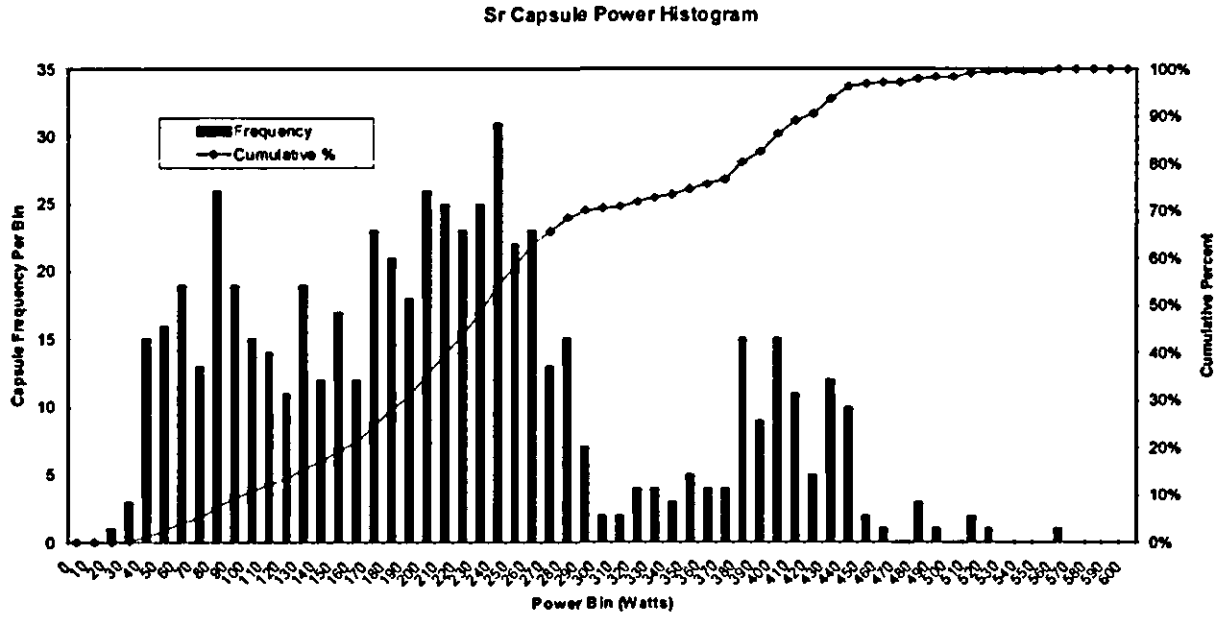

Figure 3-13. Strontium Capsule Power Histogram and Cumulative Fraction (Based on Decay to July 1, 2003).

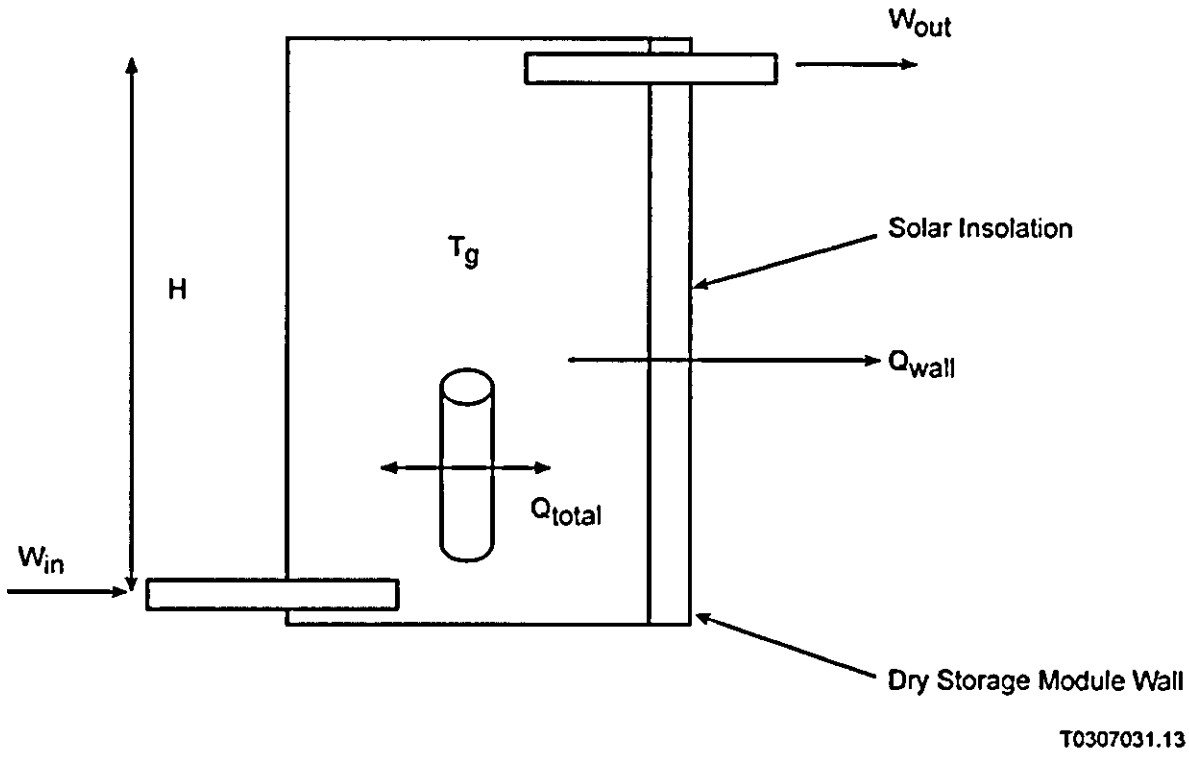

Figure 3-14. Conceptual Configuration of Dry Storage Module with Overpacks.

Table 3-1. Cesium Chloride Capsule Dimensions.

Component (see Figure 3-1)	Item	Capsule type		
Inner capsule (316L), in.		1	2	3[1]
Inner diameter[2]	a	2.060	2.044	1.983
Outer diameter	b	2.250 ± 0.005	2.250 ± 0.005	2.255 ± 0.010
Nominal wall thickness (midplane)(Δt)[3]		0.095 ± 0.009	0.103 ± 0.009	0.136 ± 0.012
Overall capsule length (including end caps)[4]		19.725	19.725	19.725
Top and bottom end cap thickness		0.400	0.400	0.400
Outer capsule (316L), in.		1	2	3[1]
Inner diameter	c	2.407 ± 0.008	2.407 ± 0.008	2.385 ± 0.015
Outer diameter[5]	d	2.625	2.645	2.657
Nominal wall thickness (midplane)(Δt)[3]		0.109 ± 0.009	0.119 ± 0.009	0.136 ± 0.012
Overall capsule length (including end caps)[4]		20.775	20.775	20.775
Top and bottom end cap thickness		0.400	0.400	0.400
Type W overpack (316L), in.				
Inner diameter		3.000		
Outer diameter		3.250		
Nominal wall thickness (midplane)(Δt)[3]		0.125		
Overall capsule length (including end caps)[4]		21.825		
Top and bottom end cap thickness		0.400		

[1]The majority, but not all of the CsCl capsules were fabricated using Type 3 tubing.

[2]Calculated using nominal dimensions: ID = OD – 2*Δt.

[3]Minimum wall (endcap weld cutback): inner capsule = 0.079 in.; outer capsule = 0.099 in.; Type W overpack = 0.099 in.

[4]Each end cap recessed 0.1 in.

[5]Calculated using nominal dimensions: OD = ID + 2*Δt.

ID = inside diameter.

OD = outside diameter

Table 3-2. Strontium Fluoride Capsule Dimensions.

Component (See Figure 3-2)	Dimension, cm (in.)
Inner capsule (Hastelloy C-276), in.	
Inner diameter	5.105 (2.010)
Outer diameter	5.715 (2.250)
Nominal wall thickness (midplane)(Δt)[1]	0.305 (0.120)
Overall capsule length (including end caps)[2]	48.387 (19.050)
Top and bottom end cap thickness	1.016 (0.400)
Outer capsule (316L), in.	
Inner diameter	6.058 (2.385)
Outer diameter	6.668 (2.625)
Nominal wall thickness (midplane)(Δt)[1]	0.305 (0.120)
Overall capsule length (including end caps)[2]	51.054 (20.100)
Top and bottom end cap thickness	1.016 (0.400)

[1]Min. wall (endcap weld cutback): inner capsule = 0.292 cm (0.115 in.), outer capsule = 0.251 cm (0.099 in.)

[2]Each end cap recessed 0.25 cm (0.1 in.).

Table 3-3. Derived Statistical Data for the Cesium and Strontium Capsules (Decayed to July 1, 2003)

	Cesium (W)	Strontium (W)
Count	1,335	600[1]
Mean	157.7[2]	217.2[3]
Median	157.5	209.9
Standard Deviation	15.5	114.4
Range	196.6	545.0
Minimum	17.9	24.8
Maximum	214.5	569.8

[1]Does not include one zero power tracer capsule produced with natural strontium.

[2]Thermal analyses assumed a mean cesium capsule power of 160 W.

[3]Thermal analyses assumed a mean strontium capsule power of 218 W

Table 3-4. Conceptual Dry Storage Module Assumed Dimensions and Derived Quantities.

	Dry Storage Module Dimensions, meters (in.)				
Height	6.10 (240)				
Shell Inner Diameter	1.87 (73.5)				
Shell Outer Diameter	3.37 (132.5)				
Shell Inner Radius	0.93 (36.75)				
Shell Outer Radius	1.68 (66.25)				
Wall Thickness	0.75 (29.50)				
Derived Quantities					
Loss coefficient (k)	1	2	3	4	5
Bottom Duct Area, m^2	0.39	0.274	0.223	0.194	0.173
Top Duct Area, m^2	0.39	0.274	0.223	0.194	0.173
Heat Transfer Wall Area	m^2	50.10[1]			
Interior Volume	m^3	8.30[2]			

[1]Heat transfer wall area is based on average shell diameter and height.

[2]Interior volume assumes 50% void, shell inner diameter, and height.

4.0 MIDPLANE CAPSULE MODELS AND STEADY-STATE ANALYSIS RESULTS

4.1 DRY STORAGE MODEL INTEGRAL BEHAVIOR

The purpose of this section is to estimate the gas exit temperature (T_g) to be used as a boundary condition for an overpack container in a dry storage module (see Sections 4.2 and 4.3). A secondary purpose is to demonstrate that a dry storage module can be designed that does not significantly challenge attainment of the performance specification for the salt-metal interface temperature.

The gas temperature within the conceptual dry storage module is primarily a function of total heat load, configuration and size of inlet/outlet flow areas, and elevation difference driving natural circulation flow (the stack height).

The dry storage module analyses assumed a total heat load of 24 kW,

- Loss coefficients are 3.0, or discharge coefficients are 0.58 ($1/\sqrt{3}$), and,
- Stack height is equal to 4.5 m, for reasons explained below.

These inputs are treated parametrically to evaluate uncertainties.

4.1.1 Dry Storage Module Thermal Model

The conceptual configuration of the dry storage module was discussed in Section 3.2. Figure 3-14 presents a diagram of a conceptual dry storage module containing a number of overpacks subject to a total decay power load. Table 3-4 presents the assumed dry storage module dimensions and derived quantities.

The dry storage module is designed to allow passive heat removal from overpack containers. This is mainly accomplished by natural circulation flow induced by the density difference between the interior gas and the ambient environment. A simplified steady state energy balance on the dry storage module is:

$$Qtotal = Qgas + Qwall \qquad \text{Equation 4.1-1a}$$

Q_{total} = total capsule heat load (W),
Q_{gas} = power (W) removed by gas circulation,
Q_{load} = power (W) removed through overpack walls, top, and bottom.

For simplicity, the dry storage module walls may be modeled as one vertical cylindrical wall, neglecting the contribution through the module top, and assuming an adiabatic bottom. Assumptions about heat transfer through the walls eventually prove to be unimportant because natural circulation removes nearly all the heat load. Solar insolation is neglected in this initial

calculation but is treated as part of the parametric calculations later on. Power removed by the gas and through the walls may be expressed in terms of temperature differences:

$$Q_{total} = w \cdot C_p \cdot (T_g - T_a) + \overline{U} \cdot A_w \cdot (T_g - T_a) \qquad \text{Equation 4.1-1b}$$

where:

w	=	natural circulation flowrate due to the stack effect (kg/s),
$\overline{U}$	=	average overall heat transfer coefficient ($W/m^2/K$) over the height of the module,
A_w	=	wall heat transfer area (m^2),
T_g	=	dry storage module gas temperature at the top exit,
T_a	=	ambient air temperature, and
C_p	=	constant pressure specific heat of air (J/kg/K).

In Equation 4.1-1b, given that T_g is identified as the gas exit temperature, its use in the wall heat removal term is an approximation. Gas heats up from the inlet ambient temperature as it enters the dry storage module interior at low elevation and passes by overpack containers, and it also cools down somewhat by heat transfer to the module inside wall at elevations above the overpacks. The approximation is justified simply because this term is negligible compared to the gas flow term. If the total capsule heat load is known, this equation can be solved for T_g once w and $\overline{U}$ are written in terms of T_g.

The stack effect mass flow rate w (kg/s) is found by writing the Bernouilli equation along an imaginary streamline from the low elevation inlet of the dry storage module, upward through the dry storage module, and exiting the dry storage module at a high elevation. The only significant pressure drops due to flow are at the dry storage module inlet and exit ports. Assuming these are of equal flow area and using the ambient density as an average value, the flow rate is given by the orifice equation:

$$w = A_f \cdot C_D \cdot \sqrt{\overline{\rho} \cdot \Delta P} \qquad \text{Equation 4.1-2}$$

where:

W	=	flow rate (kg/s)
$\overline{\rho}$	=	average gas density, (kg/m^3),
A_f	=	flow area (m^2),
ΔP	=	sum of pressure drops through dry storage module inlet and outlet paths, ($kg/m/s^2$),
C_D	=	combined orifice coefficient for dry storage module inlet and outlet paths in series; this is the effective coefficient for one path divided by $\sqrt{2}$, and the coefficient for a single path considers expansions, bends, contractions, etc.

The pressure drop is the static head difference, which is found by knowing the variation of gas density with elevation in the dry storage module interior:

$$\Delta P = \int_0^{H_{act}} (\rho(z)-\rho_a)\cdot g\cdot dz = \rho_a \cdot g\cdot B\cdot \int_0^{H_{act}} (T(z)-T_a)\cdot dz \qquad \text{Equation 4.1-3}$$

where:

$\rho(z)$	=	local gas density (kg/ m^3),
ρ_a	=	ambient gas density (kg/ m^3),
G	=	acceleration of gravity (m^2/s),
β	=	coefficient of volume expansion (1/K),
$T(z)$	=	local temperature (K),
T_a	=	ambient temperature (K), and
H_{act}	=	actual stack height (m).

Overpack containers are imagined to occupy a lower portion of the dry storage module, and their power is therefore added over this height, which will be referred to as a heated length. With no knowledge of how overpacks may be stacked, a good approximation is simply to assuming uniform heating over this length. If heat losses to the walls are indeed small, then gas temperature remains nearly constant above the heated length. On this basis a simple linear expression for the local temperature is as follows:

$$T(z)-T_a = (T_g - T_a)\cdot \frac{z}{H_Q} \qquad \text{if } 0 < z < H_Q \qquad \text{Equation 4.1-4a}$$

$$T(z)-T_a = (T_g - T_a) \qquad \text{if } H_Q < z < H_{act} \qquad \text{Equation 4.1-4b}$$

where, H_Q is the heated length. Assuming $H_Q = H/2$, the integral yields

$$\Delta P = \rho_a \cdot g\cdot B\cdot (T_g - T_a)\cdot \frac{3}{4}\cdot H_{act} \qquad \text{Equation 4.1-5}$$

It is convenient to define an effective stack height $H = 3\,H_{act}/4$ that drives natural circulation because the fraction ¾ is merely a consequence of the assumed power addition profile, and the important feature is that heat addition over a finite distance reduces the stack height from the true interior height of the module. Using this expression for the pressure drop in the orifice equation and noting that the average density and ambient density are nearly equal yields the sought expression for the flow rate:

$$\Delta P = \bar{\rho}\cdot A_f \cdot C_D \cdot \sqrt{2\cdot B\cdot g\cdot H\cdot (T_g - T_a)} \qquad \text{Equation 4.1-6}$$

The overall heat transfer coefficient, $\bar{U}$, can be written using three heat transfer resistances:

$$\overline{U} = \frac{3/4}{\frac{1}{h_i} + \frac{r_i}{k_w} \ln\left(\frac{r_o}{r_i}\right) + \frac{1}{h_o}}$$ Equation 4.1-7

These three resistances are convection from the interior gas to the interior wall, conduction through the cylindrical wall, and convection/radiation from the outer wall to the ambient environment. In this expression, h_i is the heat transfer coefficient for convection at the inner wall surface, and h_o is the total heat transfer coefficient for convection/radiation at the outer wall surface.

At steady state for the cylindrical wall, heat transfer through the inner and outer faces is equal to conduction through the wall:

$$h_i\, 2\pi r_i \frac{3}{4} (T_g - T_i) = \frac{2\pi k_w}{\ln(r_o/r_i)} (T_i - T_o)$$

Equations 4.1-8 and -9

$$h_o\, 2\pi r_o (T_o - T_\infty) = \frac{2\pi k_w}{\ln(r_o/r_i)} (T_i - T_o)$$

where T_i and T_o are the inner and outer wall surface temperatures, respectively.

If the heat transfer coefficients are specified, the result is a system of three equations and three unknowns (T_g, T_i and T_o) that can be solved iteratively. The heat transfer coefficient, h_c, is specified, as follows, by an empirical relationship for free convection from a vertical plate within an infinite medium ("Correlating Equations for Laminar and Turbulent Free Convection from a Vertical Plate" [Churchill and Chu 1975]):

$$\overline{Nu_L} = \left[0.825 + \frac{0.387\, Ra_L^{1/6}}{\left(1+(0.492/Pr)^{9/16}\right)^{8/27}}\right]^2$$

$$Ra_L = \frac{g \beta \Delta T L^3}{\nu \alpha}$$ Equations 4.1-10, -11 and -12

$$\overline{Nu_L} = \frac{h_c L}{k_{air}}$$

Where the Prandtl number (Pr) is approximately 0.7 for air over the temperature range of concern and ΔT is the temperature difference between the exterior surface of the overpack and bulk gas within the dry storage module. For hand calculations, this correlation has the advantage of applying across the entire range of Rayleigh numbers. Equation 4-1-10 is applicable, since

the assumed scale associated with the dry storage module is large enough that well-defined boundary layers will exist.

The radiation heat transfer coefficient is of the linearized form:

$$h_r = \sigma\bar{\varepsilon}\left(T_g^2 + T_w^2\right)\left(T_g + T_w\right)$$

Equations 4.1-13 and -14

$$\bar{\varepsilon} = \frac{1}{\frac{1}{\varepsilon_g} + \frac{1}{\varepsilon_w} - 1}$$

where subscript "g" and "w" refer to gas and wall surface, respectively, ε is emissivity, and σ is the Stefan-Boltzmann constant. Radiation heat transfer from the interior gas to the inner wall "i" is not credited because air is nearly transparent over such small distances and the inner wall sees itself. Radiation from the outer wall to the ambient environment is included. Heat transfer coefficients, h_i and h_o, can now be specified and the system of equations is closed.

Table 4-1 shows the solution for interior gas temperature for a heat load of 24,000 W and flow area of 0.23 m^2, which is the actual duct area multiplied by a discharge coefficient of $1/\sqrt{3}$. To solve for the three unknown temperatures, the residual of the energy balance is set to zero, subject to the constraints that the steady state conduction through the inner wall equals that through the outer wall. The residual is as follows:

$$\text{Residual} = Q_{load} - w \cdot C_p \cdot (T_g - T_a) - \bar{U} \cdot A_w \cdot (T_g - T_a) \qquad \text{Equation 4.1-15}$$

Table 4-1 presents those values that are held static during the iterative solution for the three unknown temperatures. Table 4-1 includes intermediate calculations such as the heat transfer coefficients, natural circulation flowrate, natural circulation heat removal, and conduction heat transfer rate. The natural circulation flowrate of 0.74 kg/s (1.63 lb/sec) shows that mixed-convection correlations might be appropriate. Forced convection can be neglected whenever $Gr/Re^2 >> 1$. Grashof number, Gr, is 1.90×10^{11} (Ra/Pr). Reynolds number can be computed per Equation 4.1-16:

$$Re = \frac{w H}{\rho A_c F \nu} \qquad \text{Equation 4.1-16}$$

where A_c is the cross-sectional area of the interior, $\pi(1.87)^2/4 = 2.74$ m^2, and F is some fraction to account for obstruction; assumed to be 0.5 for the sake of this discussion. This leads to a Reynolds number of about 150,000. The ratio Gr/Re^2 is about 8, and is on the order 1 if F is as low as 0.20, so heat transfer is best described by mixed-convection rather than by pure natural convection. This point is not considered any further because the calculated heat transfer coefficient is not likely to increase much if forced convection is included (mixed-convection heat transfer coefficients are combinations of natural convection and forced convection heat transfer coefficients), and in any event losses to the wall are shown to be unimportant.

Table 4-1 shows that for a heat load of 24,000 W and a Site-average external ambient temperature of 22 °C, the interior gas temperature would be about 53 °C for the indicated flow area that accounts for the discharge coefficient. Nearly all the heat is removed by buoyancy-driven flow. The buoyancy-driven mass flow rate through the dry storage module was determined to be 0.742 kg/s.

4.1.2 Dry Storage Module Parametric Calculations

Parametric calculations consider uncertainties in flow area, heat load, ambient conditions, and the elevation difference for natural circulation.

One set of parametric calculations was made with total heat loads of 18 kW, 24 kW, and 30 kW, and loss coefficients of 2, 3, 4, and 5, which is the same as saying that the parametric flow areas are 0.274, 0.223, 0.194, and 0.173 m^2, respectively. The first part of this parametric calculation accounts for the uncertainty in the individual capsule heat loads, while the second accounts for uncertainties in natural circulation flow rates. Geometric details are unavailable, but it is certain that any pathway will include bends and obstructions for shielding purposes. Figure 4-1 shows results of the 12 parametric calculations. Assuming ambient conditions of 22 °C and 101,350 Pa, interior gas temperature can vary between 45 °C and 65 °C for total heat load between 18 kW and 30 kW.

A second set of parametric calculations was made to consider uncertainties in the elevation difference for natural convection and changes in the base case flow area. Uncertainties in elevation difference result from uncertainties in the gas temperature profile within the dry storage module. Maximum potential for natural circulation is when all heating occurs at the very bottom of the dry storage module, which would result in H = 6 m. In base case calculations, it is assumed that heating takes place over the bottom half of the storage module to get a value of H = 4.5 m. Variations in base case flow area consider potential engineered changes to the assumed dry storage module design. Figure 4-2 illustrates the results and shows that for reasonable variations in elevation difference and flow area, the interior temperature for the dry storage module is still between 40 °C and 65 °C.

Figure 4-2 suggests that interior temperature to the dry storage module is relatively insensitive to changes in *H*, the elevation difference that drives natural circulation. Looking at the energy balance again, ignoring conduction losses, and solving for the temperature rise can rationalize this:

$$Q = w \cdot C_p \cdot (T_g - T_a) = C_p \cdot (T_g - T_a) \cdot \bar{\rho} \cdot A_f \cdot \sqrt{2 \cdot B \cdot g \cdot H \cdot (T_g - T_a)} \qquad \text{Equation 4.1-17}$$

Rearranging for ΔT yields:

$$\Delta T = \left[\frac{Q}{c_p \, \bar{\rho} \, A_f \sqrt{2 \beta g H}} \right]^{2/3} \qquad \text{Equation 4.1-18}$$

which demonstrates that the temperature rise is inversely proportional to the cube root of *H* and that the predicted temperature rise is a weak function of the stack height.

Site average ambient temperature is about 14 °C, so a value of 22 °C is conservative but not bounding. Repeating the calculations with the base case assumptions (heat load = 24 kW, K = 3, and H = 4.5 m) and an ambient temperature of 50 °C gives an interior gas temperature of 82.8 °C. This should be no surprise. For the base case, temperature difference between the ambient and the dry storage module interior equals 30.9 °C. If the ambient temperature is increased to 50 °C, this temperature difference equals 32.8 °C.

4.1.3 Dry Storage Module Results and Summary

Results show that the thick storage module walls prevent heat removal and that buoyancy-driven natural circulation flow accounts for nearly all of the heat removal at steady state. Assuming ambient conditions of 22 °C and negligible solar flux, the conceptual dry storage module interior gas temperature would be somewhere between 40 °C and 65 °C, depending on the heat load and flow area available for natural circulation.

A value of 50 °C was assumed as the boundary conditions for the preliminary and revised conceptual design "midplane" thermal analyses discussed in Sections 4.2 and 4.3. This value corresponds to the gas exit temperature for a dry storage module with 24 kW of decay heat and an ambient temperature of 22 °C. This value was chosen based on preliminary results, and was determined adequate for the initial midplane scooping analyses. The more detailed integral overpack and dry storage module analyses, both steady state and transient, as discussed in Sections 5.0 and 6.0, assume a boundary condition of 53 °C consistent with the results from Table 4-1.

4.2 ONE-DIMENSIONAL MODEL DESCRIPTION AND DEVELOPMENT

A 1-D thermal model was developed based on a thermal network corresponding to a Type 3 CsCl or SrF_2 capsule within an insert within a sealed overpack. As shown in Figure 4-3, the 1-D thermal model was derived along a line projecting radially outward from the centerline of the salt to the exterior surface of the overpack. The thermal model includes: the CsCl (salt) or SrF_2 (salt), inner capsule, outer capsule, insert, overpack, and three gaps. The thermal model can accommodate a wide range of conceptual designs.

Figures 4-4 and 4-5 present the 1-D thermal networks that were developed. Figure 4-4 represents the preliminary conceptual design configuration with three gaps. Figure 4-5 represents the revised conceptual design configuration with two gaps; the third gap was eliminated by constructing the insert and overpack from a monolithic piece of stainless steel.

The geometry associated with both thermal models transitions from small cylindrical capsules with a radius on the order of a few inches to larger radii on the order of 25.4 cm (10 in.); associated with the steel insert (i.e., "ring" or "gun barrel") and overpack. This transition requires several area adjustments to accommodate the 1/16 portion (symmetry) of a full circle that is associated with only the insert and overpack. These area adjustments are critical in obtaining a realistic and accurate estimate of the temperature distribution. This represents a realistic test for reviewing the corresponding level of detail and thermal results that may be received from prospective dry storage vendors.

The thermo-physical material properties (thermal conductivity, specific heat density, and surface emissivities) for CsCl are documented in WMP-16878 and are presented in Appendix F. The 1-D thermal model will determine the thermal conductivity for a gas mixture containing up to five species (air, argon, helium, nitrogen, and hydrogen) for each of the three gaps.

As presented in Figures 4-4 and 4-5, node point number 1 corresponds to the location of the peak temperature within the CsCl or SrF_2. Node point 1 does not correspond to the centerline of the salt. The peak temperature is located behind the centerline of the salt towards the interior of the system (see Equations 4.2.2-25 and 4.2.2-42). Point 2 corresponds to the temperature associated with the inner surface of the inner capsule. Point 2 also corresponds to the salt-metal interface temperature. Contact resistance between the salt and inner capsule was neglected when a salt-metal gap was not modeled (Section 4.4.6). Point 3 corresponds to the outer surface of the inner capsule. Point 4 corresponds to the inner surface of the outer capsule. Point 5 corresponds to the outer surface of the outer capsule. Point 6 corresponds to the inner diameter or inner surface of the capsule hole within the insert, but does not correspond to the inner diameter of the insert. Point 7 corresponds to the outer surface of the insert. Point 8 corresponds to the inner surface of the overpack. Point 9 corresponds to the outer surface of the overpack. External fins are accommodated through a calculated area enhancement factor (AEF), based on a user-specified fin configuration. (The fin thickness, fin center-to-center spacing, and fin depth, must be user specified.) The gas exit temperature from the dry storage module "Tg" is fixed at 122 °F (50 °C, 323K). This corresponds to an inlet temperature of 22 °C for an average Hanford Site day for a postulated dry storage module containing a heat source of 24 kW (either Cs and/or Sr capsules) and cooled by buoyancy-driven ventilation flow, as discussed in Section 4.1.

The Cs capsule is assumed to have a total recoverable decay heat of 160 W, of which 120 W (75%) is assumed to be deposited within the CsCl (Q_1), 15 W (9.375%) within the first capsule wall (Q_2), 10 W (6.25%) within the second capsule wall (Q_3), 10 W (6.25%) within the surrounding insert/structure (Q_4), and 5 W (3.125%) within the overpack wall (Q_5). The assumed fractional amount of the total decay heat deposited within the CsCl is higher than previous studies (Sasmor et al. 1988) have indicated. The SrF_2 capsules are assumed to have 100% of the recoverable decay power deposited within the salt. However, none of the previous studies has had as many capsules in close proximity. It is expected that decay energy (gamma) from the adjacent capsules will increase the fraction of total energy deposited within the CsCl salt. A brief study, as documented within Appendix B, indicates that a very small fraction of additional energy (approximately 0.4 W) is deposited within a capsule due to radiation from the adjacent (side-to-side) capsules.

Additional analyses will be required to confirm the distribution of absorbed energy within the remaining structure. It is expected that the salt-metal interface temperature will be somewhat sensitive to the fraction of energy deposited within the CsCl.

Although the equations presented later in this section assume radial heat transfer, heat will transfer simultaneously in the radial and axial direction if the temperature gradient in the axial direction is sufficiently large and/or if the thermal resistance in the axial direction is sufficiently small compared to the thermal resistance in the radial direction. A qualitative measure of the extent of axial heat transfer, the relaxation length, can be determined by the Equation 4.2-1:

$$Z_r = \sqrt{\frac{k \cdot A_z}{2\pi \cdot r_o \cdot (h_{C9} + h_{R9})}} \qquad \text{Equation 4.2-1}$$

where:

k	=	thermal conductivity of the material,
A_z	=	cross-sectional area in the z-direction,
r_o	=	radius (RR9) of the overpack outer surface,
h_{C9}	=	heat transfer coefficient due to convection from the outermost surface, and
h_{R9}	=	radiative heat transfer coefficient from the outermost surface.

(The terms h_{C9} and h_{R9} are discussed later in this section.) Physically, the relaxation length represents the distance in the axial direction where one-half of the heat will be transferred in the axial direction and one-half in the radial direction. A value of Z_r, equal to or greater than the outer radius (r_o) of the system, infers that axial heat transport is occurring simultaneously with radial heat transport. The value of Z_r is determined for salt, first capsule, second capsule, insert, and overpack. The calculated values of Z_r are presented and discussed near the end of Section 4.2.3.2.

4.2.1 Overpack Fins

Fins increase the effective area for heat transfer. Adding fins to the exterior of the overpack will reduce the overall temperature rise necessary to reject capsule power.

A fin calculation is presented for a monolithic insert and overpack. Longitudinal fins of a rectangular profile were assumed by machining grooves axially in the external surface of the overpack. The overall outer diameter of the overpack is assumed to remain at 55.9 cm (22 in.). The following fin dimensions were assumed (user specified).

- fin thickness of 0.64 cm (0.25 in)
- center-to-center spacing of 1.91 cm (0.75 in.) (to ensure free airflow in the gap)
- fin depth of 1.27 cm (0.5 in.)

This corresponds to machining grooves 1.27 cm (0.5 in.) deep along the exterior of the overpack. This would leave 0.64 cm (0.25 in.) of steel between the capsule bore and the closest approach to the outer surface of the overpack; see Figures 3-10 and 3-11.

The following discussion conservatively assumes that the tip of each fin is insulated (adiabatic boundary condition). This simplified the mathematical relationships and allowed for a timely estimate of the impact of fins. Other boundary conditions are possible, but depend on the condition assumed for the fin tip. Furthermore, because of self-shielding, the increased fin area is not considered for radiation heat transfer (see Equation 4.2.2-28). A 50% reduction in the surface emissivity of the fins is considered as a parametric analysis (see Section 4.4.7).

The textbook expression for total heat transfer through a finned surface is:

$$q_f = \eta h A_f \Delta T \qquad \text{Equation 4.2.1-1}$$

where:

q_f = heat flux through fin, W/m^2,
h = external convective heat transfer coefficient, W/m^2-K,
η = fin efficiency,

$$= \frac{1}{BL}\tanh(BL) \qquad \text{Equation 4.2.1-2}$$

$$B = \sqrt{\frac{h P}{k S}} \qquad \text{Equation 4.2.1-3}$$

A_f = fin area, m^2,

ΔT = temperature drop, fin base to ambient, K,

L = fin depth, m,

t = fin thickness, m,

P = fin perimeter, m,

$$= 2H \text{ (for long fins)} \qquad \text{Equation 4.2.1-4}$$

S = fin cross-sectional area, m^2,

$$= \tfrac{1}{2} P t = H t \qquad \text{Equation 4.2.1-5}$$

$$BL = \sqrt{\frac{2 h L^2}{k t}} \qquad \text{Equation 4.2.1-6, and}$$

k = fin thermal conductivity, W/m-K.

Note this is a conservative expression for an adiabatic fin tip, and it may be refined to yield extra gain in heat removal efficiency.

Total heat removal is the sum of heat transfer through the finned and unfinned areas:

$$q_t = q_f + q_n = h \Delta T (\eta A_f + A_n) \qquad \text{Equation 4.2.1-7}$$

where:

q_t = total heat transfer, W/m^2,

q_n = heat transfer from unfinned area, W/m^2,

A_f = fin heat transfer area, m^2,

$= N L P = 2 N L H$ Equation 4.2.1-8

A_n = non-fin heat transfer area, m^2

$= N (x - t) H$ Equation 4.2.1-9

N = number of fins,

$= 2 \pi (R - L) / x$ Equation 4.2.1-10

H = fin length (axial), m,

R = original outer radius, and

x = center-to-center spacing between fins, m.

Heat removal without the fins is simply:

$$q_o = h A_o \Delta t \qquad \text{Equation 4.2.1-11}$$

where:

$A_o = 2 \pi R H$ Equation 4.2.1-12

The heat transfer coefficient is assumed unchanged by geometry. This is a good approximation, since the same amount of energy is expected to be removed, and the fins are separated by a distance equal to their depth. This allows the finned and unimproved (non-finned) temperature drops to be expressed as a simple ratio of finned and cylindrical geometries:

$$AEF = \frac{\Delta T_{fin}}{\Delta T_{non}} = \frac{A_o}{\eta A_f + A_n} = \left[\left(\frac{2 \eta L}{x} + \frac{x - t}{x}\right)\left(\frac{R - L}{R}\right)\right]^{-1} \qquad \text{Equation 4.2.1-13}$$

where:

AEF = area enhancement factor
ΔT_{fin} = temperature drop with fin, k, and
ΔT_{non} = temperature drop without fin, k.

For the assumed fin dimensions as discussed above, the fin efficiency was determined to be very high, greater than 95% in this case, and the overall AEF or temperature ratio is about 0.53. Therefore, the exterior temperature drop is about cut in half. The effect of fins has been incorporated into the thermal model by increasing the area associated with convection losses by the factor 1/AEF, as shown in Equation 4.2.2-28. The enhanced heat transfer area associated with the fin was not applied to the thermal radiation term, because of the self-shielding effect.

4.2.2 Thermal Model

At steady-state conditions, the following energy balance holds for an object cooled by a combination (parallel) of convection and thermal radiation from an external surface:

$$Q_{TOTAL} = \frac{\Delta T}{\sum_{i=1}^{n} R_i} = \frac{\Delta T}{\frac{1}{(h_C + h_R)\cdot A}} \qquad \text{Equation 4.2.2-1}$$

$$Q_{TOTAL} = (h_C + h_R)^* A^* \Delta T \qquad \text{Equation 4.2.2-2}$$

where:

Q_{TOTAL}	=	total heat transferred (J/s),
R_i	=	individual thermal resistances (J/[s-K]),
h_C	=	convective heat transfer coefficient (J/(s-m^2-K)) and is defined below,
h_R	=	radiative heat transfer coefficient (J/[s-m^2-K]) and is defined below,
A	=	area (m^2) associated with the exterior surface, and
ΔT	=	temperature difference (K) between external surface and the ambient temperature.

Recasting terms $(h_C + h_R)^*A$ from Equations 4.2.2-1 and 4.2.2-2 in the form of an overall heat transfer coefficient for both convection and radiation yields:

$$UA = \frac{1}{\frac{1}{h_C \cdot A + h_R \cdot A}} = (h_C + h_R)^* A \qquad \text{Equation 4.2.2-3}$$

where UA has units of J/(s-K), and A, h_C, and h_R are as previously defined.

The total energy rejected can now be written as:

$$Q_{TOTAL} = UA^* \Delta T \qquad \text{Equation 4.2.2-4}$$

The overall heat transfer coefficient (parallel) for both conduction and radiation between two cylindrical internal facing surfaces can be written, in a general form, as:

$$UA_{PARALLEL} = \frac{1}{\frac{1}{\frac{2\pi kL}{\ln(r_o / r_i)} + h_r A_i}} = \frac{2\cdot\pi\cdot k\cdot L}{\ln\left(r_o/r_i\right)} + h_r \cdot A_i \qquad \text{Equation 4.2.2-5}$$

where the subscripts "i" and "o" refer to values evaluated at the inner and outer radii, respectively, and h_r is assumed to be based on two concentric cylinders:

$$h_r = \frac{\sigma_{SB} \cdot (T_i^2 + T_o^2)(T_i + T_o)}{\left(\frac{1}{\varepsilon_i} + \left(\frac{A_i}{A_o}\right)\left(\frac{1}{\varepsilon_o} - 1\right)\right)}$$ Equation 4.2.2-6

The overall heat transfer coefficient (series) for conduction through a single cylindrical wall can be written, in a general form, as:

$$UA_{SERIES} = \frac{1}{\frac{1}{\frac{2\pi kL}{\ln(r_o / r_i)}}} = \frac{2 \cdot \pi \cdot k \cdot L}{\ln\left(r_o / r_i\right)}$$ Equation 4.2.2-7a

Equation 4.2.2-7a can be extended for conduction through a series of "n" composite concentric cylinders; the overall heat transfer coefficient (series) can be written, in general form, as:

$$UA_{SERIES,N} = \frac{2 \cdot \pi \cdot L}{\frac{\ln\left(r_2 / r_1\right)}{k_1} + \frac{\ln\left(r_3 / r_2\right)}{k_2} + \cdots + \frac{\ln\left(r_n / r_{n-1}\right)}{k_3}}$$ Equation 4.2.2-7b

where r_1 is the minimum radius and r_n is the maximum radius. The overall heat transfer coefficient for a composite cylinder does not reduce easily to a simple algebraic form.

Finally, in term of an overall heat transfer coefficient, the energy (Q_{TOTAL}) removed from the outer surface of an overpack within a dry storage module considering both convection and radiation yields:

$$U9G = \frac{1}{\frac{1}{h_{C9} \cdot AA9 + h_{R9} \cdot AA9}} = (h_{C9} \cdot AA9 + h_{R9} \cdot AA9)$$ Equation 4.2.2-8

$$Q_{TOTAL} = U9A * \Delta T9g$$ Equation 4.2.2-9

where:

- h_{C9} = convective heat transfer coefficient (J/[s-m^2-K]) from the outer surface of the overpack and is defined below,
- h_{R9} = radiative heat transfer coefficient (J/[s-m^2-K]) from the outer surface of the overpack and is defined below,
- $AA9$ = area (m^2) associated with the exterior surface, and
- $\Delta T9g$ = temperature difference (K) between external surface (Node 9) and the dry storage module gas exit temperature (Tg).

The convective heat transfer coefficient was obtained from the following correlation (Churchill and Chu 1975) for vertical cylinders in an infinite medium for Rayleigh numbers between $10^{-1} < Ra < 10^{12}$. It is recognized that the conditions within the conceptual dry storage module do not reflect an infinite medium. However, since the final design is not known, Equation 4.2.2-10 is applicable, since the assumed scale associated with the dry storage module is large enough that well-defined boundary layers will exist.

$$h_{C9} = \frac{k_{AIR}}{L} \cdot \left[0.825 + \frac{0.387 \cdot Ra^{1/6}}{\left(1 + \left(\frac{0.492}{Pr}\right)^{9/16}\right)^{8/27}} \right]^2 \qquad \text{Equation 4.2.2-10}$$

where:

$$Ra = \frac{\rho^2 \cdot g \cdot \beta \cdot \Delta T \cdot L^3}{\mu^2} \qquad \text{Equation 4.2.2-11}$$

and

$$Pr = \frac{C_P \cdot \mu}{k} \qquad \text{Equation 4.2.2-12}$$

where *Ra* and *Pr* are evaluated using the thermo-physical properties of air at the film temperature, which is defined as:

$$Tfilm = (T_{wall} + T_g)/2. \qquad \text{Equation 4.2.2-13}$$

The characteristic length (L) is assumed to be the heated length of the CsCl or 0.4318 m (17 in.).

The radiative heat transfer coefficient from the outermost surface of the overpack can be written as:

$$h_{R9} = \frac{\sigma_{SB} \cdot (T9^2 + Tg^2)(T9 + Tg)}{\left(\frac{1}{\varepsilon_{316L\_OX}} + \frac{1}{\varepsilon_{AIR}} - 1\right)} \qquad \text{Equation 4.2.2-14}$$

where σ_{SB} is the Stefan-Boltzmann constant (5.6697×10^{-8} J/(s-m^2-K^4)), and ε_{316L_OX} and ε_{AIR} are the assumed emissivities for oxidized 316L SS (0.7) and air (0.6), and *T9* and *Tg* are the overpack outer surface and dry storage module gas exit temperatures (K).

The gap sizes (0.165 cm [0.065 in.], 0.277 cm [0.109 in.], and 0.318 cm [0.125 in.]) are assumed sufficiently narrow to prevent the formation of convective cells. Heat transfer across each gap is assumed to occur by a parallel combination of conduction and radiation.

The overall heat transfer coefficients and the corresponding energy balances can be written for each node within the thermal network (Figure 4-4 and 4-5), as shown within Equations 4.2.2-15 through 4.2.2-24:

Node 9	$U9G \cdot (T9-Tg) = Q_{TOTAL}$	Equation 4.2.2-15
Node 8	$U89 \cdot (T8-T9) + Q_5 = U9G \cdot (T9-Tg)$	Equation 4.2.2-16
Node 7	$U78 \cdot (T7-T8) = U89 \cdot (T8-T9)$	Equation 4.2.2-17
Node 6	$U67 \cdot (T6-T7) + Q_4 = U78 \cdot (T7-T8)$	Equation 4.2.2-18
Node 5	$U56 \cdot (T5-T6) = U67 \cdot (T6-T7)$	Equation 4.2.2-19
Node 4	$U45 \cdot (T4-T5) + Q_3 = U56 \cdot (T6-T6)$	Equation 4.2.2-20
Node 3	$U34 \cdot (T3-T4) = U45 \cdot (T4-T5)$	Equation 4.2.2-21
Node 2	$U23 \cdot (T2-T3) + Q_2 = U34 \cdot (T3-T4)$	Equation 4.2.2-22
Node 1	$Q_1 = U23 \cdot (T2-T3)$	Equation 4.2.2-23

and, $Q_{TOTAL} = Q_1 + Q_2 + Q_3 + Q_4 + Q_5$ Equation 4.2.2-24

The Cs capsule is assumed to have a total recoverable decay heat of 160 W (Q_{TOTAL}), which is based on the power associated with an average CsCl capsule. The decay power is distributed within the salt and surrounding structure as follows:

1) 120 W (75%) is assumed deposited within the CsCl (Q_1),
2) 15 W (9.375%) within the first capsule wall (Q_2)
3) 10 W (6.25%) within the second capsule wall (Q_3)
4) 10 W (6.25%) within the surrounding insert/structure (Q_4)
5) 5 W (3.125%) within the overpack wall (Q_5).

The above fractional amount of the total decay heat deposited within the CsCl is higher than previous studies (Sasmor et al. 1988) have indicated. However, none of the previous studies has had as many capsules in close proximity. It is expected that decay energy (gamma) from the adjacent capsules will increase the fraction of total energy deposited within the CsCl salt. A brief study, as documented within Appendix B, indicates that a very small fraction of additional energy (approximately 0.4 W) is deposited within a capsule due to radiation from the adjacent (side-to-side) capsules.

Parametric analyses (Section 4.4) were performed investigating a reduction from 75% to 50% deposited within the salt, 15% within the inner capsule wall, and the balance of the decay power distribution on a volumetric basis throughout the remaining structure. It is expected that the salt-metal interface temperature will be somewhat sensitive to the fraction of energy deposited within the CsCl.

The temperature of Node 1 can be determined using the classical solution for heat conduction out of a solid rod with uniform internal heat generation:

$$T1 = T2 + \frac{VolQ_1 \cdot (R2 + \frac{R2}{25})^2}{4 \cdot k_{CsCl}} \qquad \text{Equation 4.2.2-25}$$

where $VolQ_1$ is the volumetric decay heat generation rate (W/m^3) deposited within the CsCl salt, $R2$ is the salt radius (m), and k_{CsCl} is the thermal conductivity (J/(s-m-K) of CsCl evaluated at the average temperature of $(T1 + T2)/2$. $VolQ_1$ was derived assuming a salt length of 0.4318 m (17 in.).

Due to the application of an adiabatic boundary condition to the innermost surface of the insert, the location of the peak CsCl temperatures moves toward the interior half of the capsule. This increases the expected peak salt-metal interface temperature. The radius of the salt ($R2$) has been increased by 4% to approximate the increased conduction path. The 4% adjustment has no quantitative basis, just an experience-based observation that the 1-D model will not "see" the shift in location for the peak centerline temperature. The centerline salt temperatures are calculated, but it should be noted that the controlling performance specification is the salt-metal interface temperature.

Equations 4.2.2-15 through -24 contain nine unknowns (T9, T8, T7, T6, T5, T4, T5, T3, and T2). These equations were scripted into a MathCAD file. The nodal temperatures were determined using the FIND function. An initial guess for the temperatures at each node point was specified. Equations 4.2.2-15 through 4.2.2-24 are solved using successive substitution, subject to the constraint that the temperature of each inner point must be greater than the temperature of the preceding outer point. The MathCAD script, as written, will use a set of initial temperatures to provide estimates for the above terms and will use component temperatures calculated during the process to determine the external convective heat transfer coefficient and the thermal conductivity for the gap gas mixtures and solids. A final pass is made using the calculated temperatures, to check the energy balance across the system. A convergence tolerance of 1.0 E-8 is used. If the overall energy balance (i.e., energy gains–energy losses) is greater than the tolerance value, Equations 4.2.2-15 through 4.2.2-24 are solved repeatedly until the convergence tolerance is met.

The thermal model will determine the thermal conductivity, as a function of temperature, for a user-specified gas mixture containing up to five species (air, argon, helium, nitrogen, and hydrogen) for each of the three gaps. A user-specified mole fraction for each gas must be entered for each gap. The sum of the individual mole fractions for each species for a given gap must equal 1. The thermal conductivity of a gas mixture (k_{mix}) is calculated by Equation 4.2.2-26 (*Transport Phenomena*, [Bird et al. 1960]):

$$k_{mix} = \sum_{i=1}^{n} \left(\frac{\chi_i k_i}{\sum_{j=1}^{n} \chi_j \Phi_{ij}} \right)$$ Equation 4.2.2-26

where:

$$\Phi_{ij} = \frac{1}{\sqrt{8}} \left(1 + \frac{M_i}{M_j} \right)^{-\frac{1}{2}} \cdot \left(1 + \left(\frac{\mu_i}{\mu_j} \right)^{\frac{1}{2}} \cdot \left(\frac{M_j}{M_i} \right)^{\frac{1}{4}} \right)^2$$ Equation 4.2.2-27

n	=	number of species,
k_i	=	thermal conductivity (J/s-m^2-K) for gas species i,
χ_i	=	user-specified mole fraction for species i,
M_i	=	molecular weight for species i,
M_j	=	molecular weight for species j,
μ_i	=	viscosity (kg/m-s) for species i, and
μ_j		viscosity (kg/m-s) for species j.

The following overall heat transfer coefficients are calculated progressing radially inward from the outer surface of the overpack to the salt centerline; see Figures 4-4 and 4-5.

OUTER SURFACE: $U9G = \dfrac{1}{\dfrac{1}{\dfrac{h_{C9} \cdot AA9}{AEF} + h_{R9} \cdot AA9}} \dfrac{J}{s-K}$ Equation 4.2.2-28

where: $h_{R9A} = \dfrac{\sigma_{SB} \cdot (T9^2 + Tg^2)(T9 + Tg)}{\left(\dfrac{1}{\varepsilon_{316L\_OX}} + \dfrac{1}{\varepsilon_{AIR}} - 1 \right)} \dfrac{J}{s-m^2-K}$ Equation 4.2.2-29

and *AEF* is the area enhancement factor resulting from the addition of fins to the external surface of the overpack (see Section 4.2.1) (*AEF* = 1.0, if fins are not modeled), σ_{SB} is the Stefan-Boltzmann constant (5.6697 x 10^{-8} J/(s-m^2-K^4)), ε_{316L_OX} and ε_{AIR} are the assumed emissivities for oxidized 316L SS (0.7) and air (0.6), and *T9* and *Tg* are the overpack outer surface and dry storage module gas exit temperatures (*K*). On the other hand, because of the self-shielding effect, the increased exposed area is not considered for radiation heat transfer. *AA9* and h_{C9} are as previously defined.

OVERPACK:

$$U89 = \frac{1}{\frac{1}{\frac{2\pi \cdot k89 \cdot L}{\ln\left(\frac{RR9}{RR8}\right) \cdot N}}} \quad \frac{J}{s-K} \qquad \text{Equation 4.2.2-30}$$

where *k89* is the thermal conductivity of 316L SS overpack evaluated at the average temperature of the overpack ((*T8* + *T9*)/2), *L* is the heated length (0.4318 m), *N* is the number of capsules per overpack, and *RR9*and *RR8* correspond to the outer and inner radii of the overpack, respectively.

OUTER GAP:

$$U78 = \frac{1}{\frac{1}{\frac{2\pi \cdot k_{OUTER} \cdot L}{\ln\left(\frac{RR8}{RR7}\right) \cdot N} + h_{R78} \cdot AA7}} \quad \frac{J}{s-K} \qquad \text{Equation 4.2.2-31}$$

where, k_{OUTER} is the thermal conductivity of the gas mixture within the third gap, as evaluated by Equations 4.2.2-26 and 4.2.2-27 at the average temperature of ((*T8*+*T7*)/2), *RR8* and *RR7* correspond to the inner radius of the overpack and the outer radius of the insert, respectively, and *AA7* corresponds to 1/16 of the outer surface area (m^2) of the insert.

and:

$$h_{R78} = \frac{\sigma_{SB} \cdot (T7^2 + T8^2)(T7 + T8)}{\left(\frac{1}{\varepsilon_{316L\_OX}} + \left(\frac{AA7}{AA8}\right)\left(\frac{1}{\varepsilon_{AIR}} - 1\right)\right)} \quad \frac{J}{s-m^2-K} \qquad \text{Equation 4.2.2-32}$$

where *AA8* correspond to 1/16 of the inner surface area (m^2) of the overpack.

If the outer gap is eliminated, as shown in Figure 4-5, by constructing a monolithic insert and overpack, the following overall heat transfer coefficient (conduction only) is assumed:

$$U78 = \frac{1}{\frac{1}{\frac{2\pi \cdot k78 \cdot L}{\ln\left(\frac{RR8}{RR7}\right) \cdot N}}} = \frac{J}{s-K} \qquad \text{Equation 4.2.2-33}$$

where *k78* is the thermal conductivity of the stainless steel, evaluated at the average temperature of ((*T8*+*T7*)/2), and *RR8* and *RR7* correspond to the inner radius of the overpack and the outer radius of the insert, respectively.

INSERT:

$$U67 = \frac{1}{\frac{1}{\frac{2\pi \cdot k67 \cdot L}{\ln\left(\frac{R7}{R6}\right)}}} \quad \frac{J}{s-K}$$ Equation 4.2.2-34

where *k67* is the thermal conductivity of 316L SS for the insert evaluated at the average temperature ((*T7* + *T6*)/2) of the insert, and *R7* and *R6* correspond to the equivalent outer radius and the actual inner radius of the insert capsule hole, respectively.

MIDDLE GAP:

$$U56 = \frac{1}{\frac{1}{\frac{2\pi \cdot k_{MIDDLE} \cdot L}{\ln\left(\frac{R6}{R5}\right) \cdot AR} + h_{R56} \cdot A5}} \quad \frac{J}{s-K}$$ Equation 4.2.2-35

where k_{MIDDLE} is the thermal conductivity of the gas mixture within the second (middle) gap, as evaluated by Equations 4.2.2-26 and 4.2.2-27 at the average temperature of ((*T6*+*T5*)/2), *R6* and *R5* correspond to the inner radius and the outer radius of the second gap, respectively, and *A5* corresponds to the outer surface area (m^2) of the second capsule.

The term *AR* increases the resistance term for conduction and is based on a ratio of the actual area (*A6*) associated with the inner radius of the insert capsule hole and the effective reduced area (*RA6*) through the narrow portion (i.e., pinch point) of the insert. Figure 4-6 presents the geometrical relationship between *A6* and the term *RA6*. The actual area (*A6*) is shown as a solid line and the reduced area (*RA6*) as a dotted line. The ratio *AR* is automatically updated based on the number of capsules and is not allowed to decrease less than 1.0 or increase beyond 2.0. An *AR* of 1.0 corresponds to a condition with uniform heat transfer from *A6*. This is the case when the number of capsules within an insert decreases ($N < 8$) such that the resulting thickness of the pinch point increases and does not add additional resistance to heat transfer. An *AR* of 2.0 corresponds to a pinch point thickness of 0.0 ($N > 16$) and complete isolation of the rear half of the capsule and insert.

$$AR = \frac{A6}{RA6} \text{ for } N = 16 \quad AR = 1.78$$ Equation 4.2.2-36

and:

$$h_{R56} = \frac{\sigma_{SB} \cdot (T5^2 + T6^2)(T5 + T6)}{\left(\frac{1}{\varepsilon_{316L\_ASRECEIVED}} + \left(\frac{A5}{A6}\right)\left(\frac{1}{\varepsilon_{316L\_OX}} - 1\right)\right)} \quad \frac{J}{s-m^2-K}$$ Equation 4.2.2-37

where *A6* corresponds to inner surface area (m^2) of the insert, $\varepsilon_{316L\_ASRECEIVED}$ and ε_{316L_OX} are the emissivities assumed for "as-received" (0.3) and oxidized (0.7) 316L SS, respectively.

OUTER CAPSULE: $$U45 = \frac{1}{\frac{1}{\frac{2\pi \cdot k45 \cdot L}{\ln\left(\frac{R5}{R4}\right)}}} \quad \frac{J}{s \cdot K}$$ Equation 4.2.2-38

where *k45* is the thermal conductivity of 316L SS for the second capsule evaluated at the average temperature ((*T5* + *T4*)/2) and *R5* and *R4* correspond to the outer and the inner radii of the second capsule, respectively.

INNER GAP: $$U34 = \frac{1}{\frac{1}{\frac{2\pi \cdot k_{INNER} \cdot L}{\ln\left(\frac{R4}{R3}\right)} + h_{R34} \cdot A3}} \quad \frac{J}{s \cdot K}$$ Equation 4.2.2-39

where k_{INNER} is the thermal conductivity of the gas mixture within the first gap, as evaluated by Equations 4.2.2-26 and 4.2.2-27 at the average temperature of ((*T4*+*T3*)/2), *R4* and *R3* correspond to the inner radius of the second capsule and the outer radius of the first capsule, respectively, and *A3* corresponds to outer surface area (m^2) of the first capsule.

and: $$h_{R34} = \frac{\sigma_{SB} \cdot (T3^2 + T4^2)(T3 + T4)}{\left(\frac{1}{\varepsilon_{316L\_ELECTRO}} + \left(\frac{A3}{A4}\right)\left(\frac{1}{\varepsilon_{316L\_ASRECEIVED}} - 1\right)\right)} \quad \frac{J}{s \cdot m^2 \cdot K}$$ Equation 4.2.2-40

where *A4* corresponds to the inner surface area (m^2) of the second capsule, $\varepsilon_{316L\_ELECTRO}$ and $\varepsilon_{316L\_ASRECEIVED}$ are the surface emissivities assumed for electro-polished (0.1) and "as-received" (0.3) 316L SS, respectively.

INNER CAPSULE: $$U23 = \frac{1}{\frac{1}{\frac{2\pi \cdot k23 \cdot L}{\ln\left(\frac{R3}{R2}\right)}}} \quad \frac{J}{s \cdot K}$$ Equation 4.2.2-41

where *k23* is the thermal conductivity of 316L SS for the first capsule evaluated at the average temperature ((*T2* + *T3*)/2), and *R3* and *R2* correspond to the outer and the inner radii of the first capsule, respectively.

SALT CENTERLINE: $$T1 = T2 + \frac{VolQ_1 \cdot (R2 + \frac{R2}{25})^2}{4 \cdot k_{CsCl}} = 371.4°C$$ Equation 4.2.2-42

where $VolQ_1$ is the decay heat deposited within the CsCl salt (W/m^3), k_{CsCl} is the thermal conductivity (J/s-m-K) of CsCl evaluated at the average temperature of $((T1 + T2)/2)$, and $(R2 + R2/25)$ is the adjusted radius (m) of the CsCl to approximate the off-center location of the peak salt temperature.

4.2.3 Cesium Chloride Thermal Analysis Results

The results of the thermal analyses for the preliminary conceptual design are presented in Section 4.2.3.1. The results of the thermal analyses for the revised preliminary conceptual design are discussed in Section 4.2.3.2.

The preliminary conceptual design meets the salt-metal interface performance specification of 317 °C (603 °F), but for only 8 capsules per overpack. The revised conceptual design meets the specified salt-metal interface temperature of 317 °C (603 °F) for 16 capsules per overpack.

4.2.3.1 Preliminary Conceptual Design.

The results of the1-D thermal analyses for the preliminary conceptual design are presented in Tables 4-2 through 4-4. Tables 4-2 and 4-3 present the temperature distributions for each of nine nodes for 8, 12, and 16 capsules per overpack for a given gas mixture within each of the three gaps. The temperature difference across each gap is also presented. Table 4-4 summarizes the peak centerline and salt-metal interface temperatures obtained from Tables 4-2 and 4-3. The performance specification for the salt-metal interface temperature is shown.

The analyses were performed for an assumed capsule power of 160 W, variable number (N = 8, 12, and 16) capsules per overpack, and combinations of backfill gases, including air, helium, and a nitrogen-argon-hydrogen mixture (*Characterization of an Aged WESF Capsule* [Kenna and Schultz 1983]) within the inner gap. The analyses were performed for the preliminary configuration assuming all three gaps were present with no external fins. These results can be compared to the HADCRT results presented in Section 4.3.1.

Table 4-2 represents a case where the gas mixture associated with the innermost gap is based on a set of measured data obtained from a destructive analysis of Cs capsule C-117 (Kenna and Schultz 1983) and dry air is assumed for the remaining two gaps (i.e., middle and outer). A peak salt temperature (t_1) of approximately 521 °C (970 °F) is obtained for an overpack containing 16 capsules. The corresponding salt-metal interface temperature (t_2) is approximately 443 °C (829 °F). The peak salt temperatures decrease to approximately 467 °C (873 °F) and 400 °C (752 °F), respectively, for 12 and 8 capsules per overpack. The corresponding salt-metal interface temperatures decrease to 397 °C (747 °F) and 341 °C (645 °F), respectively, for 12 and 8 capsules per overpack.

Table 4-3 presents the same conditions as Table 4-2, but with helium in the middle and outermost gap. A peak salt temperature (t_1) of approximately 432 °C (810 °F) is obtained for an overpack containing 16 capsules. The corresponding salt-metal interface temperature (t_2) is 367 °C (693 °F). The peak salt temperatures decrease to approximately 384 °C (722 °F) and 326 °C (619 °F), respectively, for 12 and 8 capsules per overpack. The corresponding salt-metal interface temperatures decrease to approximately 327 °C (620 °F) and 278 °C (533 °F), respectively, for 12 and 8 capsules per overpack. The salt-metal interface temperature

performance specification of 317 °C is met only for the preliminary conceptual design with 8 average power Cs capsules per overpack with helium as the backfill gas. (A revised preliminary conceptual design was developed and analyzed and is discussed in Section 4.1.3.)

From Tables 4-2 through 4-4, large temperature drops occur across the gaps. The temperature drop across each gap is dependent on the size of the gap, location of the gap, and backfill gas/mixture within each gap. By engineering smaller gaps or eliminating the outermost gap by constructing the insert/shield plug and overpack out of a continuous piece of steel, it is anticipated that the salt-metal interface temperature performance specification can be met with a helium backfill and 16 capsules per overpack.

4.2.3.2 Revised Conceptual Design Configuration.

The revised conceptual design configuration, as discussed in Section 4.1.3, contains two gaps. The third or outermost gap was eliminated by constructing the insert and overpack from a monolithic piece of stainless steel. Fins were also added to the external surface of the overpack.

A series of baseline parametric analyses were performed for an assumed capsule power of 160 W, variable number (N = 8, 12, and 16) capsules per overpack, and combinations of backfill gases, including air, helium, and a nitrogen-argon-hydrogen mixture (Kenna and Schultz 1983) within the inner gap. The analyses were performed for the baseline configuration assuming the third gap was eliminated and fins are present on the external surface of the overpack. The extent of axial heat transfer was also investigated.

The results of the analyses are presented in Tables 4-5 through 4-7. Tables 4-5 and 4-6 present the temperature distributions for each of nine nodes for 8, 12, and 16 capsules per overpack for air and helium within the second gap. The temperature difference across each gap is also presented. Table 4-7 summarizes the salt-metal interface and centerline temperatures for the representative baseline conditions in Tables 4-5 and 4-6.

Table 4-5 presents the temperature distribution versus number of capsules for a measured (Kenna and Schultz 1983) gas mixture consisting of 90% nitrogen, 8% argon, and 2% hydrogen within the first or innermost gap and dry air in the remaining middle gap. Table 4-6 presents the temperature distribution versus number of capsules for a measured (Kenna and Schultz 1983) gas mixture consisting of 90% nitrogen, 8% argon, and 2% hydrogen within the first or innermost gap and helium in the remaining middle gap.

Table 4-5 represents a case where the gas mixture associated with the innermost gap is based on a set of measured data obtained from a destructive analysis of Cs capsule C-117 (Kenna and Schultz 1983), and dry air is assumed for the remaining middle gap. A peak salt temperature (t_1) of approximately 430 °C (807 °F) is obtained for an overpack containing 16 capsules. The corresponding salt-metal interface temperature (t_2) is approximately 363 °C (686 °F). The peak salt temperatures decrease to approximately 398 °C (747 °F) and 355 °C (671 °F), respectively, for 12 and 8 capsules per overpack. The corresponding salt-metal interface temperatures decrease to 334 °C (632 °F) and 295 °C (563 °F), respectively, for 12 and 8 capsules per overpack.

Table 4-6 presents the same conditions as Table 4-5, but with helium in the middle gap. A peak salt temperature (t_1) of approximately 371 °C (701 °F) is obtained for an overpack containing 16 capsules. The corresponding salt-metal interface temperature (t_2) is 310 °C (590 °F). The peak salt temperatures decrease to approximately 336 °C (637 °F) and 296 °C (565 °F), respectively, for 12 and 8 capsules per overpack. The corresponding salt-metal interface temperatures decrease to approximately 278 °C (533 °F) and 242 °C (467 °F), respectively, for 12 and 8 capsules per overpack. The salt-metal interface temperature of 310 °C (590 °F) meets the performance specification of 317 °C for the baseline configuration with 16 average power Cs capsules per overpack.

Table 4-7 summarizes the peak centerline and salt-metal interface temperatures obtained from Tables 4-5 and 4-6. The performance specification for the salt-metal interface temperature is shown.

From Tables 4-5 and 4-6, large temperature drops occur across the gaps. The temperature drop across each gap is dependent on the size of the gap, location of the gap, and backfill gas/mixture within each gap. The salt-metal interface temperature performance specification was met by eliminating the outer gap (monolithic insert and overpack) and using a helium backfill and 16 capsules per overpack. Using helium as a cover gas is far more effective than reducing the number of capsules in order to control the salt-metal interface temperature.

The results presented by Table 4-6 are based on an increased surface area associated with the addition of fins and are consistent with the specified fin thickness of 0.64 cm (0.25 in.), fin depth of 1.27 cm (0.5 in.), and a center-to-center spacing of 1.91 cm (0.75 in.) around the perimeter of the overpack. The combination of only two gaps and external fins meets the salt-metal performance specification of 317 °C for 16 capsules per overpack, given helium as the backfill gas for the middle gap, an assumed gas mixture for the inner gap, and assumed surface emissivities as follows:

Inner capsule outer surface:	0.1
Outer capsule inner surface:	0.3
Outer capsule outer surface:	0.3
Insert inner surface:	0.7
Overpack outer surface:	0.7

The emissivities for the surfaces between the inner and outer capsule were conservatively assumed to reflect an electro-polished surface (contamination removal) with a value of 0.1 and an "as-received" unoxidized condition with a value of 0.3. The emissivities associated with the insert and overpack are representative of an oxidized surface. Nevertheless, technical justification and support will be required for any emissivity used in the final design.

Enhancing axial heat transfer within the overpack can reduce the salt-metal interface temperature even further. The following summary presents the calculated relaxation length for the CsCl,

inner capsule, outer capsule, insert, and overpack and can be used as a qualitative measure of the importance of axial heat transfer for each component.

Region	Relaxation Length, Z_r (m)
Cesium Chloride	0.0109
Inner Capsule	0.0430
Outer Capsule	0.0459
Insert	0.4827
Overpack	0.1022

The maximum calculated relaxation length (Z_r = 0.4827m) is for the insert. The Z_r for the insert is greater than the assumed outer radius (r_o = 0.2794m [11.0 in.] []) of the overpack. Consequently, heat transferring out the outer (second) capsule into the insert will attempt to conduct along the axial direction until the temperature gradients in the axial direction decrease. When this occurs, heat will transfer in the radial direction to the outermost surface of the overpack. However, as shown in Figures 3-5 and 3-8, the insert stops just below the massive upper shield plug. The thermal network is "open" at this point. Axial heat transport is very limited beyond this point and radial heat transport will prevail. As shown in Figures 5-1 and 5-2, it is possible to increase the available surface area for heat rejection by modifying the conceptual design presented within this report to allow contact between the insert and shield plug and/or annular flow. This will promote axial heat transport by allowing the combined surface areas of the overpack and shield plug (side and top surfaces) to reject heat. This will reduce the salt-metal interface temperature. Axial heat transport was one of the concepts used by the BUSS for heat rejection when loaded with 16 Cs capsules.

4.2.4 Type W Overpack

A small number of Cs capsules with suspect integrity, as well as materials from capsule destructive examinations and test programs, were sealed inside an additional welded container for additional assurance against leakage. These capsules are referred to as Type W overpacks. Twenty-three Type W overpacks were fabricated and are currently stored in WESF.

The Type W overpack capsules have an additional annulus/gap and capsule wall that impacts thermal analysis and thus the design. The additional gap increases the thermal resistance and requires a rise in temperature to reject the same amount of energy. The additional gap is assumed to only affect the temperatures internal to the Type W overpack.

Tables 4-8 and 4-9 present the results of estimated salt-metal and centerline temperatures for a variable number of Type W capsules within an overpack with fins for two different fill gases (air and helium). The temperatures were determined by doubling the resistance across the middle gap given the reference conditions from Table 4-5 for air and Table 4-6 for helium. The actual temperatures are expected to be slightly different due to the increased surface areas associated with the Type W overpack and amount of energy deposited within the Type W capsule wall.

Table 4-8 summarizes the salt-metal and salt centerline temperatures within an overpack with dry air in the gap between the outer surface of the outer capsule and inner surface of the Type W overpack and between the outer surface of a Type W overpack and inner surface to the insert capsule bore. This represents a system containing all dry air, except the gap between the inner two capsules, which is assumed to contain a gas mixture consistent with Kenna and Schultz (1983). The Type W analyses assumed a 50 °C boundary condition consistent with the previous section and based on the exit conditions from a dry storage module during an average Hanford Site day. The Type W thermal analyses were performed assuming a mean Cs capsule power of 160 W and other attributes consistent with the results from Table 4-5.

Table 4-8 indicates that a Type W overpack with an additional air-filled gap significantly increases the salt-metal and salt centerline temperatures. The Type W overpack adds approximately 60 °C to the reference values for the salt-metal interface temperature. The Type W overpack adds approximately 70 °C to the reference values for the salt centerline temperature. The minimum salt-metal interface temperature is approximately 354 °C for eight capsules per overpack. This does not meet the salt-metal interface performance specification of 317 °C. If air were used as the backfill gas, then less than eight Type W capsules per overpack would be required.

Table 4-9 summarizes the salt-metal and salt centerline temperatures within an overpack with helium in the gap between the outer surface of the outer capsule and inner surface of the Type W overpack and between the outer surface of a Type W overpack and inner surface to the insert capsule bore. This represents a system containing all helium, except the gap between the inner two capsules, which is assumed to contain a gas mixture consistent with Kenna and Schultz (1983). The Type W analyses assumed a 50 °C boundary condition consistent with the previous section and based on the exit conditions from a dry storage module during an average Hanford Site day. The Type W thermal analyses were performed assuming a mean Cs capsule power of 160 W and other attributes consistent with the results from Table 4-6.

Table 4-9 indicates that the additional helium-filled gap increases the salt-metal and salt centerline temperatures by approximately 20 to 30 °C. This is significantly less than the air-filled system discussed in the previous paragraph. The salt-metal interface temperature is approximately 260 °C for 8 Type W capsules per overpack, approximately 301 °C for 12 Type W capsules per overpack, and approximately 335 °C for 16 Type W capsules per overpack. (Because the Type W capsules are larger diameter due to the additional capsule wall, 16 capsules will not fit into an overpack, but the analysis was performed anyway for comparison purposes.) A suggested design solution to accommodate these in the dry storage system is to limit the number of Type W capsules loaded in an overpack to 8 or 12, which will maintain the salt-metal interface temperature less than the performance specification of 317 °C.

4.2.5 Strontium Fluoride Capsules

A series of steady-state thermal analyses were performed for the SrF_2 capsules for various decay heat loads. The analyses were performed using the 1-D radial midplane model, as discussed in Section 4.2. The results are compared to the Sr salt-metal interface performance specification of 540 °C.

The following assumptions are made.

1) The mean and maximum capsule powers are consistent with Table 3-3.
2) Wall thickness and inner gap size are consistent with Table 3-2.
3) The inner capsule wall is manufactured from Hastelloy C-276.
4) The outer capsule wall is manufactured from 316L SS.
5) 100% of the decay energy is deposited within the SrF_2 salt.
6) The thermal conductivity of SrF_2 is reduced by approximately 55% to account for the porous nature of the salt and the buildup of zirconium as ^{90}Sr decays.
7) The gap between the inner two capsules is assumed to contain a gas mixture consistent with measurements performed for capsule C-117 (Kenna and Schultz 1983).
8) Air or helium is the backfill gas.
9) The gas exit temperature from a dry storage module is consistent with a boundary condition of 50 °C.

Table 4-10 presents the results of the thermal analyses for SrF_2 capsules assuming air as the backfill gas for various capsule powers. Sr capsule powers of 160, 218 (mean), 320, 480, and 570 (maximum) W were analyzed. The number of Sr capsules within an overpack is reduced as capsule power increases. This was done in an attempt to maintain the total overpack power less than 2,540 W. (This was not possible in all cases, but the total overpack power is close. In some cases, the total overpack power is based on the maximum number of capsules that can be loaded without exceeding 2,540 W.) The results for 160 W can be compared with the corresponding results for Cs.

Table 4-10 indicates that the salt-metal interface performance specification of 540 °C is exceeded for high-power Sr capsules with air as the backfill gas of choice.

Table 4-11 indicates that the salt-metal interface temperature for the maximum Sr capsule is approximately 502 °C based on a helium backfill. The corresponding centerline temperature is approximately 571 °C. The salt-metal interface performance specification of 540 °C is not exceeded for the highest power (570 W) Sr capsule with helium as the backfill gas of choice. However, if a SrF_2 capsule were operating at the performance specification for salt-metal interface temperature of 540 °C, the centerline temperature could approach 600 °C. This is well below any temperatures at which a phase transition or melting could occur for Sr capsules.

It is very apparent that helium must be used as the backfill gas and that a loading strategy will be required to maintain the total overpack power less than 2,540 W. Potential loading strategies include; mixing high- and low-power capsules, limiting the total number of capsules, and preventing the placement of high-power capsules next to one another.

It was recently "discovered" that some of the Sr capsules were fabricated with both inner and outer walls of Hastelloy C-276 rather than a 316L SS outer capsule over a Hastelloy C-276 inner capsule. Documentation in use by the CDSP did not identify this design for the Sr capsules. This shortfall in the capsule documentation as well as some apparent discrepancies in the capsule database must be corrected. It is recommended that the original capsule fabrication documentation be reviewed to verify the validity of the capsule descriptions and to validate the data in the capsule database that is pertinent to the CDSP.

4.3 MIDPLANE MODEL FOR CS CAPSULES IN OVERPACK CONTAINER

A 2-D model was developed to determine the midplane behavior of 16 capsules arranged in an insert and overpack container and is described in this section. Results are presented for Cs capsules. This model is intended to correspond to the 1-D approach described in Section 4.2. Later, this model is extended in the axial direction by copying this plan view along the length of the capsules and accounting for an overpack container top and bottom.

The HADCRT computer code (see Section 1.2 and Appendix A) is used for this analysis. Dimensions and boundary conditions are consistent with those used in Section 4.2. Details of input file values are not provided here.

The evaluation basis for Section 4.3.1 is the preliminary conceptual design; i.e., three gaps and no fins. The evaluation basis for Section 4.3.2 is the revised preliminary conceptual design; i.e., two gaps and the external fins. The revised design is considered a refinement to the preliminary conceptual design discussed in Sections 4.2.1 and 4.3.1

4.3.1 Midplane Model Nodalization

The nodalization of an axial midplane symmetry section is shown in Figure 4-7. The insert and capsules can be divided into a 1/32 symmetry section, with one line of symmetry dividing the capsule in half, and the other line of symmetry dividing the steel insert midway between a pair of adjacent capsules. These lines of symmetry are adiabatic boundaries insofar as adjacent capsules are of equal power. Heat conductors are numbered as shown in the figure, divided by solid lines, and generally, each heat conductor is subdivided into roughly 10 interior nodes to provide a temperature distribution. Only three (3) nodes are used for capsule wall conductors because they are so thin. Dotted lines signify the existence of interior temperature nodes but not necessarily the actual number.

The capsule is divided azimuthally into 8 pie-shaped (i.e., wedge) slices. The primary direction of heat transfer is radial, but adjacent interior nodes communicate azimuthally. Gap conductances are calculated by the code based on local temperatures, considering conduction and radiation, for the interior capsule gap (i.e., between conductors 3 and 2), the gap between the capsule and the insert (i.e., between conductors 2 and 1), and the gap between the insert and

overpack wall (i.e., between conductors 18 and 17). Nodes between adjacent conductors are coupled for true 2-D conduction; i.e., azimuthally conduction occurs within the salt (conductors 4 to 8, etc.) and within the inner and outer capsule walls (conductors 3 to 7, etc., and 2 to 6, etc., respectively).

4.3.2 Midplane Model Results

Reference case conditions for the preliminary conceptual design calculation are 16 Cs capsules, at 160 W each within an overpack; air in all three gaps; and a dry storage module gas exit temperature of 50 °C (see Section 4.1). Power is distributed among the salt and steel, as discussed in Section 4.2. The resultant steady-state temperature distribution is shown in Figure 4-8. Temperature values are arranged in Figure 4-8 to correspond to the nodalization of Figure 4-7. The left edge is the insert interior surface. The right edge is the overpack external wall. The top edge is continuous insert steel along a symmetry line between capsules. The bottom edge is along a symmetry line cutting through the capsule center. Interior temperatures along the bottom edge are steel insert at gap surface, average capsule outer wall, average capsule inner wall (i.e., salt-metal interface), capsule maximum, average capsule inner wall (toward insert exterior), average capsule outer wall, and average temperature of insert between capsule gap and insert outer periphery. The inner capsule wall temperature is shown by eight values arranged as a semicircle around the maximum value. The outer capsule wall temperature is shown by eight values just outside inner wall values. The "I" insert temperature at the capsule gap is shown by seven values nearest to outer wall values (three to left, three to right, one above).

A peak salt temperature of approximately 519 °C was determined. The peak salt-metal interface temperature is about 451 °C. These results can be compared with the results of the 1-D analyses presented in Section 4.2.1. Table 4-2 indicates a peak centerline salt temperature of approximately 521°C and salt-metal interface temperature of 443 °C. This is remarkable agreement between HADCRT and the 1-D thermal model.

There is noticeable azimuthal temperature variation in the steel insert around the outer surface of the capsule. A high value of about 389 °C is found on the symmetry line toward the insert interior, and a low value of 352 °C is found toward the exterior, for a difference of 37 °C. However, significant azimuthal conduction occurs in the capsule inner and outer walls, so that the peak temperature difference along this symmetry line at the salt-metal interface is 451 - 445.5 = 4.5 °C.

Large temperature drops occur in the gaps as expected. Temperature drop across the inner capsule gap varies from about 37 °C (toward insert interior) to 44 °C (toward insert exterior); temperature drop across the gap between insert and capsule varies from about 15 °C (toward insert interior) to 49 °C (toward insert exterior); temperature drop across the gap from insert to overpack wall is about 97 °C. A film temperature drop of 207 °C is required to reject heat from the overpack wall to the dry storage module condition.

A similar calculation is performed for the case of an overpack backfilled with helium gas. This increases conductance in the two overpack gaps, but air is still the gas used to characterize

conductance internal to the capsule. The corresponding temperature map is given in Figure 4-9. See Figure 4-7 for the corresponding nodalization diagram.

The salt peak temperature is reduced to 429 °C, a reduction of 90 °C compared to the air case, as presented in Figure 4-8. The maximum salt-metal interface temperature is reduced to 375 °C. This represents a drop of about 76 °C compared to the air case. Note that overpack container wall temperature is nearly identical, but the temperature drop across the gap from the insert to this wall is only about 44 °C, somewhat more than half the air case value. Temperature drop across the insert-capsule gap varies from 10 °C to 25 °C, again about half the air value.

These results can be compared with the results of the 1-D analyses presented in Section 4.2.1. Table 4-3 indicates a peak centerline salt temperature of approximately 432 °C and salt-metal interface temperature of 367 °C. This is remarkable agreement between the 2-D HADCRT and 1-D MathCAD thermal models.

4.3.3 Midplane Model Nodalization Refinements

The revised nodalization of an axial midplane symmetry section is shown in Figure 4-10. The revised nodalization pattern corresponds to the revised preliminary conceptual design with two internal gaps and external fins. The insert and capsules can be divided into a 1/32 symmetry section, with one line of symmetry dividing the capsule in half, and the other line of symmetry dividing the steel insert midway between a pair of adjacent capsules. These lines of symmetry are adiabatic boundaries insofar as adjacent capsules are of equal power. Heat conductors are numbered as shown in the figure, divided by solid lines, and generally, each heat conductor is subdivided into roughly 10 interior nodes to provide a temperature distribution. Only three nodes are used for capsule wall conductors because they are so thin. Dotted lines signify the existence of interior temperature nodes but not necessarily the actual number.

The volume and heat transfer area of heat conductors are scaled such that one entire 0.4318 m (17-in.) fueled height of the overpack is represented by the model.

The capsule is divided azimuthally into 8 pie-shaped wedges. The primary direction of heat transfer is radial, but adjacent interior nodes communicate azimuthally. Gap conductance is calculated by the code based on local temperatures, considering conduction and radiation, for the interior capsule gap (i.e., between conductors 3 and 2), and the gap between the capsule and the insert (i.e., between conductors 2 and 1). Conductors are selected to have homogenous composition, and concatenated for simultaneous solution of the temperature distribution. Nodes between adjacent conductors are coupled for true 2-D conduction. For example, azimuthal conduction occurs within the salt (conductors 4 to 8, etc.) and within the inner and outer capsule walls (conductors 3 to 7, etc., and 2 to 6, etc., respectively).

Fins on the overpack wall increase the area available for convective heat transfer. Based on the overall AEF of 0.53 determined in Section 4.2.1, the convective heat transfer rate multiplier of 1.9 (input parameter FHHS in HADCRT) was used in the calculation. On the other hand, because of self-shielding effect, the increased exposed area is not considered for radiation heat transfer.

4.3.4 Midplane Model Results

Reference case conditions for the baseline calculation are 16 Cs capsules, all with 160 W power in an overpack, and an exterior temperature of 50 °C. Power is distributed between the salt and steel as in Section 4.1.2. The steady-state temperature distribution is shown in Figure 4-11. Temperature values are arranged in Figure 4-11 to correspond to the nodalization of Figure 4-10.

Figure 4-11 shows the steady state temperature map (°C) for 160 W capsule, 16 capsules per overpack, and helium in outer gap, 90% nitrogen, 8% argon, 2% hydrogen mixture in the inner gap.

The peak salt temperature is about 371 °C, and peak salt-metal interface temperature is about 316 °C. This is very near the project specification of 317 °C, leaving virtually no margin for error. These results can be compared with the results of the 1-D analyses presented in Section 4.2.2 and Table 4-6. Table 4-6 indicates a peak centerline salt temperature of approximately 371 °C and salt-metal interface temperature of 310 °C. This is remarkable agreement.

There is noticeable azimuthal temperature variation in the steel insert at the inside of the gap with the capsule: A high value of about 256 °C is found on the symmetry line toward the insert interior, and a low value of 218 °C is found toward the exterior, for a difference of 38 °C. However, azimuthal conduction occurs in the capsule inner and outer walls, so that the peak temperature difference along this symmetry line at the salt-metal interface is $316.0 - 310.5 = 5.5$ °C.

Large temperature drops occur in the gaps as expected. Temperature drop across the inner capsule gap varies from about 48 °C (toward insert interior) to 61 °C (toward insert exterior); temperature drop across the gap between insert and capsule varies from about 11 °C (toward insert interior) to 32 °C (toward insert exterior). A temperature drop of about 170 °C is required to remove heat from the overpack wall to the ambient gas.

The fact that the capsule maximum temperature is almost on the centerline demonstrates effective azimuthal conduction in capsule walls, which directly implies that axial variations in the exterior gap widths will not result in significant variation in the salt-metal interface temperature.

4.4 PARAMETRIC ANALYSES

The results of a series of parametric analyses are presented and discussed within this section and Table 4-12. It is not possible to completely investigate all possible sensitivities here, but the following are believed to be important in determining the potential for temperature variation and potential hot spots. In any case, the potential exists to use loading strategy to maintain the total overpack decay power less than 2,540 W and to minimize hot spots within the overpack. This will have to be assessed and technically justified for any final design. However, loading limits/strategies may include, but are not limited to: mixing high- and low-power capsules,

limiting the total number of capsules within an overpack, or simply preventing the placement of high-power capsules adjacent to one another.

The parametric analyses were performed assuming a reference condition associated with the revised preliminary conceptual design for cesium capsules with helium as the backfill gas, as discussed in Section 4.2.3.2 and summarized in Table 4-6.

The results of the analyses indicate that the assumption of 75% deposited power is a conservative assumption and clearly bounds the several secondary effects, including reduced thermal conductivity of CsCl, Type 1 capsules, and a salt-metal gap.

4.4.1 Peak Salt and Salt-Metal Interface Temperatures Versus Capsule Power

Peak salt and salt-metal interface temperatures vs. Cs capsule power were determined. The analyses were performed by varying the capsule power and keeping all other quantities, such as the number of capsules per overpack (N=16), the same. The capsule power was varied between 100 and 300 W. This bounds the maximum expected Cs capsule power of 211 W from Table 3-3.

The results are summarized in Table 4-13 and Figure 4-12. The results indicate a salt-metal interface temperature of approximately 234 °C for a capsule power of 100 W. For a capsule power of 200 W, the salt-metal interface temperature is approximately 354 °C, which exceeds the salt-metal interface criterion of 317 °C. The potential exists to use loading strategy to maintain the total overpack decay power less than 2,540 W and to minimize hot spots within the overpack. This will have to be assessed and technically justified for any final design. However, loading limits/strategies may include, but are not limited to: mixing high- and low-power capsules, limiting the total number of capsules within an overpack, or simply preventing the placement of high-power capsules adjacent to one another.

4.4.2 Revised Power Deposition (Case #2)

The subject thermal analyses assumed 75% of the total decay heat was deposited within the CsCl. This is higher than previous studies have indicated. However, none of the previous studies has had as many capsules in close proximity. It is expected that decay energy (gamma) from the adjacent capsules will increase the fraction of total energy deposited within the CsCl salt.

Nevertheless, a parametric analysis was performed to determine the peak salt and salt-metal interface temperatures assuming a revised power deposition fraction within the salt and inner capsule wall. The analyses were performed using the same reference (case #1) conditions associated with the revised preliminary conceptual design with helium. However, the analyses assumed a power deposition fraction of 50% (120 W) within the salt, 15% (24 W) within the inner capsule wall, the remaining balance of 35% (56 W) distributed uniformly throughout the remaining structure, and keeping all other quantities the same.

The results are summarized in Table 4-12. The results indicate a salt-metal interface temperature of approximately 290 °C and a salt centerline temperature of 329 °C for a total capsule power of

160 W. These values represent a significant drop from the reference values of 310 °C and 371 °C.

Decreasing gamma deposition in salt from a conservative value of 75% to a possibly more realistic estimate of 50% results in about 20 °C reduction in interface and 40 °C reduction in centerline values.

As an indicator of how complete each vendor's basis is for the corresponding thermal analysis, an MCNP analysis could have been performed to determine the fraction of power deposited within the salt and remaining structure.

4.4.3 Reduced Cesium Chloride Conductivity (Case #3)

The thermal conductivity of CsCl is expected to change due to removal of impurities by corrosion of the capsule wall and by the introduction of barium by the radioactive decay of ^{137}Cs. A parametric analysis was performed to determine the peak salt and salt-metal interface temperatures assuming a reduced thermal conductivity for CsCl. The analyses were performed using the same reference conditions as case #2, but applied a 35% reduction in the thermal conductivity of CsCl.

The results are summarized in Table 4-12. The results indicate a salt-metal interface temperature of approximately 290 °C and a salt centerline temperature of 351 °C for a total capsule power of 160 W. The salt-metal interface temperature remains the same as case #2 (Section 3.3.2), since the heat flux across the inner capsule has not changed. However, reducing salt thermal conductivity by 35% to account for barium build-in can increase centerline temperature by about 22 °C.

4.4.4 Maximum Capsule Gap (Case #4)

The revised preliminary conceptual design discussed in Sections 4.1.3 and 4.2.3.2 assumed a configuration based on Type 3 Cs capsules. This configuration results in the largest salt radius and a minimum gap between the inner and outer capsule walls.

A parametric analysis was performed to determine the peak salt and salt-metal interface temperatures assuming a Type 1 configuration, which results in a smaller salt radius and the maximum gap between the inner and outer capsule walls. The analyses were performed using the same reference conditions as case #3, but assuming a Type 1 capsule.

The results are summarized in Table 4-12. The results indicate a salt-metal interface temperature of approximately 300 °C and a salt centerline temperature of 362 °C for a total capsule power of 160 W. The salt-metal interface and salt centerline temperatures have increased from the case #3 values due to the decreased salt radius and increased gap. Variations in capsule type (except Type W) are only worth about 11 °C.

4.4.5 Revised Radial Power Distribution (Case #5)

The reference Cs capsule thermal models assume a uniform heat generation rate across the salt. This may not be appropriate, since decay gamma created near the perimeter of the salt will have a higher probability of escaping the salt than a gamma created near the centerline. The actual power deposition may be a function of radius. This will result in a centerline peaked power distribution that will lead to increased centerline temperatures and lower salt-metal interface temperatures.

Nevertheless, a parametric analysis was performed to determine the peak salt and salt-metal interface temperatures assuming a revised radial power distribution across the salt (Appendix C). The amount of energy deposited within the salt was kept the same as in case #2, but the distribution was shifted toward the centerline. The maximum centerline temperature was determined as previously presented by Equation 4.2.2-42, but the volumetric heat generation rate was increased by the ratio of 7/6 (see Appendix D). All other quantities were kept the same as case #4.

The results are summarized in Table 4-12. The results indicate a salt-metal interface temperature of approximately 300 °C and a salt centerline temperature of 373 °C for a total capsule power of 160 W. Rendering gamma deposition non-uniform in salt increases centerline temperature by about 9 °C. However, the salt centerline temperature has increased by 9 °C. This is not a significant increase, but it represents an uncertainty that can best be resolved by performing an MCNP analysis to determine both the fraction of power deposited within and radial power distribution across the salt.

4.4.6 Salt-Metal Interface Gap

A salt-metal interface gap ranging from 5 to 7 mils has been observed during gamma scans of some Cs capsules. A parametric analysis was performed assuming a 10-mil salt-metal interface gap. The gap was assumed backfilled with a gas mixture obtained from a destructive analysis of Cs capsule C-117 (Kenna and Schultz 1983). The salt-metal gap is assumed to consist (% mole fraction) of 34% argon, 46% helium, and 20% nitrogen. The conditions are the same as case #6, except a 10-mil salt-metal interface gap was added.

The results are summarized in Table 4-12. The results indicate a salt-metal interface temperature of approximately 300 °C and a salt centerline temperature of 376 °C for a total capsule power of 160 W. The salt-metal interface temperature has not changed, since the heat flux across the inner capsule wall has not changed. However, allowing a gap between salt and cladding inner surface increases centerline temperature by about 5 °C. This is a trivial change and is easily bounded by a conservative assumption for the fraction of power deposited within the salt.

4.4.7 Reduced Emissivity of Fins

The emissivity of the fins was reduced approximately 50% (from 0.7 to 0.359) to approximate self-shadowing between the adjacent fins (see Appendix E).

The results are summarized in Table 4-12. The results indicate a salt-metal interface temperature of approximately 319 °C and a salt centerline temperature of approximately 398 °C. This represents an increase of 25 to 30 °C. Self-shadowing of fins has a significant affect on the salt-metal interface and centerline temperatures, especially for natural circulation systems where radiative heat transfer provides a large fraction of energy rejected from the system. The correct view factor or effective emissivity must be determined for a given fin design. Underprediction of the salt-metal and salt centerline temperatures can result, if the appropriate fin view factor is not applied.

4.4.8 External Overpack Surface Temperatures Versus Time

The temperature distribution within a capsule overpack within a dry storage module was determined vs. time for long-term storage conditions. Time was varied from 0 to 100 years. The overpack and dry storage decay powers were reduced consistent with Equation 4.1-1. The exit gas temperature (boundary condition for the overpack) within the dry storage module was reduced to inlet conditions as the decay power decreased with increasing time. The 1-D thermal model was used to obtain "snapshots" of the temperature distribution at 5- to 25-year intervals.

The results are presented in Table 4-14. The results at time zero correspond to the reference condition associated with the revised preliminary conceptual design discussed in Sections 4.1.3 and 4.2.3.2. After 50 years, the average capsule power has decreased to approximately 51 W. The exit temperature from the dry storage module has decreased to approximately 31 °C and the estimated salt-metal interface temperature is approximately 141 °C. The external surface for an overpack exposed to dry storage outlet conditions has decreased to approximately 103 °C. The external surface for an overpack exposed to dry storage inlet conditions has decreased to approximately 94 °C.

The results indicate that sometime between 40 and 50 years, depending on how close the overpack was loaded to 2,540 W, the external surface temperature will drop to the point where moisture could collect on the stainless steel. The presence of dust and other surface contaminants could raise the temperature at which condensation occurs and could introduce chlorides with the resultant potential for stress corrosion cracking in the overpacks.

The results presented within Table 4-14 can be used in support of CAP analyses, such as corrosion (WMP-16937) evaluations. It is recommended that a long-term thermal analysis be performed with more detail in support of the final design. This analysis will support confidence that the overpack material (316L) is durable against corrosion and thermal aging.

4.5 SUMMARY AND CONCLUSIONS

Table 4-15 summarizes the progression of salt-metal interface and centerline salt temperatures for the preliminary conceptual design. A revised preliminary conceptual design for dry storage of CsCl capsules is noted that meets the salt-metal performance specification of 317 °C (603 °F). These results demonstrate the feasibility of designing a viable dry storage system. Salt-metal interface temperatures ranging from approximately 310 °C (590 °F) to 316 °C (601 °F) were determined. Additional salt-metal and centerline salt temperature reductions were achieved by

modeling axial conduction within the capsule overpack. The results were derived assuming a dry storage module gas exit temperature of 50 °C given an inlet ambient temperature of 22 °C.

Parametric analyses indicate that the assumption of a 75% power deposition fraction within the salt is conservative and bounds numerous effects including: (1) a 50% power deposition fraction, (2) reduced thermal conductivity of CsCl due to impurities and Ba build up, (3) capsule types, (4) revised radial power distribution across the salt, and (5) a 10-mil salt-metal gap. The salt-metal interface performance specification of 317 °C (603 °F) is met for all parametric cases.

The conceptual design is based on the following configuration.

- 55.9 cm (22-in.) outer diameter overpack with external fins
- 16 CsCl capsules at 160 W per capsule (2,560 W per overpack) arranged in a circular array
- two gaps (no outer gap due to the monolithic construction of insert and overpack)
- helium as the backfill gas
- a measured gas mixture for the innermost gap
- surface emissivities consistent with oxidized stainless steel

The remaining surface emissivities (i.e., capsule walls) were conservatively assumed to remain at values associated with an "as-received" or electro-polished values of 0.3 and 0.1, respectively.

Significant reductions in the salt-metal interface and centerline salt temperatures were achieved through the application of external fins, helium backfill, and axial conduction. Additional reductions can be achieved for the conceptual design by one or more of the following.

- Accurately determine both the fraction of energy deposited within the CsCl salt and the radial power distribution across the salt.
- Increase the effective thermal conductivity for the gaps between the overpack and insert and between the insert and the outer capsule, or decrease the size of the middle gap.
- Modify the conceptual design assumed for this report to increase the contact area between the insert, the lower baseplate, and the upper shield plug. This will promote axial heat transport and increased heat rejection by using the combined surface areas of the overpack, baseplate, and shield plug. This was one of the concepts used by the BUSS to obtain adequate heat rejection when loaded with 16 Cs capsules.
- Modify the conceptual design to incorporate an annular design that will allow convective cooling from both the external and interior surfaces of an overpack.

The following limitations are noted.

- The subject thermal models are based on a single average power CsCl capsule within an overpack assuming symmetric placement of equal-power capsules.
- Multiple adjacent (i.e., side-to-side) capsules around the insert are modeled. The potential exists for local hot spots due to the possibility of two or more adjacent capsules with greater-than-average power. The potential exists to use loading strategy to maintain the total overpack decay power less than 2,540 W. This will have to be assessed and technically justified for any final design. Loading limits/strategies may include, but are

not limited to, mixing high- and low-power capsules, limiting the total number of capsules within an overpack, or simply preventing the placement of high-power capsules adjacent to one another.

- Contact resistance between the salt and inner capsule is neglected when a salt-metal gap was not modeled (see Section 4.4.6).
- The conceptual design does not accommodate Type W overpack capsules. However, the affect of the Type W overpacks on peak centerline and salt-metal interface temperatures can be estimated with the current thermal models.
- Only steady-state, 1-D midplane analyses were performed for the Type W and strontium fluoride capsules.
- Specific power (W/m^3) within the Cs and Sr salts was derived assuming a salt height of 0.4318 m (17 in.). Undoubtedly longer and shorter salt heights exist.
- Self-shadowing of fins is a significant affect on the salt-metal interface and centerline temperatures, especially for natural circulation systems where radiative heat transfer provides a large fraction of energy rejected from the system. The correct view factor or effective emissivity must be determined for a given fin design. Underprediction of the salt-metal and salt centerline temperatures can result, if the appropriate fin view factor is not applied.

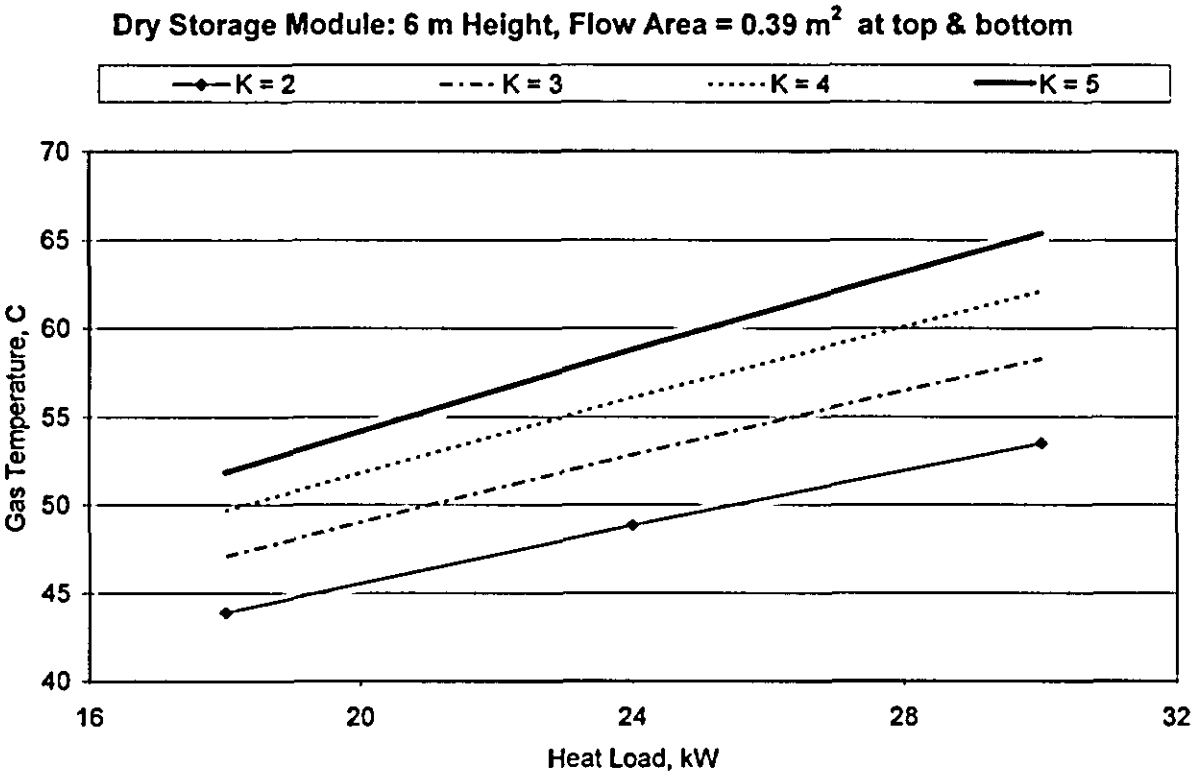

Figure 4-1. Dry Storage Module Interior Gas Temperature for Parametric Variation of Total Heat Load and Flow Loss Coefficient (6 m) Elevation Difference; Inlet Temperature 22 C; and, Top/Bottom Flow Area = 0.39 m^2 (4.2 ft^2).

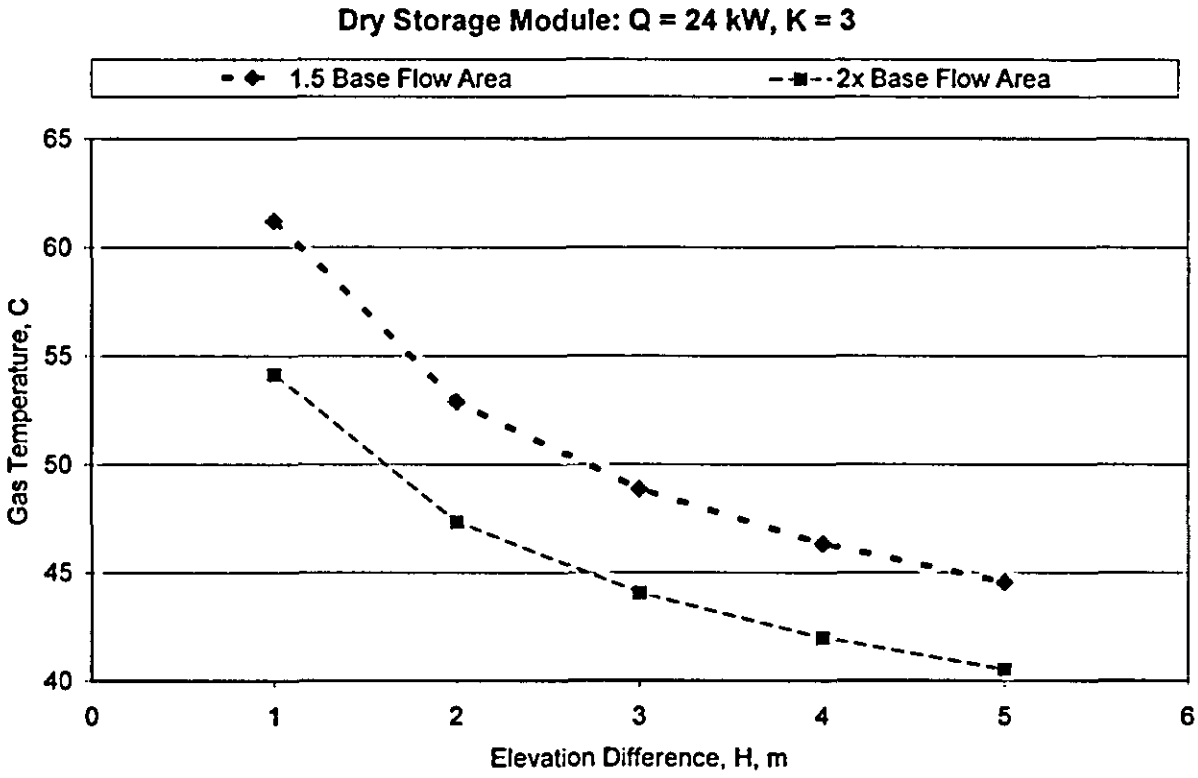

Figure 4-2. Dry Storage Module Interior Gas Temperature for Parametric Variation of Elevation Difference and Flow Area; Total Heat Load = 24 kW; Loss Coefficient (K), = 3; 22 C Ambient Temperature; and, Basecase Top/Bottom Flow Area = 0.39 m^2 (4.2 ft^2).

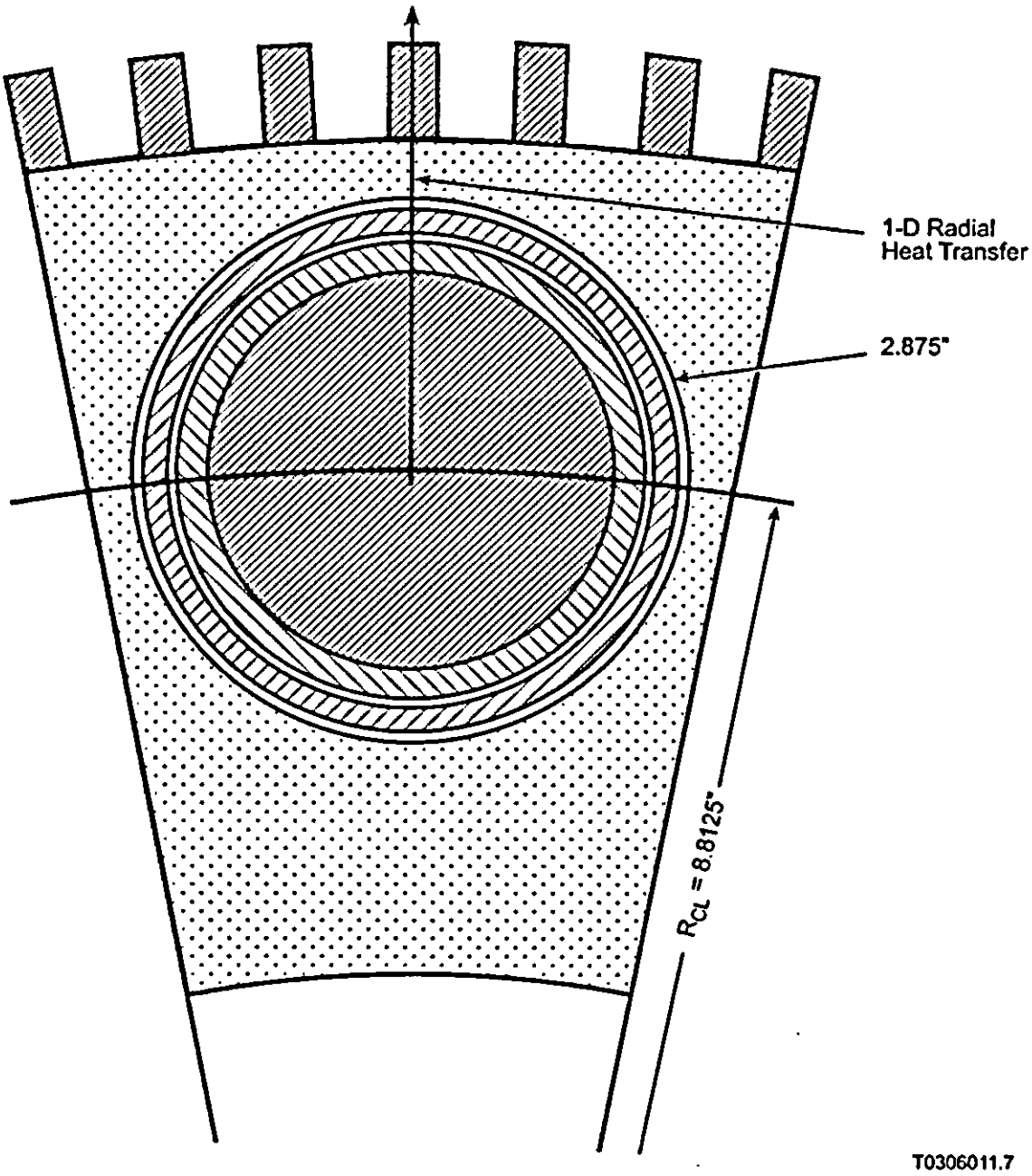

Figure 4-3. Plan View of Overpack Assembly with As-Modeled Line of 1-D Radial Heat Transfer.

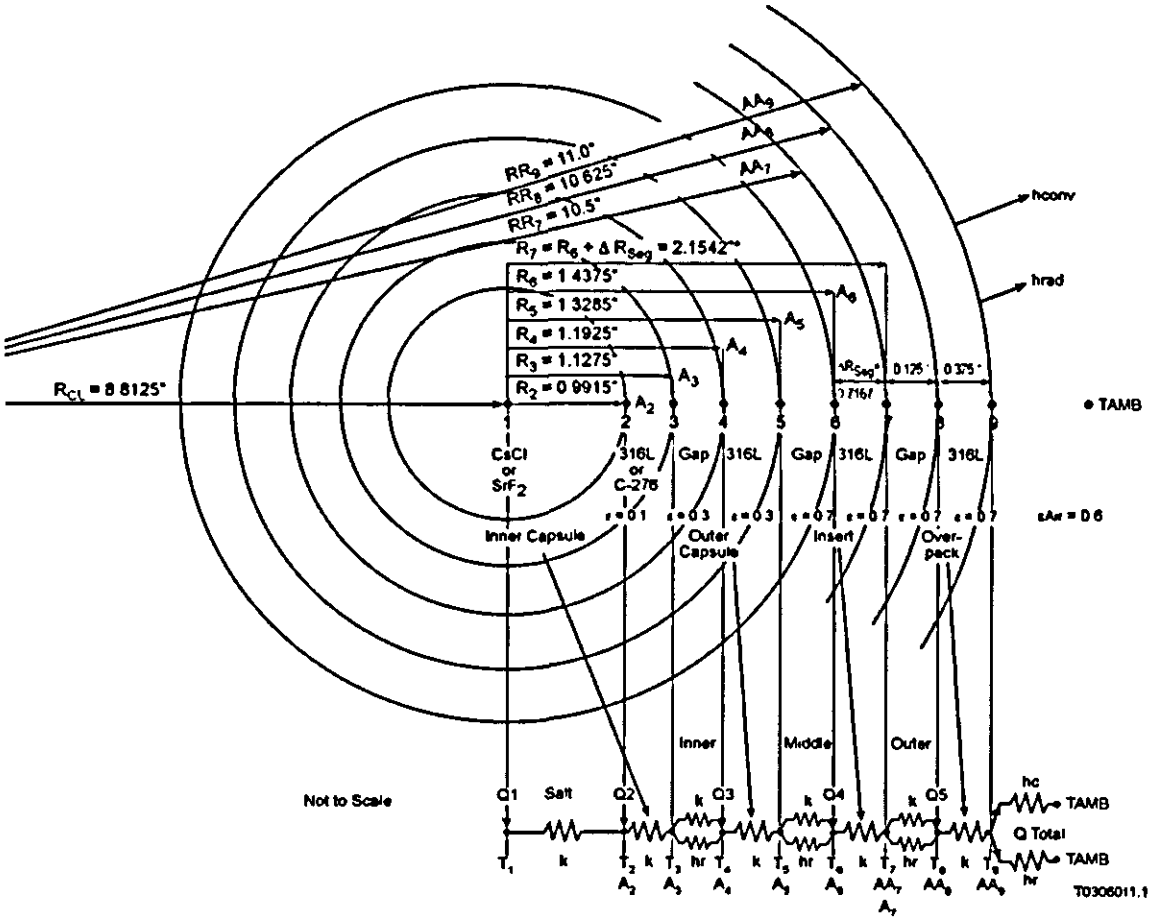

Figure 4-4. Thermal Network for 1-D Thermal Model with Three Gaps (Dimensions Representative of a Type 3 Cesium or Strontium Capsule Within an Insert with 16 Capsules per Overpack).

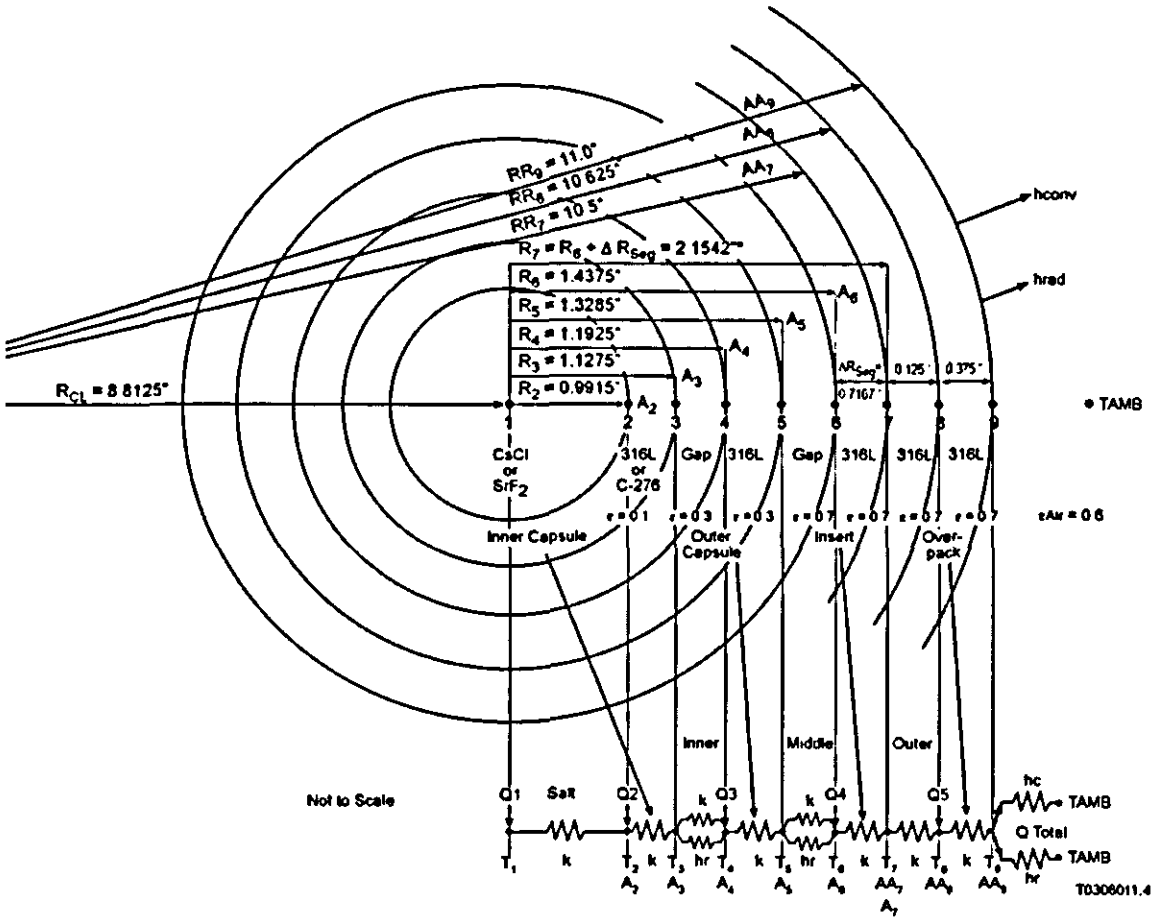

Figure 4-5. Thermal Network for 1-D Thermal Model with Two Gaps (Dimensions Representative of a Type 3 Cesium or Strontium Capsule Within an Insert with 16 Capsules per Overpack).

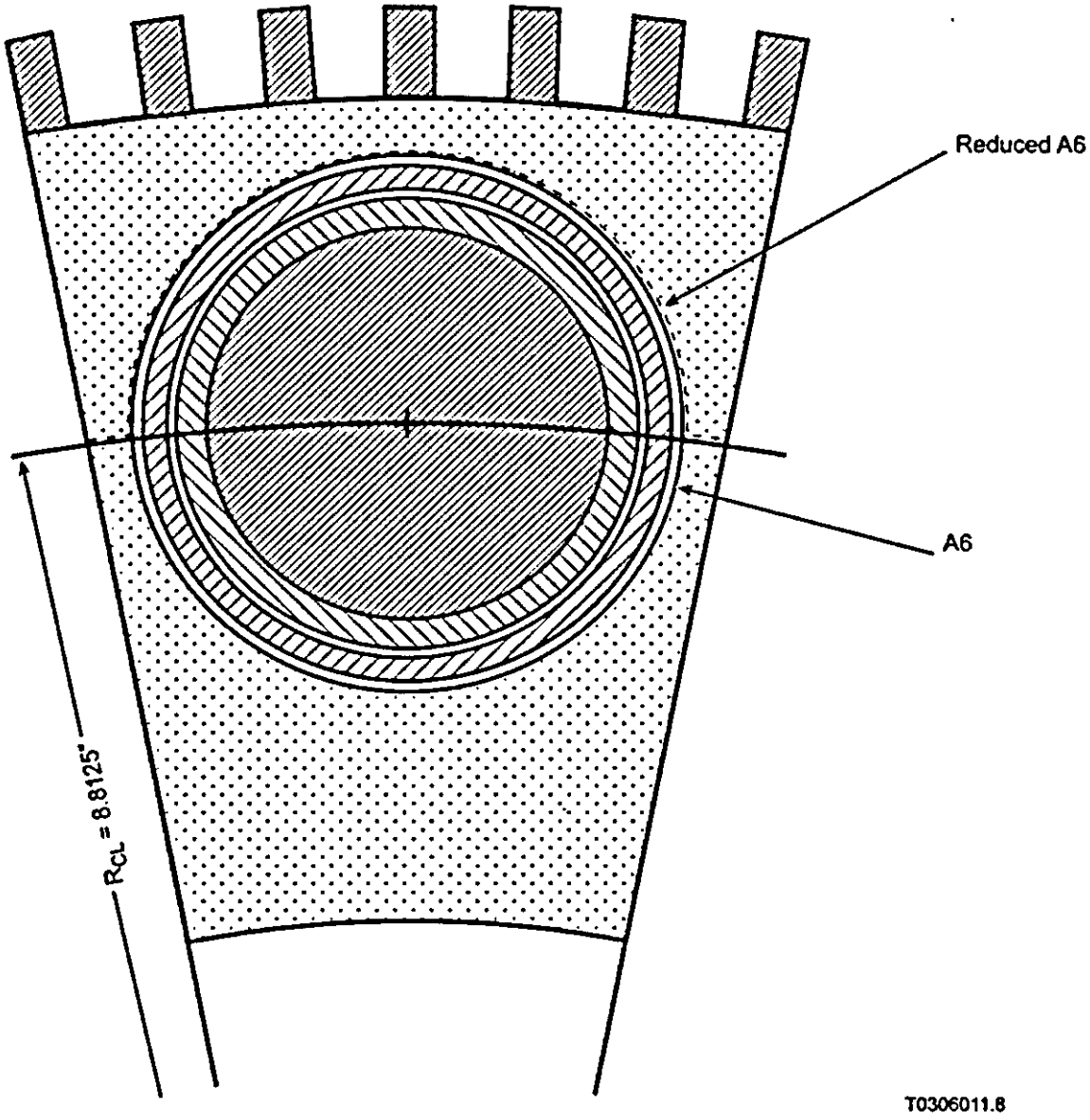

Figure 4-6. Graphical Representation of Ratio AR (AR = Area A6/Reduced Area A6).

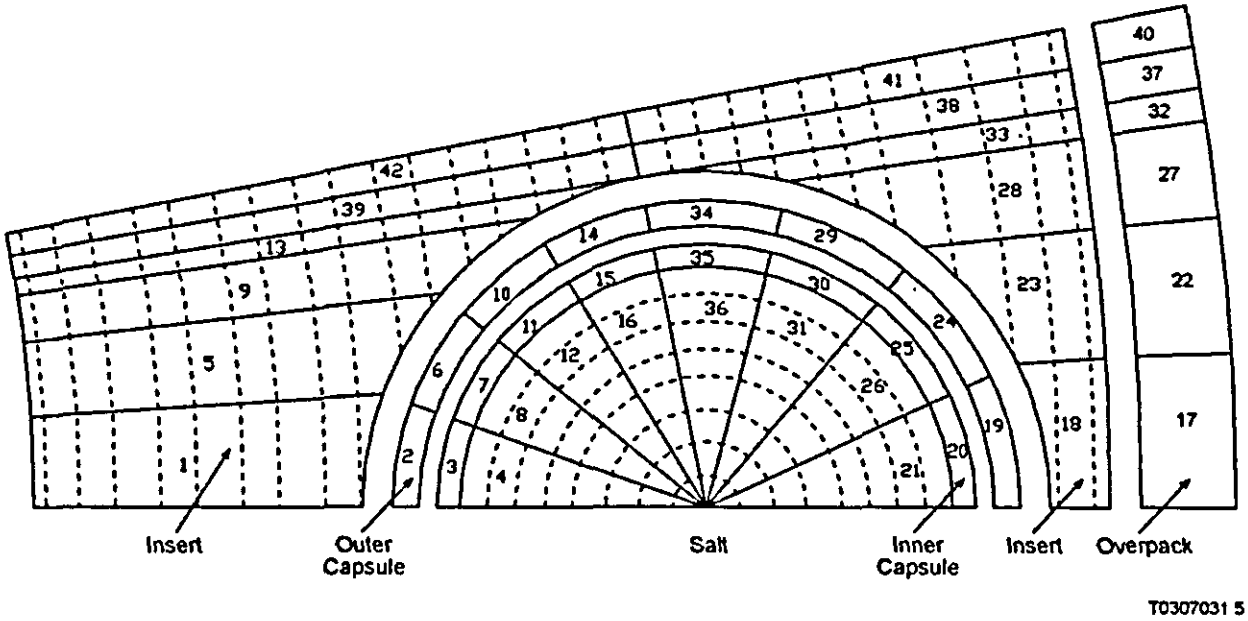

Figure 4-7. Midplane Nodalization of Preliminary Conceptual Design for Cesium Capsule and Overpack.

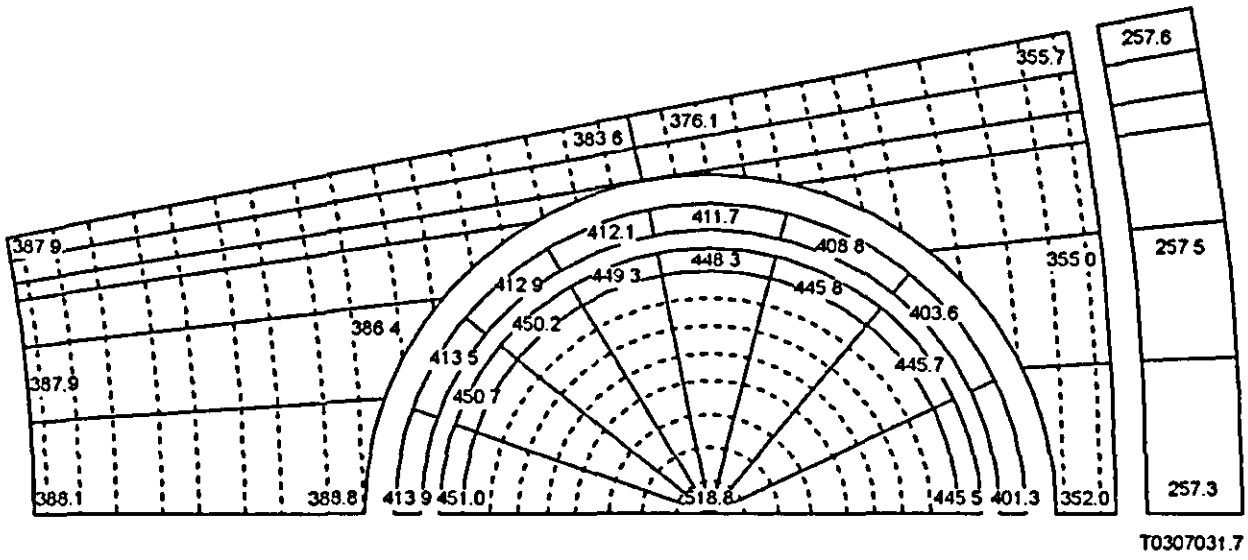

Figure 4-8. Steady State Temperature Map (°C) for 160 W per Capsule, 16 Capsules/Overpack, Air in All (Three) Gaps.

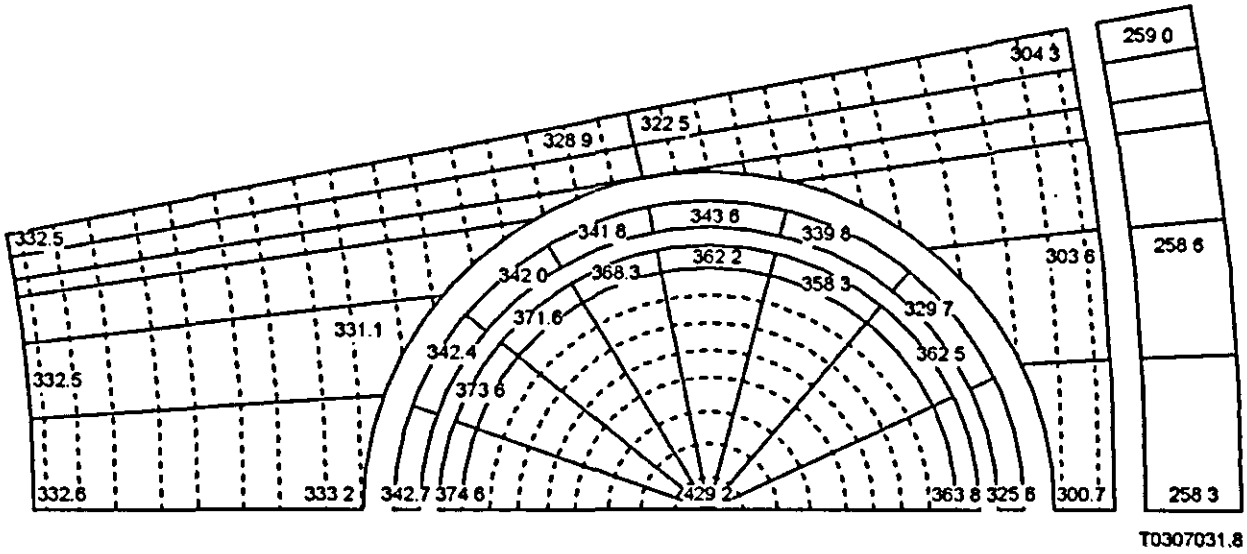

Figure 4-9. Steady State Temperature Map (°C) for 160 W Capsule, 16 Capsules/Overpack, Helium-Filled Overpack (Air in Capsule Gap).

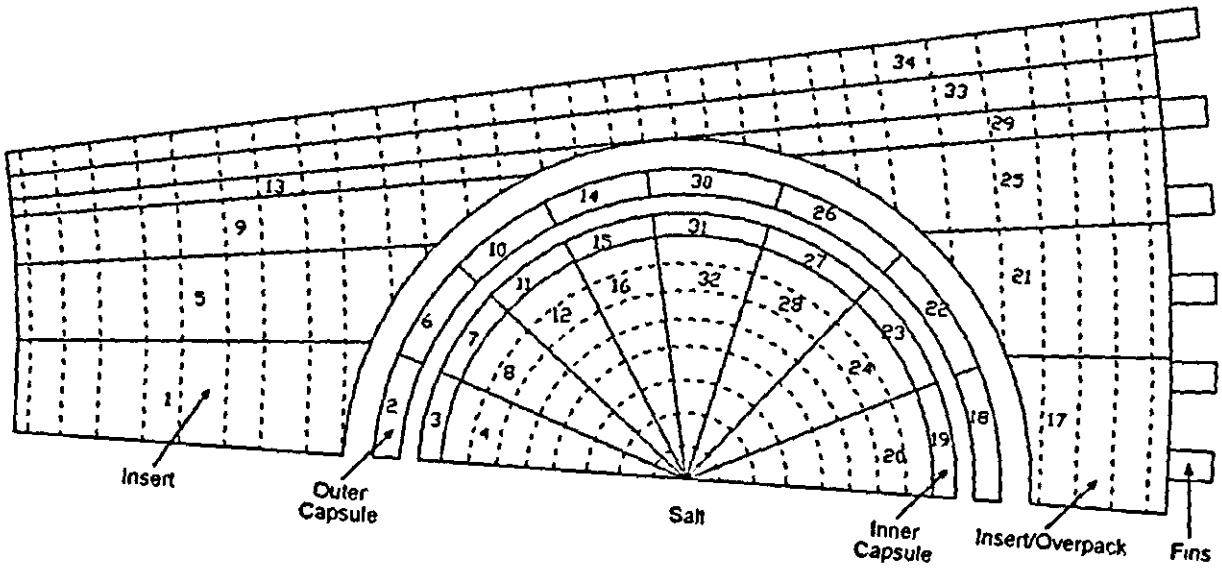

Figure 4-10. Midplane Nodalization for Baseline Configuration Design for Cesium Capsule and Overpack.

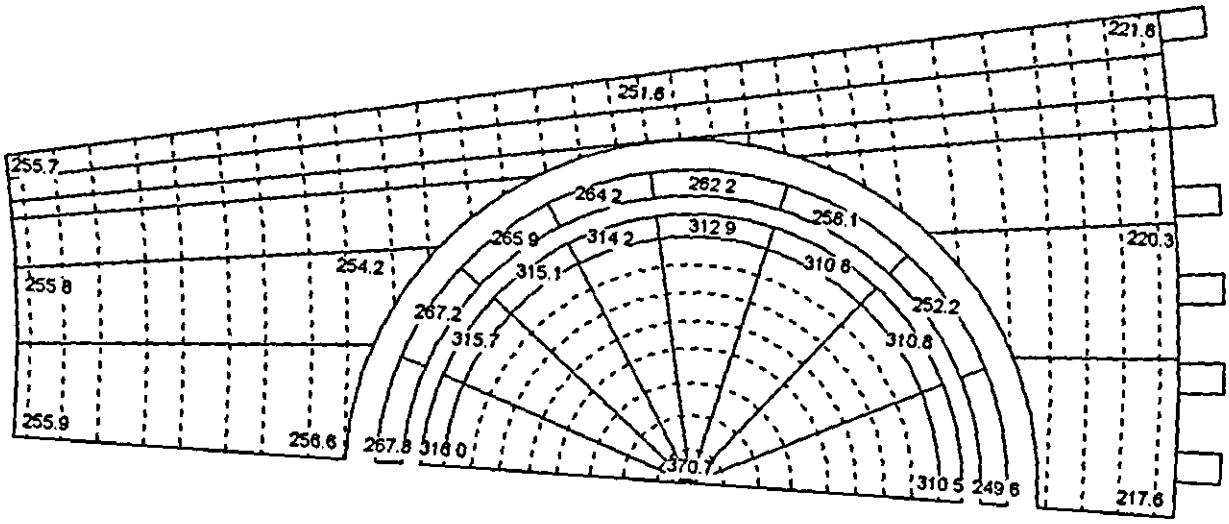

Figure 4-11. Steady State Temperature Map (°C) for Model Nodalization Refinements (Two Gaps, Helium Backfill, External Fins).

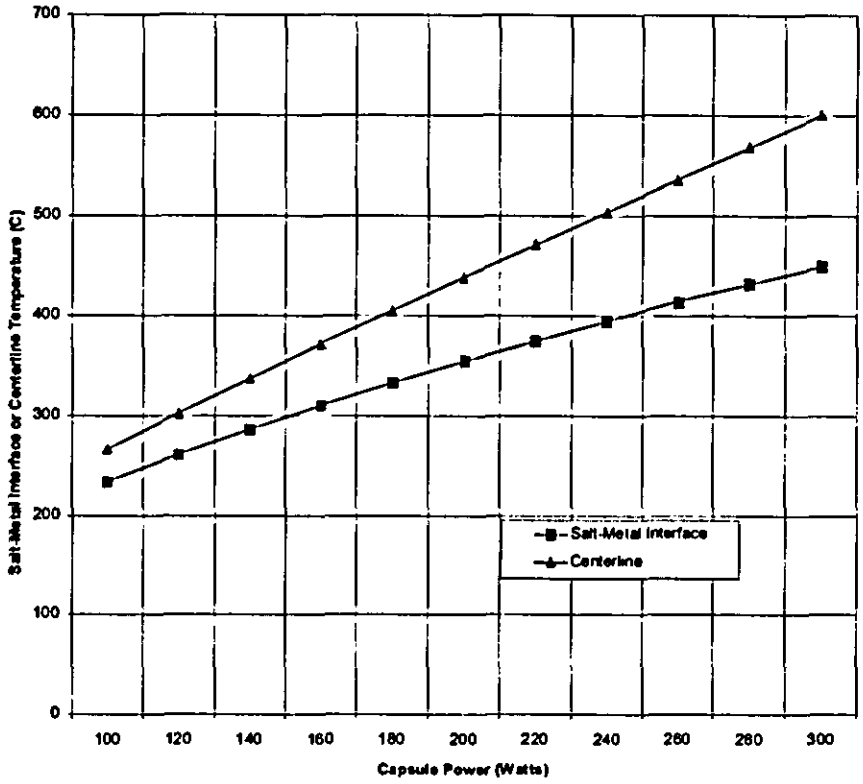

Figure 4-12. Salt-Metal Interface and Salt Centerline Temperature vs. Cesium Capsule Power for Revised Configuration and 16 Capsules per Overpack (1-D Thermal Model).

Table 4-1. Temperature Results for Conceptual Dry Storage Module.

Inputs	
Heat Load, W	24,000
Ambient Temperature, C	22.00
Wall Inner Radius, m	0.93
Wall Outer Radius, m	1.68
Elevation Difference, H, m	4.50
Wall Height, L, m	6.00
Air thermal conductivity, W/m/K	0.027
Air viscosity @ 325 K, m^2/s	1.80E-05
Air thermal diffusivity @ 325 K, m^2/s	2.50E-05
Concrete thermal conductivity, W/m/K	1.00
Air emissivity	0.700
Concrete emissivity	0.700
Prandtl No.	0.700
Air specific heat, J/kg/C	1000.0
Top/bottom duct flow area, m^2	0.23
Temperatures	
Gas Temperature, C	52.87
Inside Wall Temperature, C	42.08
Outside Wall Temperature, C	24.99

Heat Transfer Coefficients	
Overall emissivity	0.538
Inner wall Rayleigh No.	1.56E+11
Inner wall Nusselt number	853.6
Inner wall convective HX Coefficient, $W/m^2/K$	3.841
Inner wall radiative HX coefficient, $W/m^2/K$	0.000
Outer wall Rayleigh No.	4.53E+10
Outer wall Nusselt number	572.5
Outer wall convective HX Coefficient, $W/m^2/K$	2.576
Outer wall radiative HX coefficient, $W/m^2/K$	3.186
Energy Balance	
Natural circulation flowrate, kg/s	0.742
Natural Circulation Heat Removal, W	22910.19
Heat Removal Through Walls, W	1089.81
Total Heat Removal,W	24000.00
Heat Removal at Inner Face, W	1089.81
Heat Removal at Outer Face, W	1089.81
Conduction through Wall, W	1089.81
Residual Energy Imbalance, W =	**1.75E-10**

Table 4-2. Preliminary Conceptual Design—Nodal Temperature vs. Number of Type 3 Cesium Capsules Per Overpack (160 W/Capsule, Inner Gap = 90% Nitrogen, 8% Argon, 2% Hydrogen; Middle Gap = Air, Outer Gap = Air and Tg = 50 °C).

	Temperature, °C (°F)		
Node – description	8 capsules per overpack	12 capsules per overpack	16 capsules per overpack
1 - Centerline (Max.)	400.2 (752.4)	467.3 (873.1)	521.1 (969.9)
2* – Inner Capsule Inner Wall	**340.5 (645.0)**	**397.1 (746.9)**	**442.5 (828.5)**
3 – Inner Capsule Outer Wall	340.2 (644.4)	396.8 (746.3)	442.2 (828.0)
Inner Gap (t_3-t_4)	46.4 (83.5)	41.0 (73.9)	37.3 (67.1)
4 – Outer Capsule Inner Wall	293.8 (560.9)	355.8 (672.4)	404.9 (760.9)
5 – Outer Capsule Outer Wall	293.5 (560.3)	355.5 (671.9)	404.7 (760.4)
Middle Gap (t_5-t_6)	46.3 (83.1)	51.0 (91.9)	53.0 (95.4)
6 – Insert Inner Wall	247.3 (477.2)	304.5 (580.0)	351.7 (665.0)
7 – Insert Outer Wall	245.0 (473.0)	302.8 (577.1)	350.5 (662.9)
Outer Gap (t_7-t_8)	64.4 (115.9)	79.0 (142.1)	89.6 (161.3)
8 – Overpack Inner Wall	180.6 (357.1)	223.9 (435.0)	260.9 (501.6)
9 – Overpack Outer Wall	179.6 (355.3)	222.4 (432.4)	259.1 (498.3)

* Salt-metal interface temperature.

Table 4-3. Preliminary Conceptual Design - Nodal Temperature vs. Number of Type 3 Cesium Capsules Per Overpack (160 W/Capsule, Inner Gap = 90% Nitrogen, 8% Argon, 2% Hydrogen; Middle Gap = Helium, Outer Gap = Helium and Tg= 50 °C).

	Temperature, °c (°f)		
Node – description	**8 capsules per overpack**	**12 capsules per overpack**	**16 capsules per overpack**
1 - Centerline (Max.)	326.2 (619.2)	383.5 (722.4)	432.1 (809.8)
2* – Inner Capsule Inner Wall	**278.1 (532.6)**	**326.5 (619.6)**	**367.4 (693.4)**
3 – Inner Capsule Outer Wall	277.8 (532.0)	326.2 (619.1)	367.1 (692.8)
Inner Gap (t_3-t_4)	53.7 (96.5)	48.0 (86.3)	43.7 (78.7)
4 – Outer Capsule Inner Wall	224.1 (435.5)	278.2 (532.8)	323.4 (614.1)
5 – Outer Capsule Outer Wall	223.8 (434.9)	277.9 (532.2)	323.1 (613.6)
Middle Gap (t_5-t_6)	18.1 (32.6)	22.0 (39.6)	24.3 (43.8)
6 – Insert Inner Wall	205.7 (402.3)	255.9 (492.6)	298.8 (569.8)
7 – Insert Outer Wall	203.3 (397.9)	254.2 (489.6)	297.6 (567.6)
Outer Gap (t_7-t_8)	22.7 (40.8)	30.3 (54.6)	36.7 (66.0)
8 – Overpack Inner Wall	180.6 (357.1)	223.9 (435.0)	260.9 (501.6)
9 – Overpack Outer Wall	179.6 (355.3)	222.4 (432.4)	259.1 (498.3)

* Salt-metal interface temperature.

Table 4-4. Preliminary Conceptual Design - Summary of Peak Centerline and Salt-Metal Interface Temperatures from Tables 4-2 and 4-3.

Number of capsules per overpack	Gap gas			Temperature, °C (°F)	
	Inner	Middle	Outer	Salt-metal interface (performance specification 317 °C)	Cesium chloride centerline
16	Mix	Air	Air	442.5 (828.5)	521.1 (969.9)
	Mix	Helium	Helium	367.4 (693.4)	432.1 (809.8
12	Mix	Air	Air	397.1 (746.9)	467.3 (873.1)
	Mix	Helium	Helium	326.5 (619.6)	383.5 (722.4)
8	Mix	Air	Air	340.5 (645.0)	400.2 (752.4)
	Mix	Helium	Helium	278.1 (532.6)	326.2 (619.2)

Table 4-5. Revised Preliminary Conceptual Design - Nodal Temperature vs. Number of Type 3 Cesium Capsules Per Overpack (160 W/Capsule, Inner Gap = 90% Nitrogen, 8% Argon, 2% Hydrogen; Middle Gap = Air, With Fins, and Tg= 50 °C).

	Temperature, °c (°f)		
Node – description	**8 capsules per overpack**	**12 capsules per overpack**	**16 capsules per overpack**
1 - Centerline (Max.)	354.9 (670.8)	397.5 (747.4)	430.3 (806.5)
2* – Inner Capsule Inner Wall	**295.1 (563.2)**	**.333.5 (632.3)**	**363.1 (685.6)**
3 – Inner Capsule Outer Wall	294.8 (562.6)	333.2 (631.7)	362.8 (685.0)
Inner Gap (t_3-t_4)	58.0 (104.4)	53.9 (97.1)	51.1 (92.0)
4 – Outer Capsule Inner Wall	236.8 (458.2)	279.2 (534.6)	311.7 (593.0)
5 – Outer Capsule Outer Wall	236.5 (457.6)	278.9 (534.1)	311.4 (592.5)
Middle Gap (t_5-t_6)	81.6 (146.9)	88.1 (158.6)	88.3 (158.9)
6 – Insert Inner Wall	154.9 (310.7)	190.8 (375.5)	223.1 (433.5)
7 – Insert Outer Wall	152.3 (306.1)	189.0 (372.1)	221.8 (431.2)
Outer Gap (t_7-t_8)	-	-	-
8 – Overpack Inner Wall	151.9 (305.5)	188.5 (371.3)	221.1 (430.0)
9 – Overpack Outer Wall	150.9 (303.6)	187.0 (368.6)	219.2 (426.5)

* Salt-metal interface temperature.

Table 4-6. Revised Preliminary Conceptual Design - Nodal Temperature vs. Number of Type 3 Cesium Capsules Per Overpack (160 W/Capsule, Inner Gap = 90% Nitrogen, 8% Argon, 2% Hydrogen; Middle Gap = Helium, With Fins, and Tg= 50 °C).

	Temperature, °C (°F)		
Node – description	**8 capsules per overpack**	**12 capsules per overpack**	**16 capsules per overpack**
1 - Centerline (Max.)	295.9 (564.6)	336.2 (637.2)	371.4 (700.5)
2* – Inner Capsule Inner Wall	**241.9 (467.4)**	**278.2 (532.8)**	**310.0 (589.9)**
3 – Inner Capsule Outer Wall	241.5 (466.8)	277.9 (532.2)	309.7 (589.5)
Inner Gap (t_3-t_4)	64.5 (116.2)	59.9 (107.9)	56.4 (101.5)
4 – Outer Capsule Inner Wall	177.0 (350.6)	218.0 (424.4)	253.3 (487.9)
5 – Outer Capsule Outer Wall	176.6 (350.0)	217.7 (423.8)	253.0 (487.3)
Middle Gap (t_5-t_6)	21.8 (39.2)	26.9 (48.3)	29.9 (53.8)
6 – Insert Inner Wall	154.9 (310.7)	190.8 (375.5)	223.1 (433.5)
7 – Insert Outer Wall	152.3 (306.1)	189.0 (372.2)	221.8 (431.2)
Outer Gap (t_7-t_8)	-	-	-
8 – Overpack Inner Wall	151.9 (305.5)	188.5 (371.3)	221.1 (430.0)
9 – Overpack Outer Wall	150.9 (303.6)	187.0 (368.6)	219.2 (426.5)

* Salt-metal interface temperature.

Table 4-7. Revised Preliminary Conceptual Design - Summary of Salt-Metal Interface and Centerline Temperatures vs. Number of Capsules Per Overpack and Backfill Gas (No Outer Gap, With External Fins).

Number of capsules per overpack	Gap gas			Temperature, °C(°F)	
				Salt-metal interface (performance specification 317 °C)	Cesium chloride centerline
	Inner	Middle	Outer		
16	Mix	Air	-	363.1 (685.6)	430.3 (806.5)
	Mix	Helium	-	310.0 (589.9)	371.4 (700.5)
12	Mix	Air	-	333.5 (632.3)	397.5 (747.4)
	Mix	Helium	-	278.2 (532.8)	336.2 (637.2)
8	Mix	Air	-	295.1 (563.2)	354.9 (670.8)
	Mix	Helium		241.9 (467.4)	295.9 (564.6)

Table 4-8. Estimated Type W Overpack Salt-Metal and Salt Centerline Temperature (Air Backfill).

		Temperature[a], °C (°F)		
Node	Number of Type W capsules per overpack	N = 8	N = 12	N = 16
2	Salt-metal interface	353.8	395.8	425.5
1	Salt Centerline	420.0	466.6	499.5

[a]Gap between IC and OC = gas mixture (Kenna and Schultz 1983).
Gap between OC and Type W = air.
Gap between Type W and insert = air.

Table 4-9. Estimated Type W Overpack Salt-Metal and Salt Centerline Temperature (Helium Backfill).

		Temperature[a], °C (°F)		
Node	Number of Type W capsules per overpack	N = 8	N = 12	N = 16
2	Salt-metal interface	259.7	300.6	335.0
1	Salt Centerline	315.7	361.0	399.1

[a]Gap between IC and OC = gas mixture (Kenna and Schultz 1983).
Gap between OC and Type W = helium.
Gap between Type W and insert = helium.

Table 4-10. Temperature Distribution for Strontium Fluoride Capsules vs. Number of Capsules for Air Backfill and Tg = 50 °C.

	Temperature, °C					
Node	**CsCl Ref.[a] 160 W**	**SrF_2 160 W**	**SrF_2 (Avg.) 218 W**	**SrF_2 320 W**	**SrF_2 480 W**	**SrF_2 (Max.) 570 W**
9[b]	219.2	219.2	221.8	219.2	211.5	205.6
8	221.1	221.2	223.8	221.2	213.3	207.3
7	221.8	221.9	224.6	221.9	214.0	208.0
6	223.1	223.3	227.2	227.1	224.5	221.9
Middle Gap ΔT	**88.3**	**102.3**	**120.5**	**143.8**	**194.4**	**222.5**
5[c]	311.4	325.6	347.7	370.9	418.9	444.4
4	311.7	325.9	348.4	371.4	419.7	445.4
Inner Gap ΔT	**51.1**	**60.2**	**78.1**	**107.8**	**146.0**	**164.6**
3	362.8	386.1	426.2	479.2	565.7	610.0
2[d]	363.1	386.8	427.1	480.6	567.8	611.4
1[e]	430.3	403.0	450.6	517.7	630.5	691.6
Number of capsules	**16**	**16**	**12**	**8**	**5**	**4**
Overpack Power (W)	**2,560**	**2,560**	**2,616**	**2,560**	**2,400**	**2,280**

[a]From Table 4-5.
[b]External surface of overpack.
[c]Outer surface of outer capsule.
[d]Inner surface of inner capsule (salt-metal interface).
[e]Salt centerline.

Table 4-11. Temperature Distribution for Strontium Fluoride Capsules vs. Number of Capsules for Helium Backfill and Tg = 50 °C.

	Temperature, °C					
Node	**CsCl Ref.[a] 160 W**	**SrF_2 160 W**	**SrF_2 (Avg.) 218 W**	**SrF_2 320 W**	**SrF_2 480 W**	**SrF_2 (Max.) 570 W**
9[b]	219.2	219.2	221.8	219.2	211.5	205.6
8	221.1	221.2	223.8	221.2	213.0	207.3
7	221.8	221.9	224.6	221.9	214.0	208.0
6	223.1	223.3	227.2	227.1	224.5	221.9
Middle Gap ΔT	**29.9**	**37.0**	**41.8**	**46.3**	**65.2**	**76.9**
5[c]	253.0	260.3	269.0	273.4	289.7	298.8
4	253.3	260.6	269.4	274.1	290.6	299.9
Inner Gap ΔT	**56.4**	**67.0**	**88.2**	**124.4**	**174.2**	**199.5**
3	309.7	327.6	357.6	398.5	464.8	499.4
2[d]	310.0	328.3	358.5	399.8	466.8	501.8
1[e]	371.4	343.0	379.7	433.2	522.3	571.2
Number of capsules	**16**	**16**	**12**	**8**	**5**	**4**
Overpack Power (W)	**2,560**	**2,560**	**2,616**	**2,560**	**2,400**	**2,280**

[a]From Table 4-6.
[b]External surface of overpack.
[c]Outer surface of outer capsule.
[d]Inner surface of inner capsule (salt-metal interface).
[e]Salt centerline.

Table 4-12. Results of Parametric Analyses (1-D Midplane Model) for Revised Preliminary Conceptual Design.

		Temperature, °C	
Case	**Description**	**Salt-metal interface**	**Salt centerline**
1	Reference[1] case	310	371
2	Revised Power Deposition (50%)[2]	290	329
3	Reduced CsCl Thermal Conductivity[3]	290	351
4	Type 1 Capsule (Max. gap)[4]	300	362
5	Revised Radial Power Distribution[5]	300	373
6	Salt-Metal Gap (10 mils)[6]	300	376
7	Reduced Emissivity of Fins[7]	319	398

[1]160 W, 75% deposited in salt, monolithic overpack with fins, helium backfill, measured inner gap gas composition, Type 3 tubing, nominal CsCl conductivity, no salt-metal gap.

[2]50% deposited in salt, 15% deposited in first capsule, remaining power in structure.

[3]CsCl thermal conductivity reduced 35%.

[4]Maximum capsule gaps.

[5]Centerline temperature based on $Q_{MAX} = 7/6\ Q_{AVG}$.

[6]Based on gamma scans of some cesium capsules.

[7]Emissivity of fins reduced approximately 50% from 0.7 to 0.359 (see Appendix E).

Table 4-13. Salt-Metal Interface and Centerline Temperature Vs Cesium Capsule Power for Revised Preliminary Conceptual Design and 16 Capsule per Overpack (1-D Thermal Model).

	Temperature (°C)	
Cesium capsule power(watts)	**Salt-metal interface**	**Centerline**
100	233.6	266.1
120	260.6	302.0
140	286.0	337.1
160	310.0	371.4
180	332.7	405.0
200	354.3	438.2
220	374.9	471.1
240	394.9	503.8
260	414.0	536.3
280	432.4	568.7
300	450.0	600.9

Table 4-14. Capsule and Overpack Temperatures vs. Decay Time (Revised Preliminary Conceptual Design).

		Temperature, °C				
Time (yrs)	Capsule power (W)	Dry storage module outlet[2]	Salt centerline	Salt-metal interface	Overpack external surface (outlet conditions)	Overpack external surface (inlet conditions)
0	160.0[1]	50.0	371.4	310.0	219.2	191.2
5	142.6	46.9	339.3	287.1	203.2	178.3
10	127.1	44.2	310.1	265.7	188.3	166.1
15	113.2	41.8	283.6	245.7	174.4	154.6
20	100.9	39.6	259.6	227.2	161.6	144.0
25	89.9	37.7	237.8	210.0	149.8	134.1
30	80.1	36.0	217.9	194.1	138.9	124.9
35	71.4	34.4	199.8	179.4	128.9	116.5
40	63.6	33.1	183.4	165.8	119.7	108.6
45	56.7	31.9	168.3	153.1	111.1	101.2
50	50.5	30.8	154.6	141.4	103.2	94.4
60	40.1	29.0	130.9	121.0	89.4	82.4
75	28.4	26.9	103.0	96.5	73.0	68.1
100	16.0	24.7	71.3	67.9	53.9	51.2

[1]Reference case.

[2] Based on constant flow rate from reference case. Total heat load within dry storage module decays with time.

Table 4-15. Summary of Key Thermal Results for Cesium Capsules.

		Temperature, °C	
• **Preliminary Conceptual Design**[1]	**Backfill Gas**	**1-D**	**2-D**
Salt-Metal Interface	Air	443	446–451
Salt Centerline	Air	521	519
Salt-Metal Interface	Helium	367	364–375
Salt Centerline	Helium	432	429
• **Revised Preliminary Conceptual Design**[2]	**Backfill Gas**	**1-D**	**2-D**
Salt-Metal Interface	Helium	310	311–316
Salt Centerline	Helium	371	371
• **Integral Dry Storage Module With Overpacks (With Axial Conduction)**[3]			**3-D**
Salt-Metal Interface	Helium	—	291–295
Salt Centerline	Helium	—	348

[1]Tables 3-2 and 3-3, Figures 3-8 and 3-9.

[2]Table 3-6 and Figure 3-11.

[3]Figure 4-7.

5.0 STEADY-STATE ANALYSIS OF OVERPACKS IN DRY STORAGE MODULE

Section 4.0 discussed the methodology, and presented and compared the results of the 1- and 2-D midplane models for the preliminary and revised conceptual design of a Cs capsule overpack. This section extends the revised conceptual design of the overpack model by incorporating axial conduction and modifying the conceptual dry storage module to account for multiple tiers of overpacks.

5.1 OVERPACK (AXIAL) MODEL DESCRIPTION

A 3-D model (i.e., detail overpack model) of the revised conceptual design of the overpack was developed by concatenating the insert heat conductors to those of the bottom plate below and the shield plug above, as shown in Figures 5-1 and 5-2.

The bottom plate, in good contact with the insert, provides an additional heat removal path for the decay power deposited in the capsules and in the insert. A 1/32 symmetry sector of the bottom plate is modeled (see Figure 5-3). Consistent with the insert midplane model, as discussed in Section 4.3, the volume and heat transfer area of each heat conductor comprising the 1/32 symmetry sector is scaled to represent the entire plate. Furthermore, to facilitate one-to-one axial conduction coupling between the insert heat conductors and the corresponding bottom plate heat conductors, two sets of conductors are defined. One set (heat conductors 218, 220, 222, 224, 226, and 228) comprises the center portion of the plate and its internal nodes are exposed to gas on the top. The other set (heat conductors 217, 219, 221, 223, 225, and 227) comprises the annular section of the plate that is in contact with the insert on the top.

The underside of the bottom plate is assumed to be exposed to the gas in the dry storage. Although the bottom plate is in good contact with the insert, because the downward facing surface is normally warmer than the gas, no convective cooling is considered for the surface. In addition, the plate is relatively thin 2.54 cm (1 in.) and its heat capacity is small. Hence, it is expected to have a minor affect on heat removal. In reality, it might be sitting on top of another overpack, in which case the heat may be conducted downward to the shield plug of the overpack below. However, this is not currently modeled.

A similar model is constructed for the shield plug as shown in Figure 5-4. A 0.635 cm (0.25-in.) crushable stainless steel disc, as shown in Figure 5-2, is assumed to provide thermal contact between the shield plug and the insert. The thermal conductivity of the disc is assumed to be 1/3 of the stainless steel. In addition, the underside of the shield plug center is heated by the hot gas in the containment. Note that the insert has a vertical interior wall convecting to gas, and that the same gas convects to the bottom inside of the plug.

5.2 DRY STORAGE (AXIAL) MODULE MODEL DESCRIPTION

Nominal power in the dry storage module is 24 kW. The nominal power associated with an overpack is 2.56 kW. There are approximately 10 (i.e., 24/2.56 conservatively rounded up) overpacks in a dry storage module. As shown in Figure 5-5, the dry storage module is modeled

assuming two regions: a bottom and top region. The overpacks are assumed placed in parallel stacks with three tiers per stack (i.e., nine overpacks within the bottom region) and one overpack on top (top region).

The conceptual dry storage module design (Section 4.1) contains extra space above the top region. The top region is assumed to contain the extra stack space. The overpack model was assumed positioned within the top 1/6 of the volume in the dry storage. Because the gas is hotter at the top of the dry storage before it exits, the overpack is exposed to the most severe boundary condition. The bottom 5/6 is assumed to hold the remaining overpacks, and their affect is represented by a heat source equivalent to the decay power (24,000 W – 16 x 160 W = 21,440 W).

A heat conductor representing the portion of the storage wall in the region is defined for each elevation. Heat transfer due to natural convection is accounted for between the inner surface of the dry storage module wall and the annular gas space. The dry storage module wall, in turn, rejects heat to the environment by natural convection and thermal radiation from the outer surface. Because the wall is thick (0.75 m [29.5 in.]) and has low thermal conductivity (1.0 W/m/K), not much heat will be conducted through the wall.

Three junctions are defined: the inlet, the outlet, and the zero loss junction linking the upper region to the lower region. For the inlet and the outlet junctions, the flow area of 0.39 m^2 (4.2 ft^2) and local loss coefficient of 1.5 are assumed. The density difference of air inside and outside the dry storage module drives natural circulation flow through the junctions. The air density decreases steadily as the air rises and heats up through the dry storage module. The assumed height of the dry storage module is 6 m (~19.7 ft). However, because the model uses a single lower region to lump most of the air in the dry storage module, the hydrostatic head difference would be overestimated. To correct for the nonconservative flow calculation, a height of 4.5 m (~14.8 ft) is input to the dry storage module model. This will give correct static head difference for overpacks stacked to half the interior height of the dry storage module.

5.3 STEADY-STATE OVERPACK RESULTS

Figure 5-6 shows temperature and flow transients leading to a steady state condition at 24 hours. A circulation flow rate of 0.74 kg/sec (1.63 lb/sec) in the dry storage module is predicted (Table 4-1). The uni-directional (upward) flow is strong enough to suppress any counter-current exchange flows through the inlet and the outlet (upper right) ports. The resulting steady-state flow establishes a gas exit temperature of approximately 53 °C (Table 4-1) within the conceptual dry storage module, which in turn determines the temperature distribution within the overpack, insert, and capsules necessary to reject the decay heat. With such a strong circulation flow, the heat removed by the flow is an order of magnitude greater than that conducted through the dry storage module wall (lower right).

The bottom plate temperature closely follows the temperature of the insert because it is strongly coupled to the insert and has a low heat capacity (lower left). On the other hand, the shield plug has a high heat capacity and its temperature slowly approaches that of the insert.

A peak salt-metal interface temperature of 294.7 °C (562.5 °F) is predicted. This is approximately 21 °C lower than the corresponding midplane result from Figure 4-11. A peak salt temperature of 347.9 °C (658.2 °F) is predicted. This is approximately 23 °C lower than the midplane results presented by Figure 4-11. (The boundary condition in the integrated dry storage module and overpack model is about 4 °C higher than what was assumed in Sections 4.2 and 4.3). Axial heat conduction is important. By incorporating axial conduction from the insert to the shield plug and to the bottom plate, the peak salt and salt-metal interface temperatures can be significantly reduced.

Figure 5-7 presents the temperature distribution (°C) in the shield plug, the bottom plate, and the capsule and insert at the end of the 24-hour transient. The temperature map corresponds to nodalization patterns presented within Figures 4-10, 5-3, and 5-4.

The top two rows correspond to the shield plug; the first row is along a symmetry line between capsules and the second row is along a symmetry line cutting through the capsule center. The bottom two rows correspond to the bottom plate.

For the capsules and insert, the left edge is the interior surface of the insert. The right edge is the outermost surface of the overpack. The top edge is along a line-of-symmetry within the steel insert between adjacent capsules. The bottom edge is along a line-of-symmetry cutting through the capsule center from the interior surface of the insert to the outermost surface of the overpack.

The temperatures (left-to-right) along the bottom edge are: steel insert at the interior surface, steel insert at gap surface, average capsule outer wall, average capsule inner wall (i.e., salt-metal interface), salt maximum, average capsule inner wall (toward insert exterior), average capsule outer wall, and overpack wall. The inner capsule wall temperature is shown by eight values arranged as a semicircle around the maximum value. The outer capsule wall temperature is shown by eight values just outside inner wall values. The steel insert temperature at the capsule gap is shown by seven values closest to outer wall values (three to left, three to right, one above).

Figure 5-7 shows appreciable temperature variations in the cladding and in the insert, indicating the importance of a 2-D effect: 199 °C to 229 °C in the insert, 230 °C to 242 °C in the outer cladding, and 291 °C to 295 °C in the inner cladding. The temperature spreads are also shown in temperature plots in Figure 5-6 (upper left). On the other hand, azimuthal temperature variation in the shield plug and in the bottom plate is negligible as expected; only the radial temperature gradient remains prominent.

5.4 DAILY DIURNAL CYCLES - DRY STORAGE MODULE WITH OVERPACKS

The thermal performance of a dry storage module, with overpacks exposed to summertime diurnal temperature variations, was simulated for a period of 14 days. The analysis assumed a repeating series of the hottest summer day ever recorded at the Hanford Site. Solar insolation flux on the module wall was also considered. The Hanford Site-specific solar insolation data over a 24-hour period is shown in Table 5-1. See WMP-16878 for a summary table of Hanford-specific maximum day and seasonal temperatures and solar insolation values.

The ambient air temperature was used as the inlet condition to the dry storage module and as the applied boundary condition for the exterior vertical surface and horizontal top of the dry storage module. Half of the solar insolation flux was assumed applied to the outer vertical surface of the dry storage module; 100% of the insolation flux was assumed applied to the top surface. The solar flux for both surfaces was multiplied by a solar absorptivity coefficient of 0.52 (*Thermal Analysis Methods for Safety Analysis Reports for Packaging* [Irwin 2000]).
That is, $Q_{solar,side}(t) = Q_{solar}(t) \times 0.5 \times 0.52$ and $Q_{solar,top}(t) = Q_{solar}(t) \times 1.0 \times 0.52$.

Figures 5-8a and 5-8b present the results. Because most of the heat generated in the overpack is removed by natural circulation flow rather than through the module wall, the solar insolation flux on the module wall has little impact on the thermal response of the overpack. On the other hand, because of the natural circulation in the module, diurnal fluctuation of the ambient air temperature is directly felt by the overpack. Consequently, as shown in the temperature plots, the diurnal temperature fluctuation begins to propagate into the overpack. Peak temperatures in the salt and at the salt-metal interface are 360 °C and 305 °C, respectively. Normal diurnal temperature variation for the salt temperature did not exceed about 10 °C in amplitude (Figure 5-8a).

5.5 LONG-TERM Cs SALT TEMPERATURES

The purpose of this section is to provide a 50-year history of daily high- and low-temperature values at the salt-metal interface and capsule centerline. A method for estimating long-term maximum and minimum daily temperature in Cs salt was developed. The salt-metal and centerline temperatures are found by extrapolating current steady-state and diurnal temperature variation results to account for annual ambient temperature variation and decay of the Cs.

Steady-state results for a constant ambient temperature provide a convenient way of characterizing thermal resistance. Present-day values for the average salt-metal interface temperature T_i and the centerline temperature T_{cl} are related to the ambient value T_a by

$$T_i = T_a + \Delta T_{ia} \qquad \text{Equation 5.5-1}$$

$$T_{cl} = T_a + \Delta T_{ia} + \Delta T_{cli} \qquad \text{Equation 5.5-2}$$

Where ΔT_{ia} is the temperature difference between the ambient temperature T_a and the salt-metal interface temperature T_i, and ΔT_{cli} is the temperature difference between the salt-metal interface temperature T_i and the peak centerline salt temperature T_{cl}. The flow of heat through the surface of the capsule carrier, Q, is given by:

$$Q = h \cdot A \cdot \Delta T \qquad \text{Equation 5.5-3}$$

Where h is the overall heat transfer coefficient, A is the area and ΔT is the difference between the ambient and capsule carrier surface temperature that is appropriate. If the radiation affects are ignored, a simplified form for the heat transfer coefficient for natural circulation from vertical cylinders in air can be written as:

$$h = 1.31\,\Delta T^{1/3} \qquad \text{Equation 5.5-4}$$

Note that now: $Q \propto \Delta T^{4/3}$

The Q that must be dissipated from the capsule is declining exponentially because of the decay of the Cs. If we neglect the heat deposited in the metal structure of the capsule and the insert, the Q at the overpack surface and the Q generated in the salt can be equated. Neglecting differences in the constants of proportionality equals:

$$\Delta T_{ia}^{4/3}(t) = \Delta T_{ia}^{4/3}(0) \cdot e^{(-\lambda t)}, \qquad \text{Equation 5.5-5}$$

where λ is a decay constant. If both sides of the Equation5.5-5 are raisedto the ¾ power, then:

$$\Delta T_{ia}(t) = \Delta T_{ia}(0) \cdot e^{(-0.75\lambda t)} \qquad \text{Equation 5.5-6}$$

If time is expressed in years, then $\lambda = 0.693/30.07 = 0.02305$. As indicated in Figure 5-6, the salt-metal interface temperature is 295 °C and since the ambient temperature is 22 °C in these cases, $\Delta T_{ia}(0) = 272$ °C.

If ΔT_{cli} is defined as the temperature drop from the centerline to the salt-metal interface, a similar equation is obtained that decays with time given the cesium-137 decay constant. The following equation neglects the temperature dependence of thermal conduction in the salt.

$$\Delta T_{cli}(t) = \Delta T_{cli}(0) \cdot e^{(-\lambda t)} \qquad \text{Equation 5.5-7}$$

This difference in decay exponents means that the centerline temperature approaches the salt-metal interface temperature with time as presented in Figure 5-12. As indicated in Figure 5-7, centerline temperature is about 348 °C, hence $\Delta T_{cli}(0) = 53$ °C.

Calculation of the salt-metal interface and centerline temperatures, given diurnal ambient variations from Figure 5-8, shows that the amplitude of diurnal variation is reduced by slightly less than one-half, i.e., when the ambient temperature amplitude is 22 °C, the corresponding amplitude in the salt is 10 °C. Therefore, on any given day, the maximum and minimum values for the salt-metal interface are approximately given by:

$$T_{i,max}(t) = T_{a,avg}(t) + \Delta T_{ia}(t) + \frac{1}{4} \cdot \Delta T_a(t) \qquad \text{Equation 5.5-8}$$

$$T_{i,min}(t) = T_{a,avg}(t) + \Delta T_{ia}(t) - \frac{1}{4} \cdot \Delta T_a(t) \qquad \text{Equation 5.5-9}$$

where approximating the average temperature with the arithmetic average:

$$T_{a,avg}(t) = \frac{1}{2} \cdot \left[T_{a,max}(t) + T_{a,min}(t)\right] \qquad \text{Equation 5.5-10}$$

$$\Delta T_a(t) = T_{a,max}(t) - T_{a,min}(t) \qquad \text{Equation 5.5-11}$$

Values for the Hanford Site nominal maximum and minimum temperatures, respectively, are contained in WMP-16878 and are repeated in Figure 5-9 for convenience.

Figure 5-10 provides maximum and minimum values for the salt-metal interface and centerline temperatures for a one-year period based on nominal maximum and minimum ambient conditions. Since only temperatures that may lead to a phase change are of interest, the same information is expanded in Figure 5-11 for a 10-year period. If there is a transition temperature in a certain range, say 330 to 340 °C, then Figure 5-11 can be examined to determine the number of temperature cycles that could occur through this range. Actual use of this information in this section must await the specification of transition temperatures of concern to the CAP. Figure 5-12 provides maximum and minimum salt centerline and salt-metal interface temperatures for a 50-year period.

The change in the radial temperature distribution across the salt can be estimated as ambient temperature changes. Assume that the temperature profile across the salt is parabolic and that the temperature T_i at the salt-metal interface (r=R) is known from the previous discussion and ΔT_{cli} is the temperature difference from the centerline to the salt-metal interface. The radial temperature distribution can be written as:

$$T(r) = T_i + \Delta T_{cli} \cdot e^{(-\lambda \cdot t)} \left(1 - \left(\frac{r}{R}\right)\right)^2 \qquad \text{Equation 5.5-12}$$

Where, the term $e^{(-\lambda t)}$ accounts for the decay of Cs and ΔT_{cli} is 53 °C at time zero.

Figure 5-13 presents the radial temperature distribution versus salt radius for the daily high- and low-ambient temperatures for July 1 (time zero). This can be extended to determine the radial temperature distribution at any time (t).

5.6 SUMMARY AND CONCLUSIONS

Axial heat conduction is important. By incorporating axial conduction from the insert to the shield plug and to the bottom plate, the peak salt and salt-metal interface temperatures can be significantly reduced. A peak salt-metal interface temperature of 294.7 °C (562.5 °F) is predicted. This is approximately 21 °C lower than the corresponding midplane result from Figure 4-16. A peak salt temperature of 347.9 °C (658.2 °F) is predicted. This is approximately 23 °C lower than the midplane results presented by Figure 4-11. (Considering that the boundary condition in the integrated dry storage and overpack model is about 4 °C higher than what was assumed in Sections 4.2 and 4.3).

The thermal performance of a dry storage module with overpacks exposed to summertime diurnal temperature variations was simulated for a period of 14 days. The analyses indicated that

the increase in the salt centerline and salt-metal interface temperatures, due to maximum summertime diurnal cycles, is approximately 10 °C to 12 °C (18 °F to 22 °F) above the previous (no diurnal cycles) steady-state results presented in Figure 5-7. This can be easily accommodated through further optimization of the conceptual design configuration. The analysis assumed a repeating series of the hottest summer day ever recorded at the Hanford Site and included solar heating on the external surfaces of the dry storage module. The results (Figures 5-8a and 5-8b) show that the peak salt centerline temperature and salt-metal interface temperatures have increased slightly from the values presented in Figure 5-7 and oscillate (slightly out of phase) with the assumed diurnal cycles. The peak salt centerline temperature is approximately 358 °C (676 °F). The peak-to-peak difference in salt centerline temperature is approximately 10 °C (18 °F), which at the low point in the diurnal cycle is in good agreement with the value (348 °C) presented in Figure 5-7. The peak salt-metal interface temperature is approximately 305 °C (581 °F), which is less than the performance specification of 317 °C. However, this is slightly higher than the values (291 °C to 295 °C) presented in Figure 5-7. The corresponding peak-to-peak difference for the salt-metal interface temperature is approximately 10 °C to 12 °C (18 °F to 22 °F).

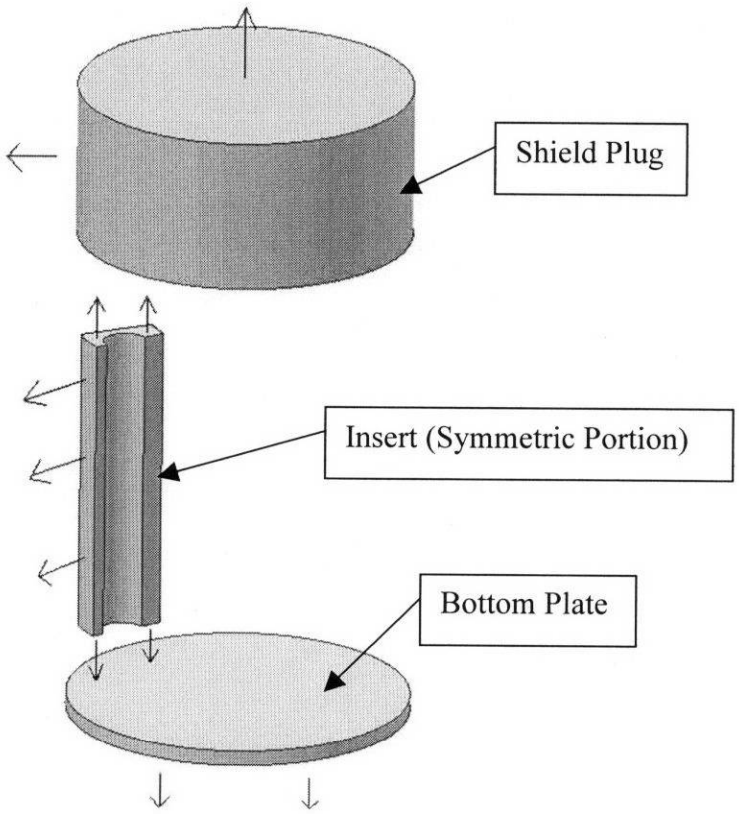

Figure 5-1. Overpack Model.

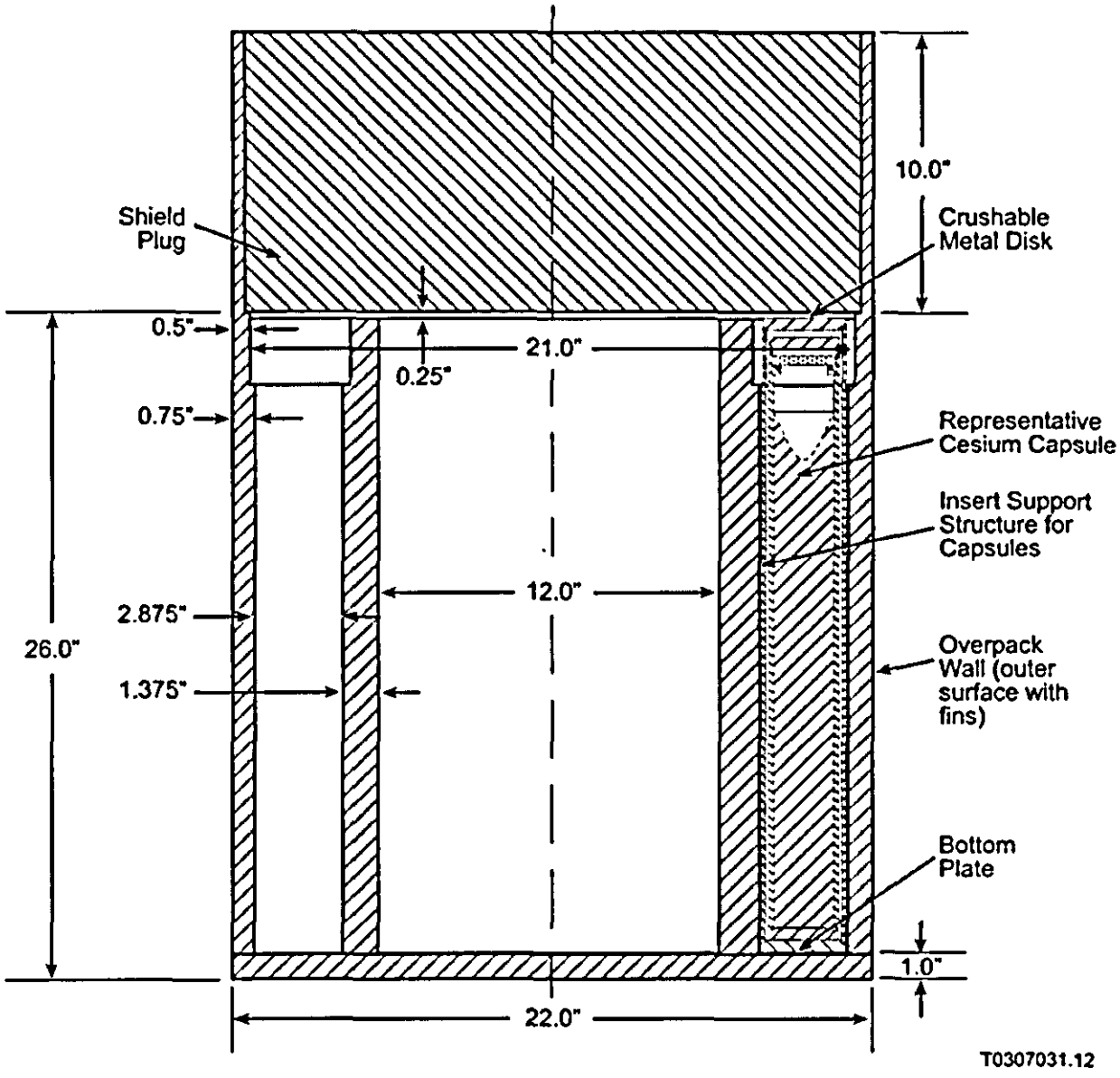

Figure 5-2. Revised Baseline Conceptual Design with Enhanced Axial Heat Transfer (Crushable Metal Disk).

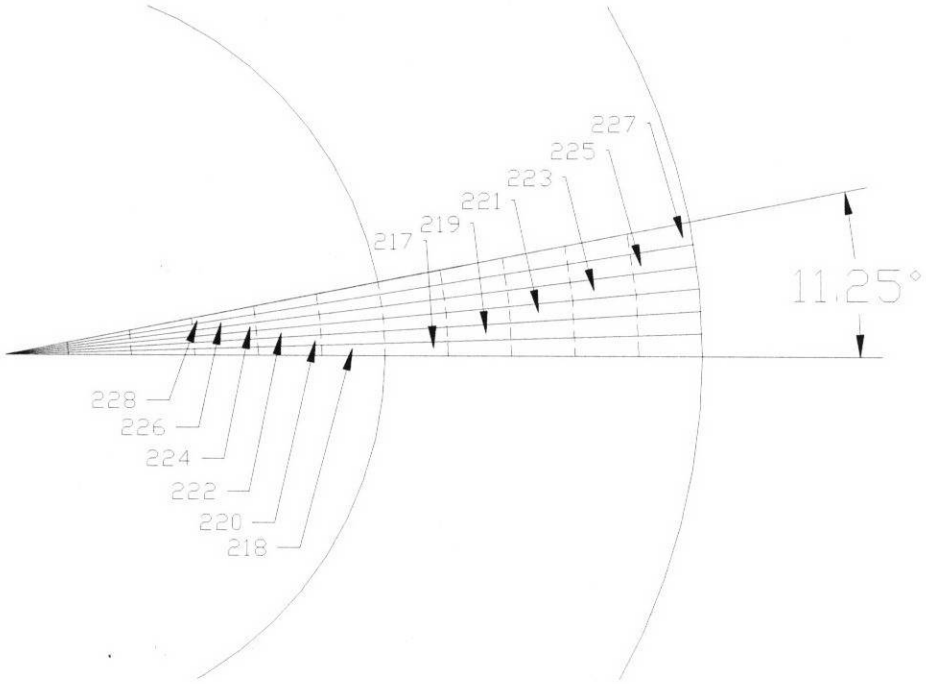

Figure 5-3. Nodalization of Bottom Plate.

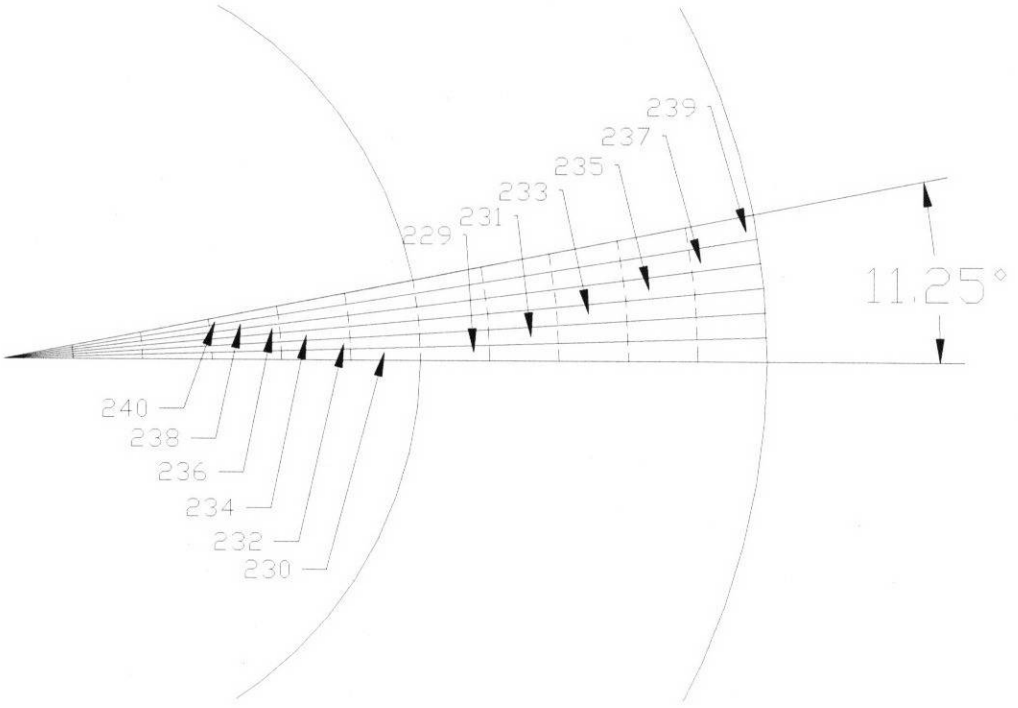

Figure 5-4. Nodalization of Shield Plug.

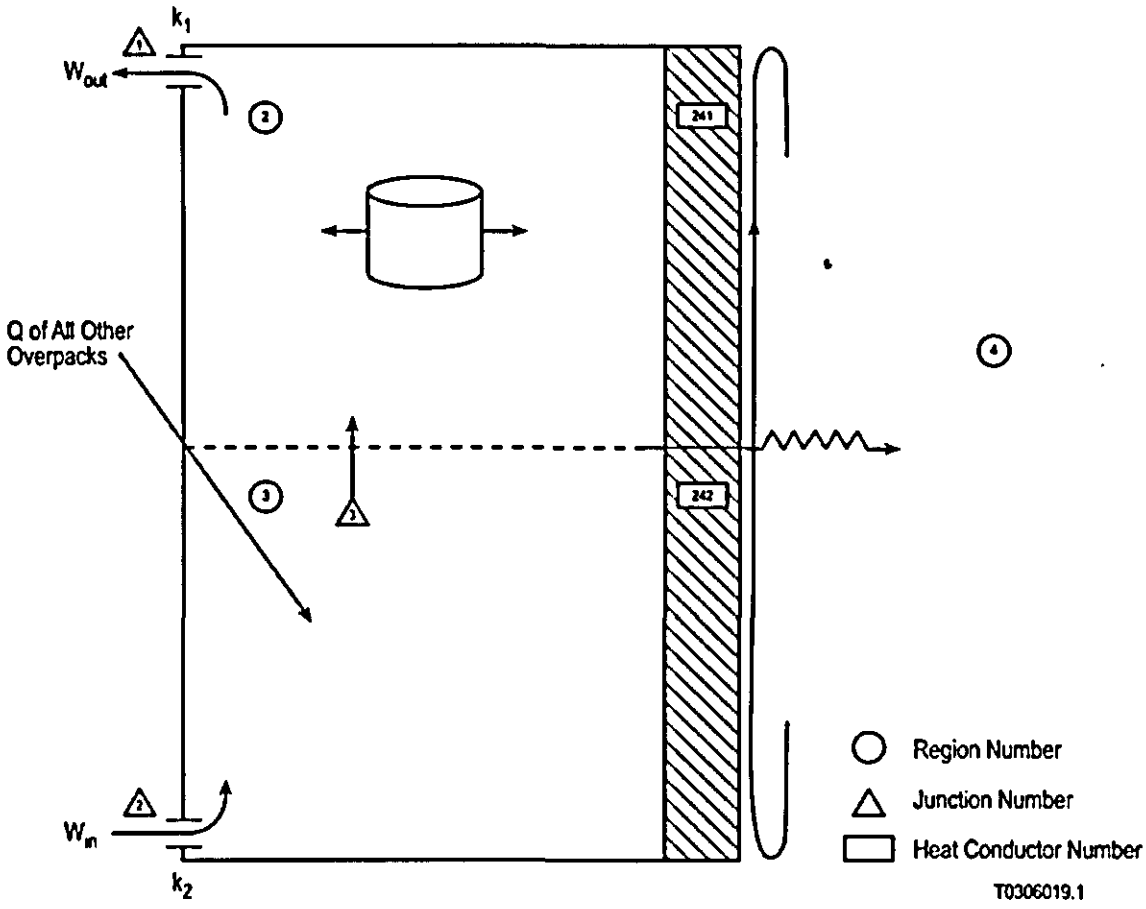

Figure 5-5. Conceptual Dry Storage Module Model with Overpacks.

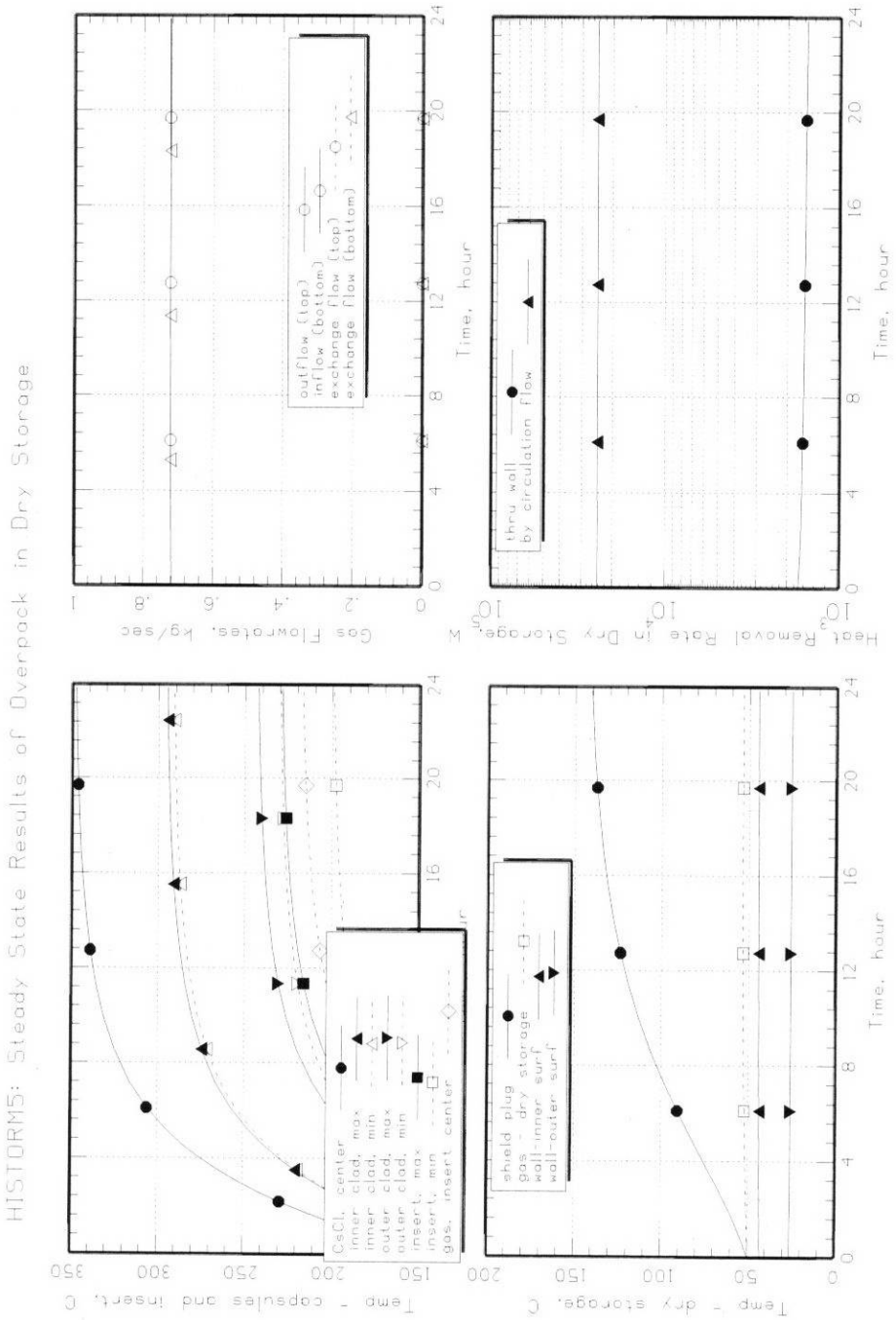

Figure 5-6. Steady State Results of Overpack in Conceptual Dry Storage Module.

Shield plug (above capsule and insert)

143.5	142.2	139.8	136.3
143.6	142.1	139.6	136.2

Capsule and Insert

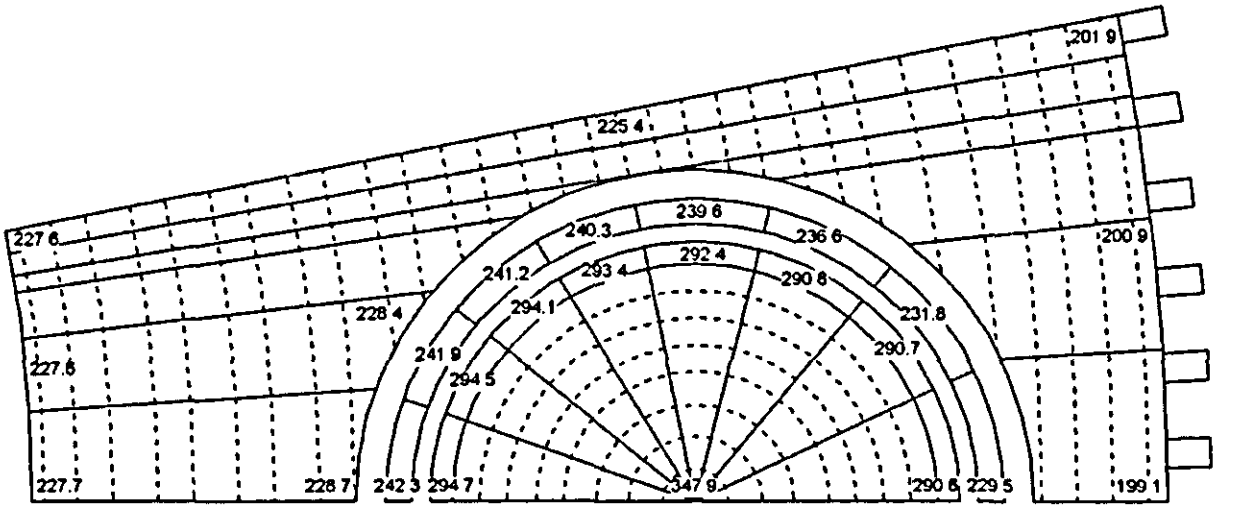

T0307031.10

Base plate (below capsule and insert)

208.7	206.7	201.3	194.2
209.2	206.4	200.9	193.9

Figure 5-7. Heat Sink Node Steady-State Temperature (°C) Results for Overpack in Conceptual Dry Storage Module.

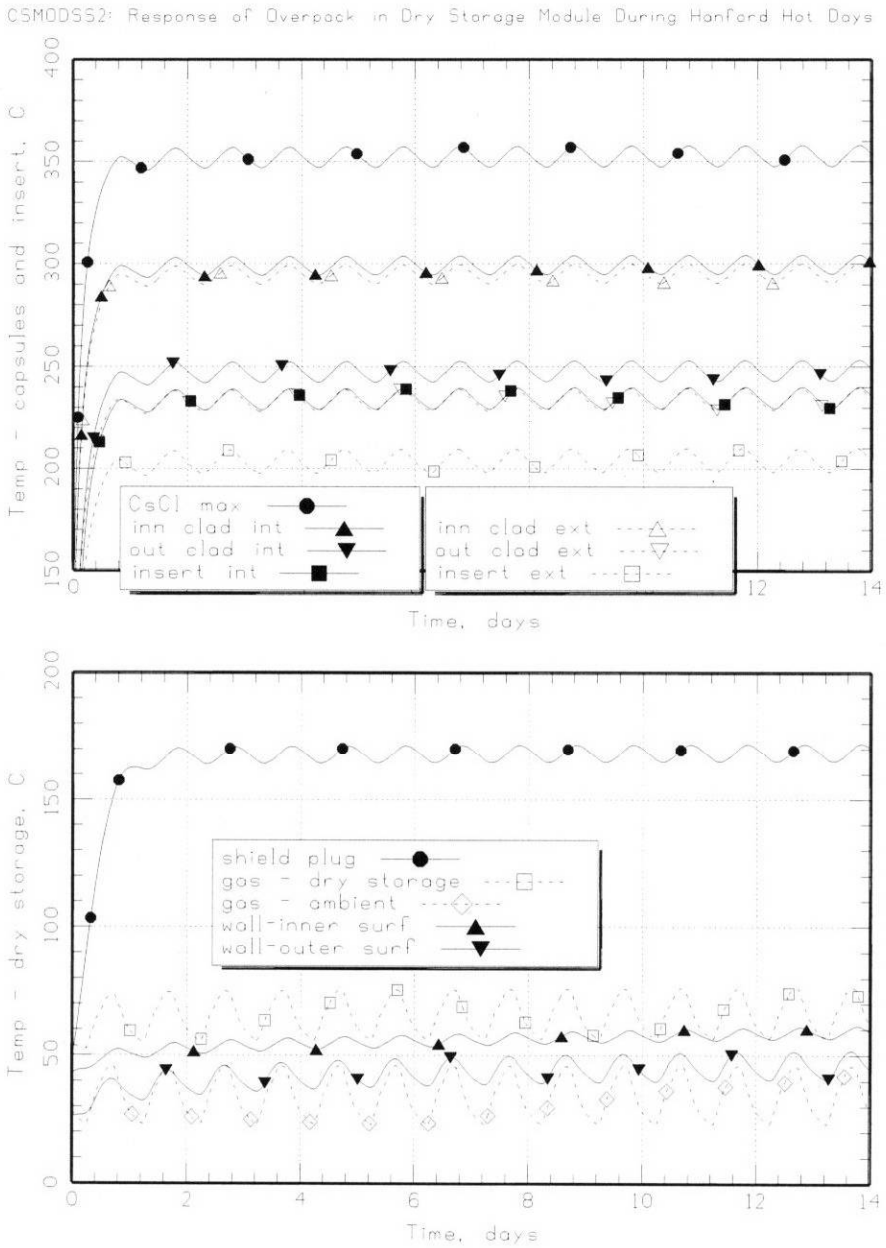

Figure 5-8a. Thermal Response of Conceptual Dry Storage Module vs. Time for Maximum Ambient Conditions (Diurnal Cycles)

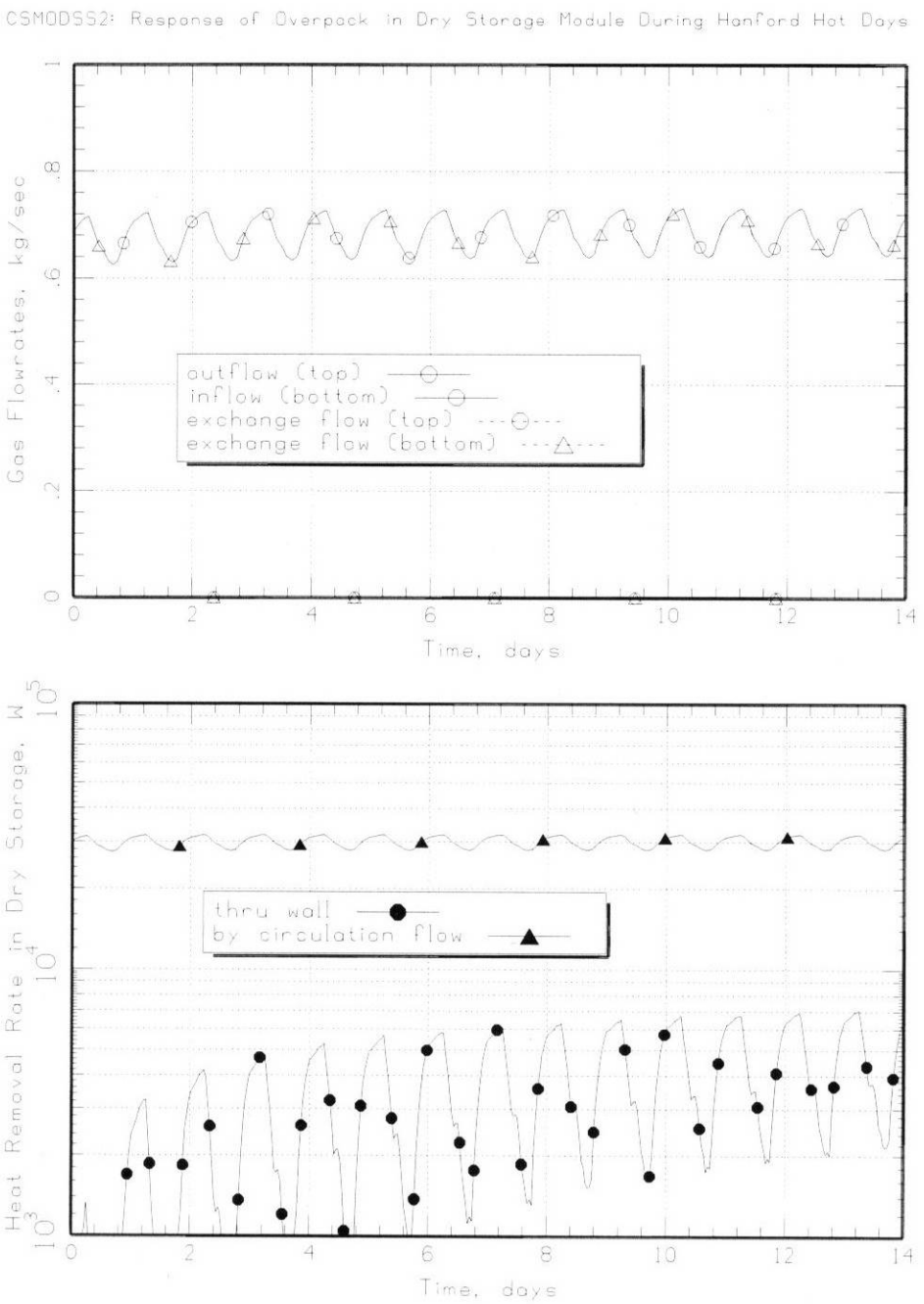

Figure 5-8b. Thermal Response of Conceptual Dry Storage Module vs. Time for Maximum Ambient Conditions (Diurnal Cycles).

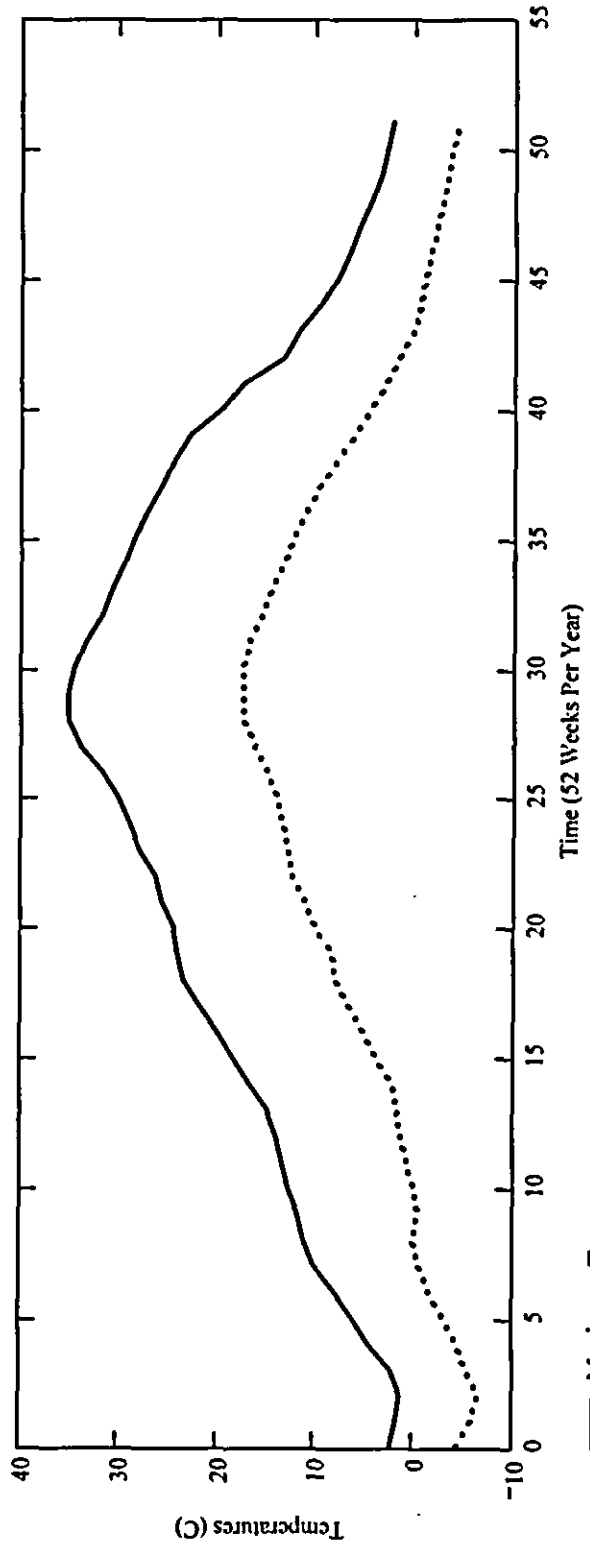

Figure 5-9. Hanford Nominal Maximum and Nominal Minimum Temperature vs. Time (One Year).

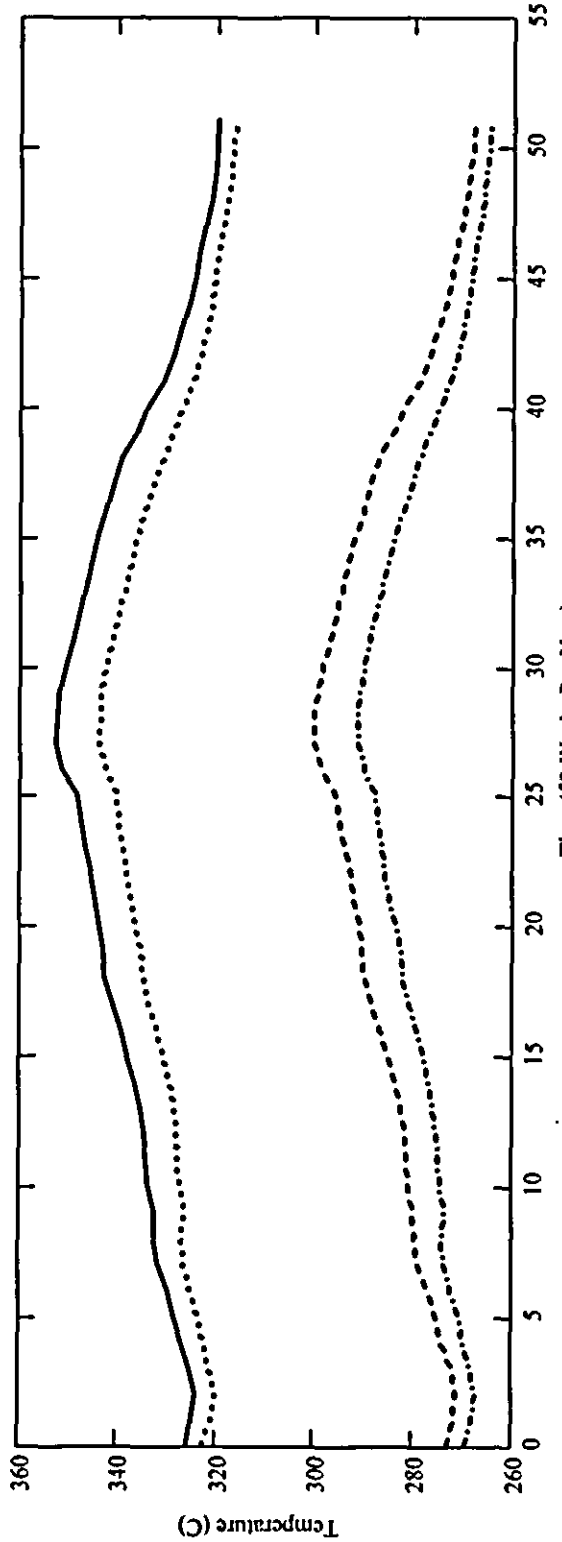

Figure 5-10. Maximum and Minimum Salt Centerline and Salt-Metal Interface Temperatures vs. Time (One Year).

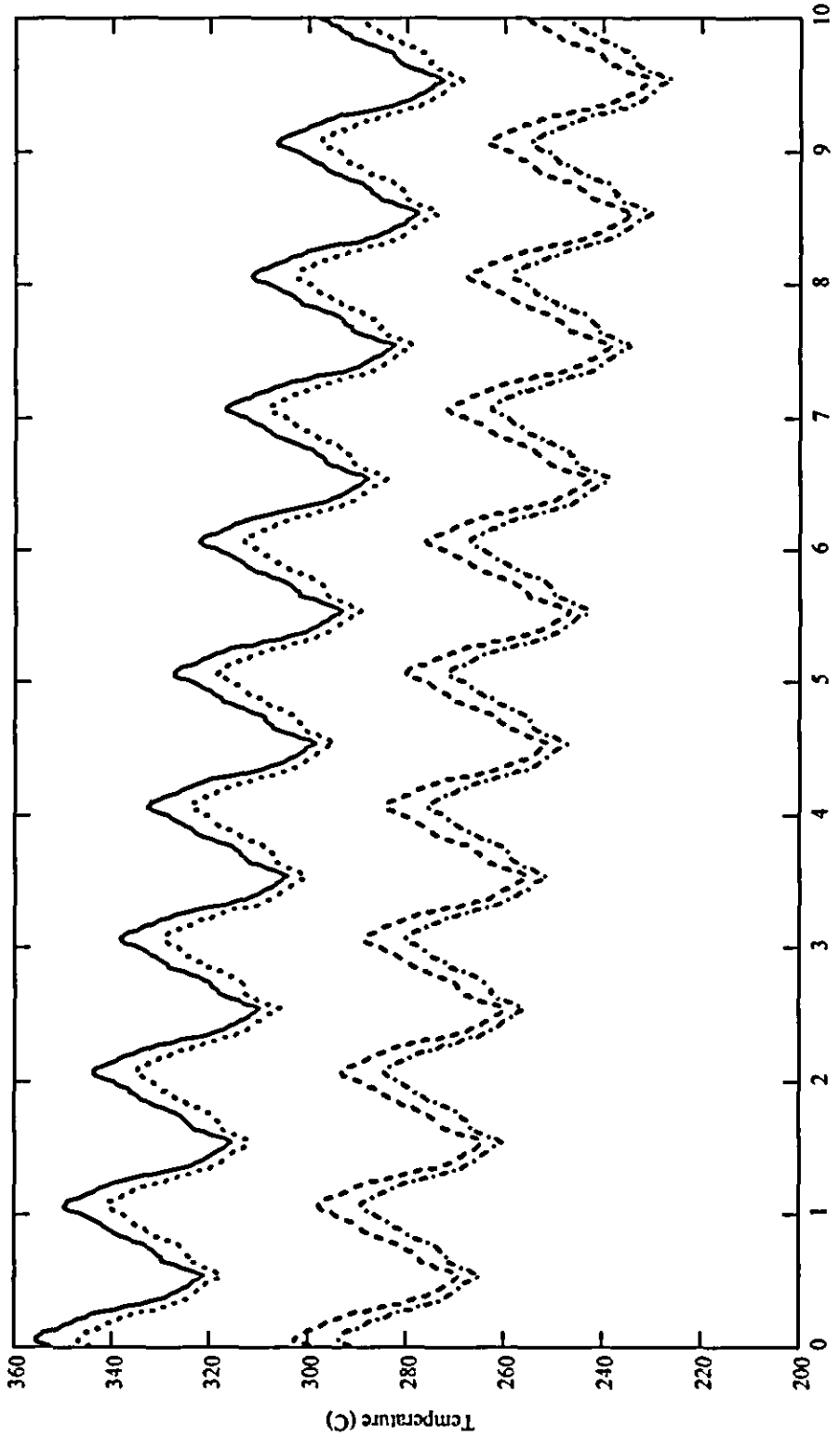

Figure 5-11. Maximum and Minimum Salt Centerline and Salt-Metal Interface Temperatures vs. Time (Ten Years).

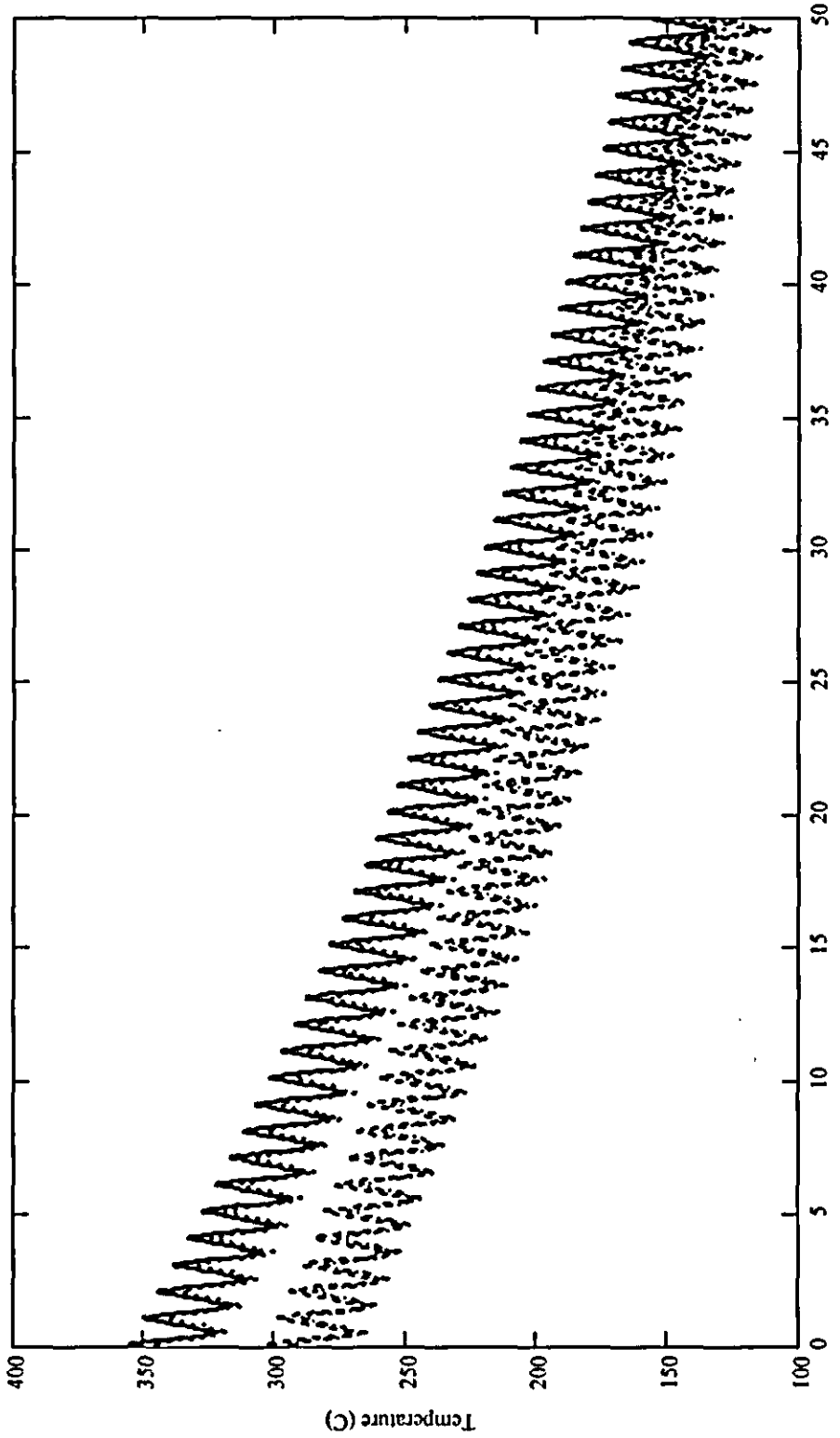

Figure 5-12. Maximum and Minimum Salt Centerline and Salt-Metal Interface Temperatures vs. Time (Fifty Years).

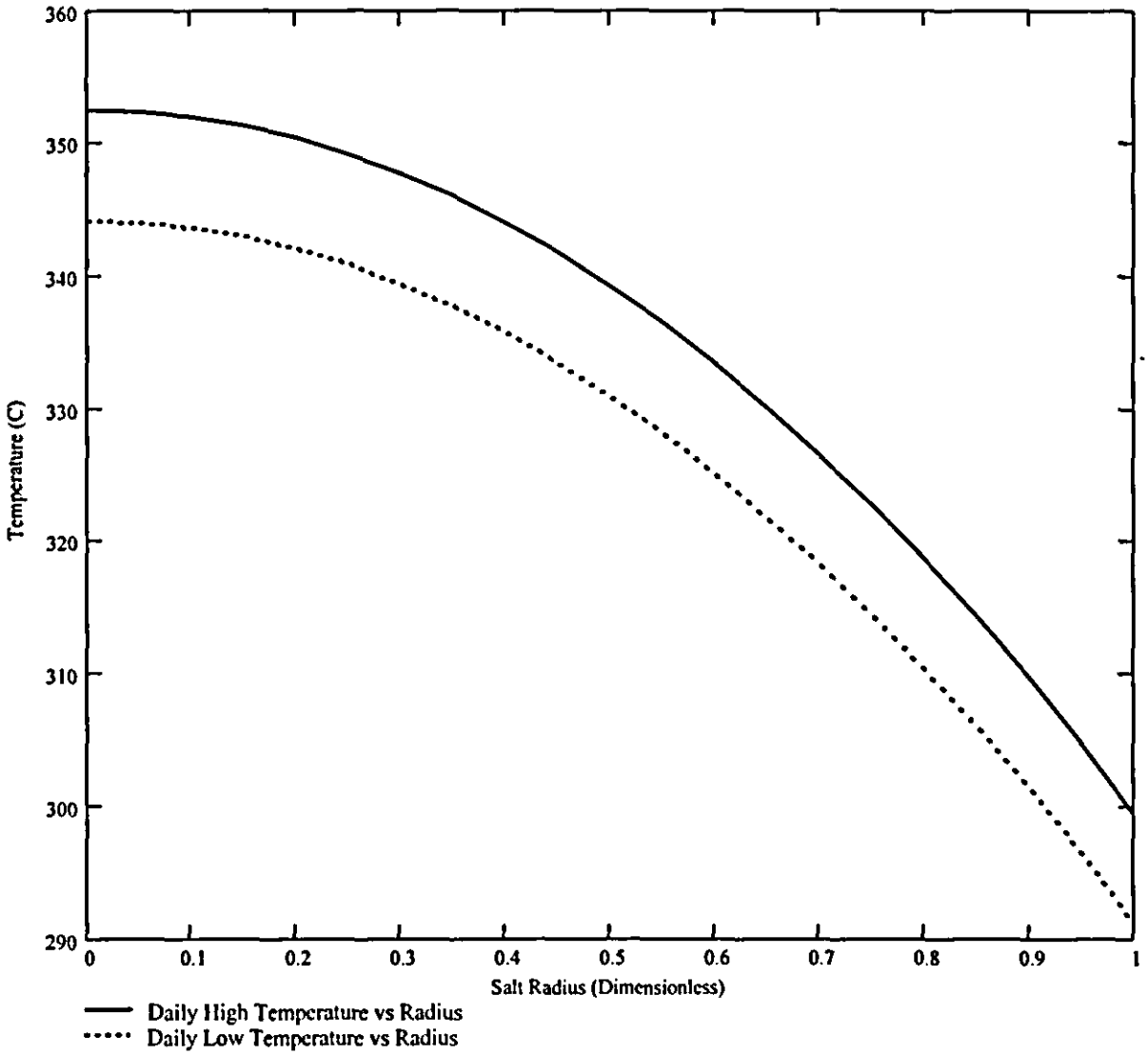

Figure 5-13. Radial Temperature vs. Normalized Salt Radius for Daily High and Low Ambient Temperature (July 1).

Table 5-1. Solar Insolation Data for Hanford Site (Irwin 2000).

Time	Insolation Langleys[1]	Insolation Btu/ft^2	Time	Insolation Langleys[1]	Insolation Btu/ft^2
12 –01 a.m.	0	0	12 – 01 p.m.	71.9	265.1
01 – 04 a.m.	0	0	01 – 02 p.m.	67.8	250.0
04 –05 a.m.	2.5	9.2	02 – 03 p.m.	60.5	223.1
05 – 06 a.m.	908	36.1	03 – 04 p.m.	49.9	184.0
06 – 07 a.m.	22.1	81.5	04 – 05 p.m.	37.2	137.2
07 – 08 a.m.	36.6	134.9	05 – 06 p.m.	23.6	87.0
08 – 09 a.m.	49.9	184.0	06 – 07 p.m.	11.3	41.7
09 – 10 a.m.	60.7	223.8	07 – 08 p.m.	2.9	10.7
10 – 11 a.m.	68.3	251.8	08 – 09 p.m.	0	0
11 – 12 a.m.	72.1	265.8	09 – 12 p.m.	0	0
			Sum	647.1	2386

[1]A Langley is defined as 1 gram-calorie/cm^2. To convert to Langley's to a heat flux (J/s-m2) given a one hour (3600 seconds) interval multiply by 11.6306.

Irwin, J. J., 2000, *Thermal Analysis Methods for Safety Analysis Reports for Packaging*, WHC SD-TP-RPT-005, Rev. 1, Fluor Hanford, Inc., Richland, Washington.

6.0 TRANSIENT ANALYSIS OF OVERPACKS IN DRY STORAGE MODULE

6.1 PROCESS PROOF-OF-DRYNESS

Processing conditions, such as a vacuum test for capsule dryness, will increase the capsule temperatures for a few hours to a few days.

Steady-state response of the overpack was simulated for an end-state vacuum condition. No conduction (just radiation) between the outer surface of the outer capsule and the inner wall of the capsule bore was assumed. The boundary conditions for the outer surface of the overpack will depend on the WESF hot cell conditions. Based on measured conditions within a "G all" cell with a BUSS cask containing 16 Cs capsules, the cell ambient condition obtained was 35 °C (95 °F). A "G" cell wall emissivity of 0.5 corresponding to smooth white walls was assumed for the emissivity of the ambient gas to which the overpack wall radiates.

Figure 6-1 presents a "snapshot" of the steady-state temperature distribution within the shield plug, the bottom plate, the capsule, and the insert. See Figures 4-10, 5-3, and 5-4 for corresponding nodalization diagram. The top two rows are shield plug; the first row is along a symmetry line between capsules and the second row is along a symmetry line cutting through the capsule center. The bottom two rows are bottom plate. For the capsules and insert, the left edge is the overpack insert interior surface, the right edge is the overpack wall, the top edge is along the line-of-symmetry between capsules, and the bottom edge is along a symmetry line cutting through the capsule center. Interior temperatures along the bottom edge are steel insert at gap surface, average capsule outer wall, average capsule inner wall (i.e., salt-metal interface), capsule maximum, average capsule inner wall (toward insert exterior), average capsule outer wall, and overpack wall.

The inner capsule inner wall temperatures are shown by eight values arranged as a semicircle around the maximum value. The outer capsule outer wall temperatures are shown by eight values just outside inner wall values. The steel insert temperature at the capsule gap is shown by seven values closest to outer wall values (three to left, three to right, one above).

With a vacuum condition within the overpack, an appreciable temperature drop develops in the gap between the outer capsule and the capsule borehole: 187°C vs. 30°C when the overpack is filled with helium. Consequently, significantly higher temperatures are observed in the salt and salt-metal interface temperature. The maximum salt temperature for the proof-of-dryness test is about 480 °C for the preliminary conceptual design and exceeds a possible minimum melting point value of 430 °C (Figure 6-2a). The maximum salt-metal interface temperature during the process proof-of-dryness test is approximately 413 °C. This is less than the performance specification for 450 °C for the salt-metal interface temperature during process or process upset events. Clearly the design can be refined to reduce the maximum temperature if necessary. Note that in this case only a fraction of the salt in its interior would be molten.

Figure 6-2a presents the transient temperature distribution. Steady-state conditions are reached after a day and a half. Figure 6-2b presents the heat removal from various surfaces within the overpack: 1,380 W by convection on the overpack wall, 600 W by radiation on the overpack

wall, 290 W by convection on the shield plug surface, and 230 W by radiation on the shield plug surface, for the total of 2,500 W. It is slightly less than the assumed power of the individual overpack, 2,560 W, because the overpack has not reached a perfect steady-state condition.

6.2 DRY STORAGE MODULE LOSS OF VENTILATION

Figures 6-3a and 6-3b present the thermal response of the overpack in the conceptual dry storage module over the 24 hours following an assumed complete blockage of the inlet ports. The steady-state case presented in Section 5.3 provides the initial temperature distribution. Counter-current flow-in exit ports are disabled as a conservative assumption.

As shown in Figure 6-3a, as soon as the flow stops in the storage module, the storage gas temperature rises rapidly (within the first few minutes) from approximately 54 °C to about 120 °C. This establishes the temperature gradient (difference) between the gas and the wall necessary to transfer the assumed decay power to the wall in the absence of flow. Over the next 24 hours, the storage gas temperature gradually increases another 70 °C to reach 190 °C. This parallels the wall inner surface temperature increase. The storage gas temperature sets the ambient condition for the overpack. Consequently, the CsCl center temperature increases about 100 °C to reach almost 450 °C over the 24 hours. Maximum salt temperature approaches, but does not exceed, a possible minimum melting point of 430 °C for the dry storage module loss-of–flow (LOF) accident condition during a 24-hour mission time (Figure 6-3a).

One key observation this simulation reveals is the large heat capacity of the storage wall in absorbing the decay power rejected by the overpacks. On the other hand, poor thermal conductivity (1.0 W/m-K) of the relatively thick dry storage wall (0.75 m [29 in.]) causes the thermal wave to propagate only a fraction of the thickness after one day (upper right). The outer surface of the dry storage module feels no impact from the loss of cooling inside.

6.3 DRY STORAGE MODULE EXTERNAL FIRE

The dry storage module is engulfed by a fire at 800 °C for 30 minutes. A 600-minute cool down phase was assumed. A total transient time of 630 minutes was simulated. This is a restart run continuing from the steady state condition established in the overpack and the dry storage module (see Section 5.3).

The fire was simulated by introducing 800 °C carbon dioxide gas into the dry storage module at the rate of 10 kg/sec (4.5 lb/sec) as a species source. The inlet to the dry storage was blocked to prevent atmospheric air from entering. The outside ambient temperature was fixed at 800 °C. During the first 30 minutes, the overpack and the dry storage module walls were heated by convection and radiation heat transfer from the gas. After 30 minutes, the fire was assumed over; the carbon dioxide gas source was turned off, the ambient temperature was restored to 22 °C, and the inlet junction was opened. Air flowing through the dry storage module will cool the overpack and the module walls.

The results are shown in Figures 6-4a and 6-4b. The upper portion of Figure 6-4a presents the transient temperatures in the capsule; note how the outer structure "leads" and the inner values "lag." The maximum salt-metal interface temperature (upward-pointing open triangle) peaks at

about 470 °C at 34 minutes. Maximum salt temperature is just over 520 °C. This assumes a pure conduction without melting. Note how energy stored in the system impedes a cooldown of the salt. Bulk salt melting may occur during a fire scenario (Figure 6-4a). The present fire scenario is likely conservative, so this result may not be representative of performance of a final design.

The lower portion of Figure 6-4a presents the dry storage module temperatures. The dry storage module gas temperatures are clipped since the scale only goes to 400 °C; the fire is 800 °C. The shield plug obtains a maximum temperature of approximately 310 °C. The upward pointing triangle is the inner surface of the dry storage module wall; it shows the major affect in energy storage.

The upper portion of Figure 6-4b presents the transient temperatures in the dry storage module wall. Most of the energy is deposited within the first four cm as would be expected given the relatively short duration of the fire and the low thermal diffusivity of the dry storage module wall. The low thermal diffusivity impedes the after-fire cool down.

The lower portion of Figure 6-4b presents a heat balance over the module wall. During the fire, the wall receives heat on both surfaces. After the fire, the wall rejects the stored heat on both surfaces. During the fire, a significant amount of heat is absorbed by the wall , up to 2,000 kW on the inner surface.

6.4 STRONTIUM CAPSULES

Table 4-10 indicates that the salt-metal interface and centerline temperatures of the maximum Sr capsule are approximately 611 °C and 692 °C, respectively, when air is the backfill gas. Table 4-11 indicates that the salt-metal interface and centerline temperatures of the maximum Sr capsule are approximately 502 °C and 571 °C, respectively, when helium is the backfill gas. Therefore, the project specification of 540 °C salt-metal interface temperature for normal storage is attainable (501 °C is based on the maximum capsule power with helium backfill).

The next step is to relate these temperatures to those expected during process operations and accident conditions such as a flow blockage and fire accident. Because total power in a module is assumed the same for either capsule type, and because the heat capacities are dominated by structural steel, the same temperature increase observed for a Cs capsule under vacuum conditions or during a flow blockage or fire event is a good first order estimate of what would be predicted for the Sr capsule overpacks.

During process operations, such as a vacuum test for capsule dryness, temperatures will rise for a duration of a few hours to several days. From Figures 6-1 and 6-2a, a temperature rise of approximately 140 °C was noted over the reference (Figure 5-7) steady-state conditions . This would result in a salt-metal interface and centerline temperature of approximately 642 °C and 712 °C, respectively, for Sr capsules. (The final temperatures under vacuum conditions are independent of the initial fill gas.) This exceeds the project specification of 540 °C for the salt-metal interface temperature and may need to be increased to as much as 700 °C. Therefore, maintaining the maximum salt-metal interface temperature less than the performance

specification of 540 °C may not be achievable for high-power Sr capsules. Temperatures of approximately 700 °C could occur without some form of active cooling.

Raising the performance specification for process and process-upset events from 540 °C to at least 700 °C, and possibly higher, is a viable option. Note that if a loss of helium backfill constitutes a process-upset condition, then the project specification of 540 °C will need to be increased to 700 °C.

The flow blockage results from Figure 6-3a indicate a temperature rise of approximately 100 °C. This results in a Sr capsule salt-metal interface and centerline temperature of approximately 602 °C and 671 °C, respectively. Hence, the salt-metal interface performance specification of 800 °C for accident conditions is adequate for this accident condition.

Response during a fire is driven by external heat load and heat capacity of the overpack and not by capsule power. From Figure 6-4a, a 200 °C increase from nominal conditions would be expected and would result in a Sr capsule salt-metal interface and centerline temperature of approximately 702 °C and 771 °C, respectively. Hence, the salt-metal interface performance specification of 800 °C is adequate for this accident condition.

6.5 SUMMARY AND CONCLUSIONS

Significantly, higher temperatures are estimated during processing and accident conditions. It is recommended that the final design include an in-depth thermal analysis of all process events, process upsets, and postulated accident conditions. The results of these analyses are used for corrosion analysis in WMP-16937. It is recommended that these significantly higher temperatures also be considered with respect to metal properties and weld properties. In addition, it is recommended that these temperatures be considered with respect to cracking, fracture, or rupture of capsules.

The process proof-of-dryness transient for CsCl capsules indicates that significantly higher temperatures will occur in the salt (480 °C) and salt-metal interface temperature (413 °C).

The loss-of-ventilation results for Cl capsule overpacks indicate the dry storage module gas temperature gradually increases to reach 190 °C over 24-hours. The storage gas temperature, in turn, sets the boundary condition for the overpack. Consequently, the CsCl center temperature increases about 100 °C and reaches 450 °C over the 24 hours. The salt-metal interface temperature increases to approximately 380 °C over 24 hours.

The external fire results indicate the maximum salt-metal interface temperature for the CsCl capsules peaks at about 470 °C at 34 minutes. Maximum salt temperature is just over 520 °C. This assumes pure conduction without melting. After a simulated cool down period of six hours, the dry storage module and overpack have not yet recovered the pre-fire initial conditions.

Raising the Sr capsule performance specification for process and process-upset events from 540 °C to at least 700 °C, and possibly higher, is a viable option. With a process temperature limit of 700 °C, centerline temperatures would be less than 800 °C. This remains well below any temperatures at which phase transition or melting could occur in the Sr capsules for both process

upset and accident conditions. For accident conditions, the salt-metal interface performance specification of 800 °C is adequate for Sr capsules. Metal aging effects must be addressed.

For Cs capsules, the performance specifications for the salt-metal interface temperatures during process/process upset and accident conditions, 450 °C and 600 °C, respectively, were not exceeded.

However, with a process/process upset limit of 450 °C at the salt-metal interface, centerline temperatures in the CsCl capsules could potentially exceed 500 °C. In addition, during the fire simulation the salt centerline temperature exceeded the conservative 430 °C melting point for a period of a few hours, with a maximum temperature predicted to be approximately 520 °C.

In addition to corrosion and salt thermal expansion issues, the affects of elevated metal temperatures on the fracture toughness of metal and welds must be considered. Refer to WMP-16938 and WMP-16939 for additional discussion.

Shield plug (above capsule and insert)

150.6	149.5	147.3	144.1
150.8	149.4	147.2	144.1

Capsule and Insert

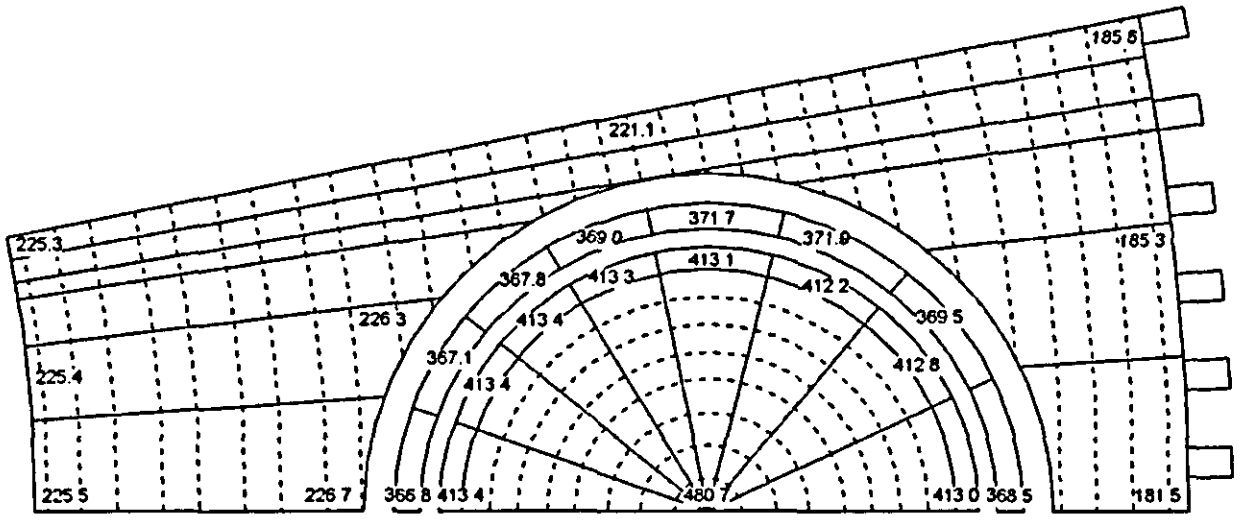

T0307031.11

Baseplate (below capsule and insert)

206.8	204.4	198.8	192.2
207.1	204.2	198.7	192.3

Figure 6-1. Steady State Heat Sink Node Temperature Map (°C) for Shield Plug, Insert with Capsule, and Bottom Plate for Vacuum Conditions. (Process Proof-of-dryness)

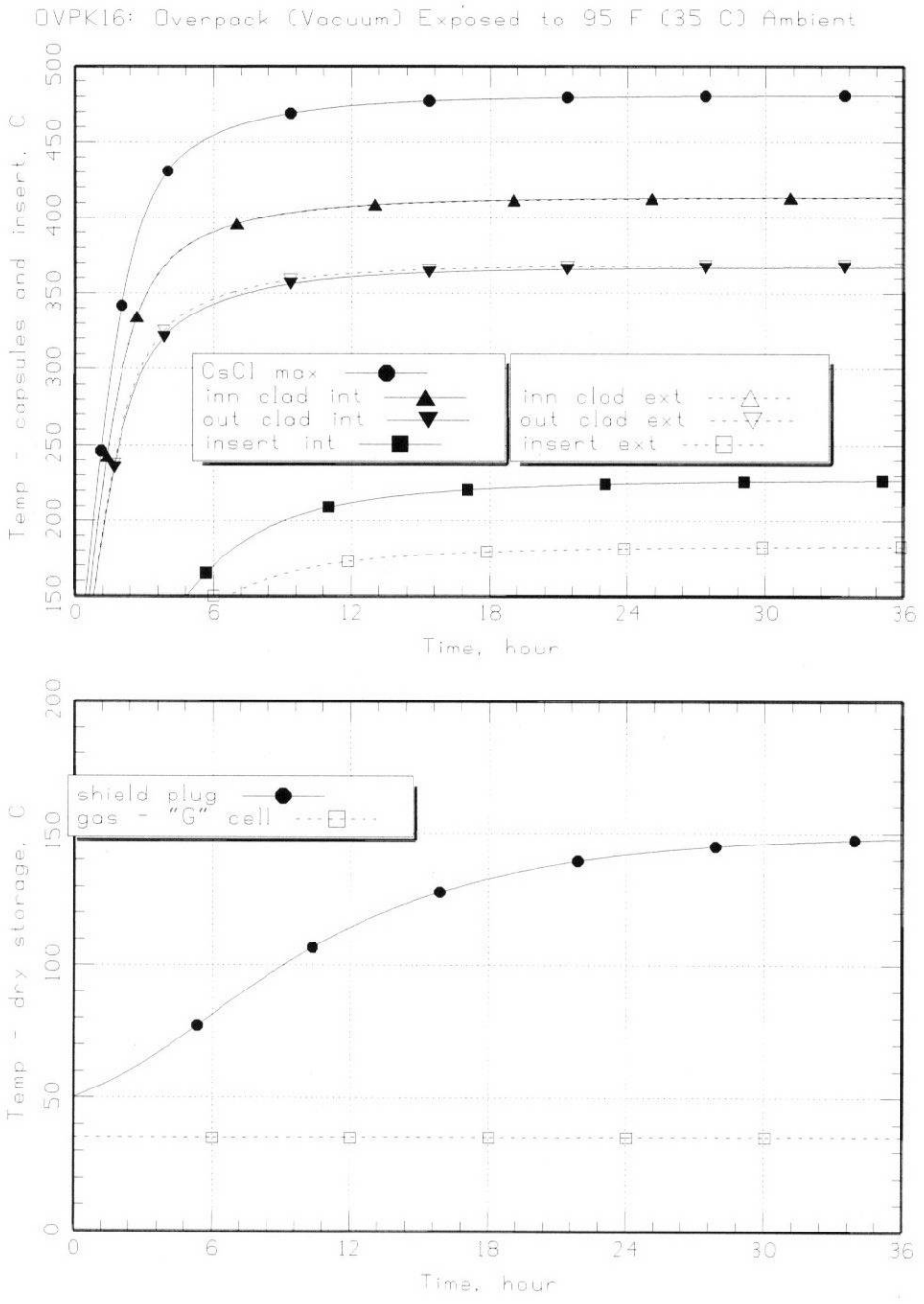

Figure 6-2a. Thermal Response of Vacuumed Overpack Exposed to 95ºF (35ºC).

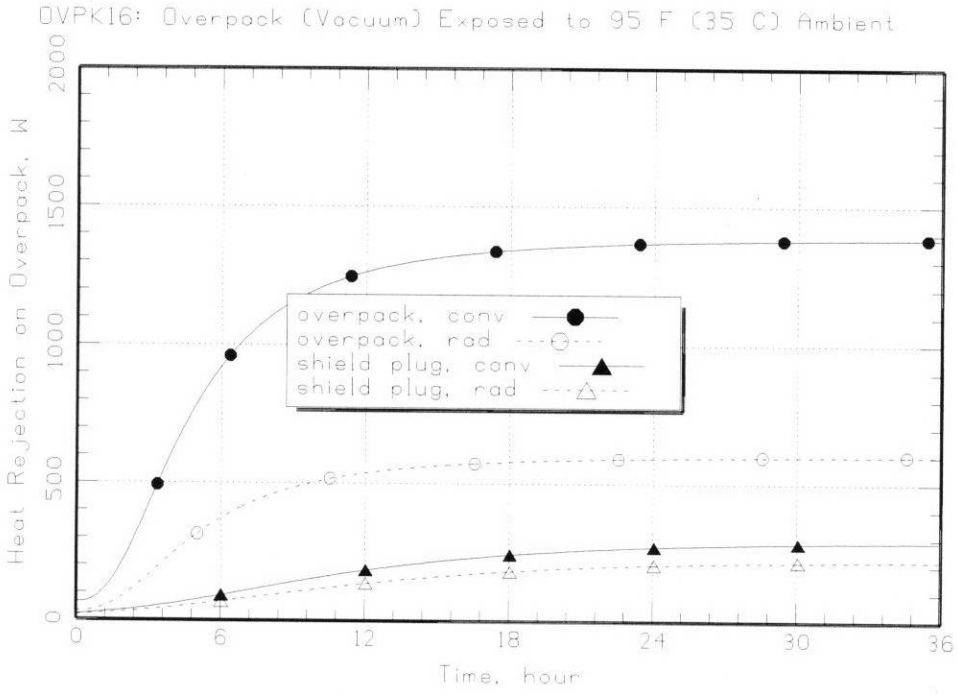

Figure 6-2b. Thermal Response of Vacuumed Overpack Exposed to 95°F (35°C).

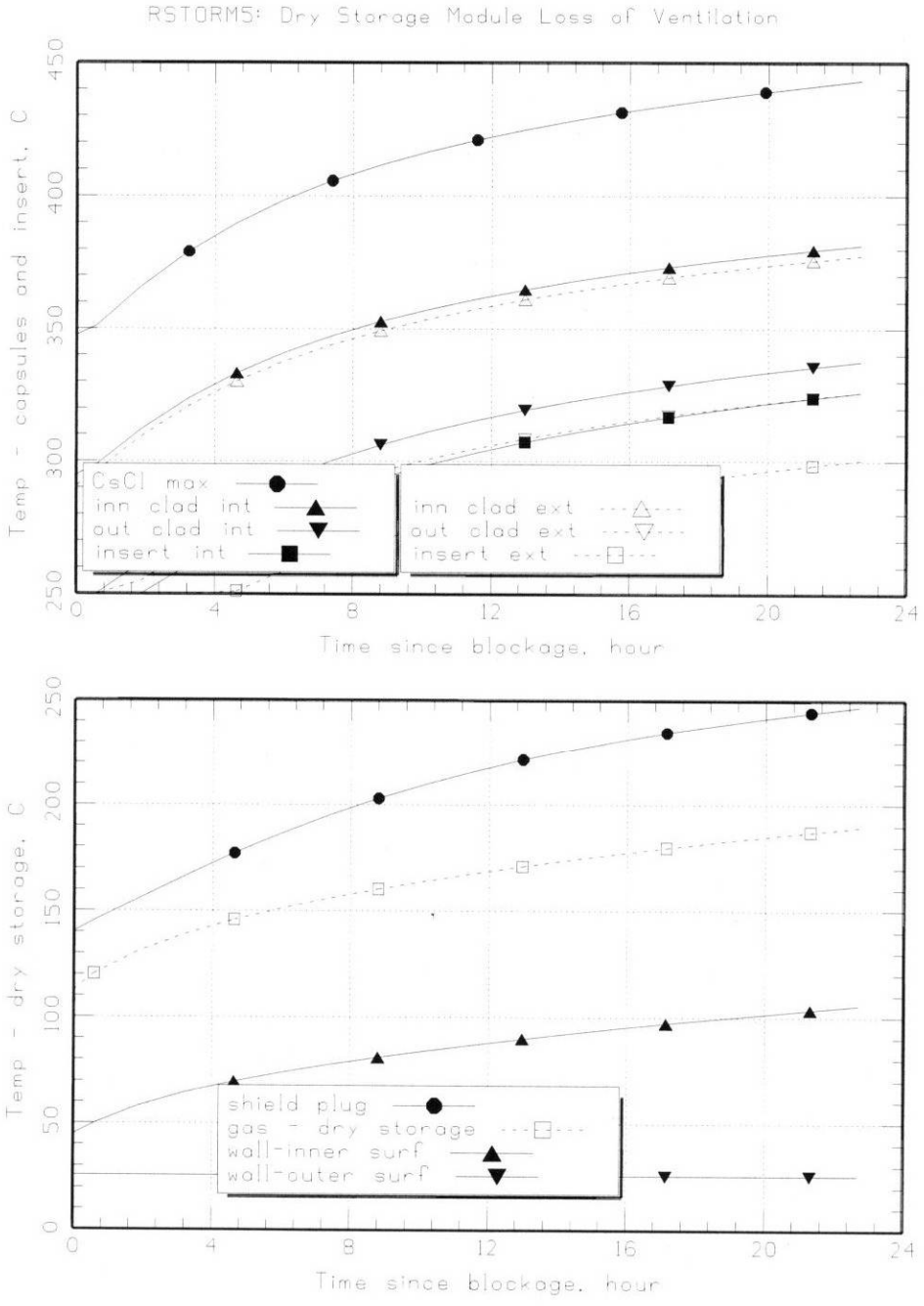

Figure 6-3a. Results of Dry Storage Loss of Ventilation Scenario.

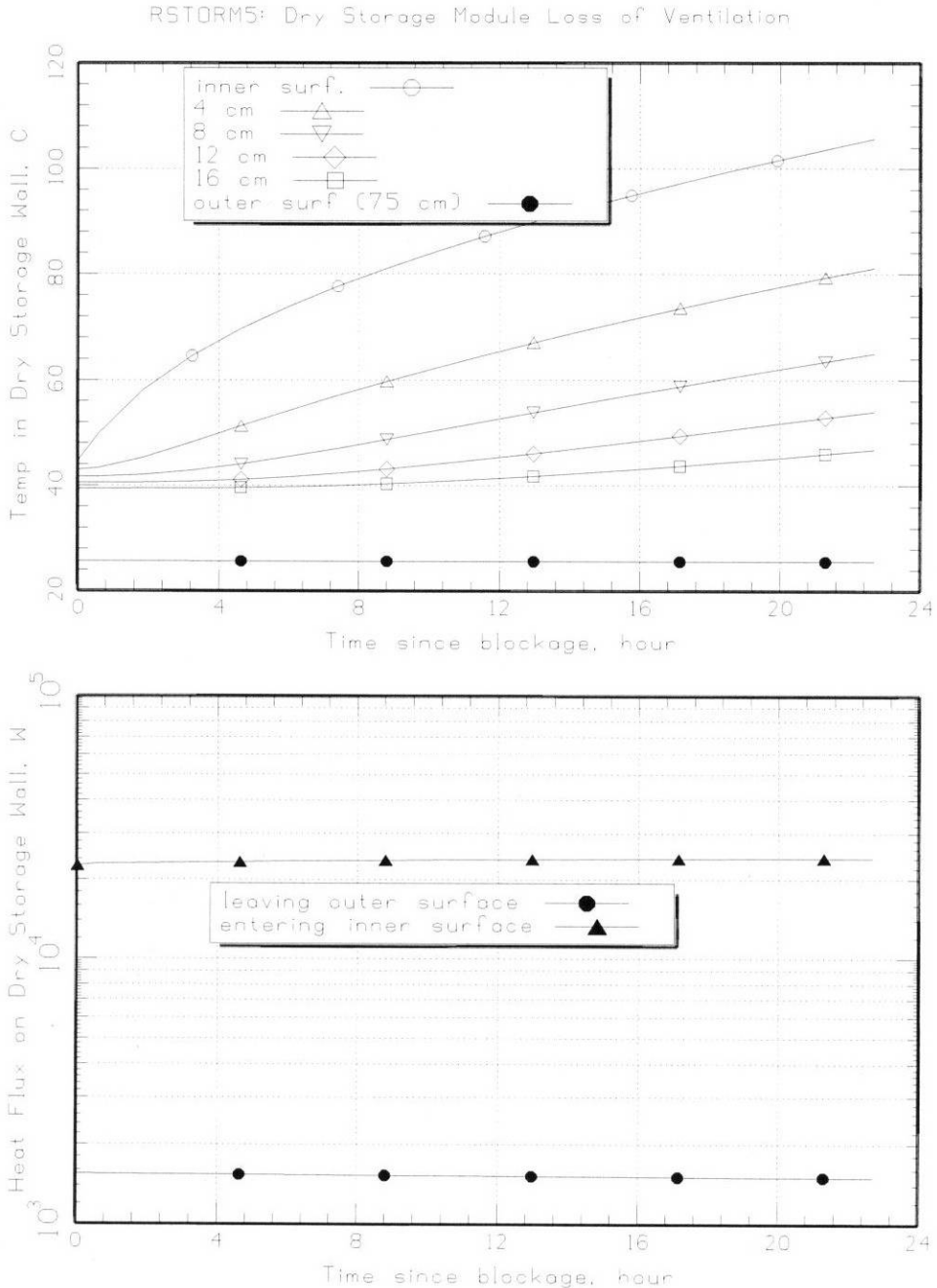

Figure 6-3b. Results of Dry Storage Loss of Ventilation Scenario.

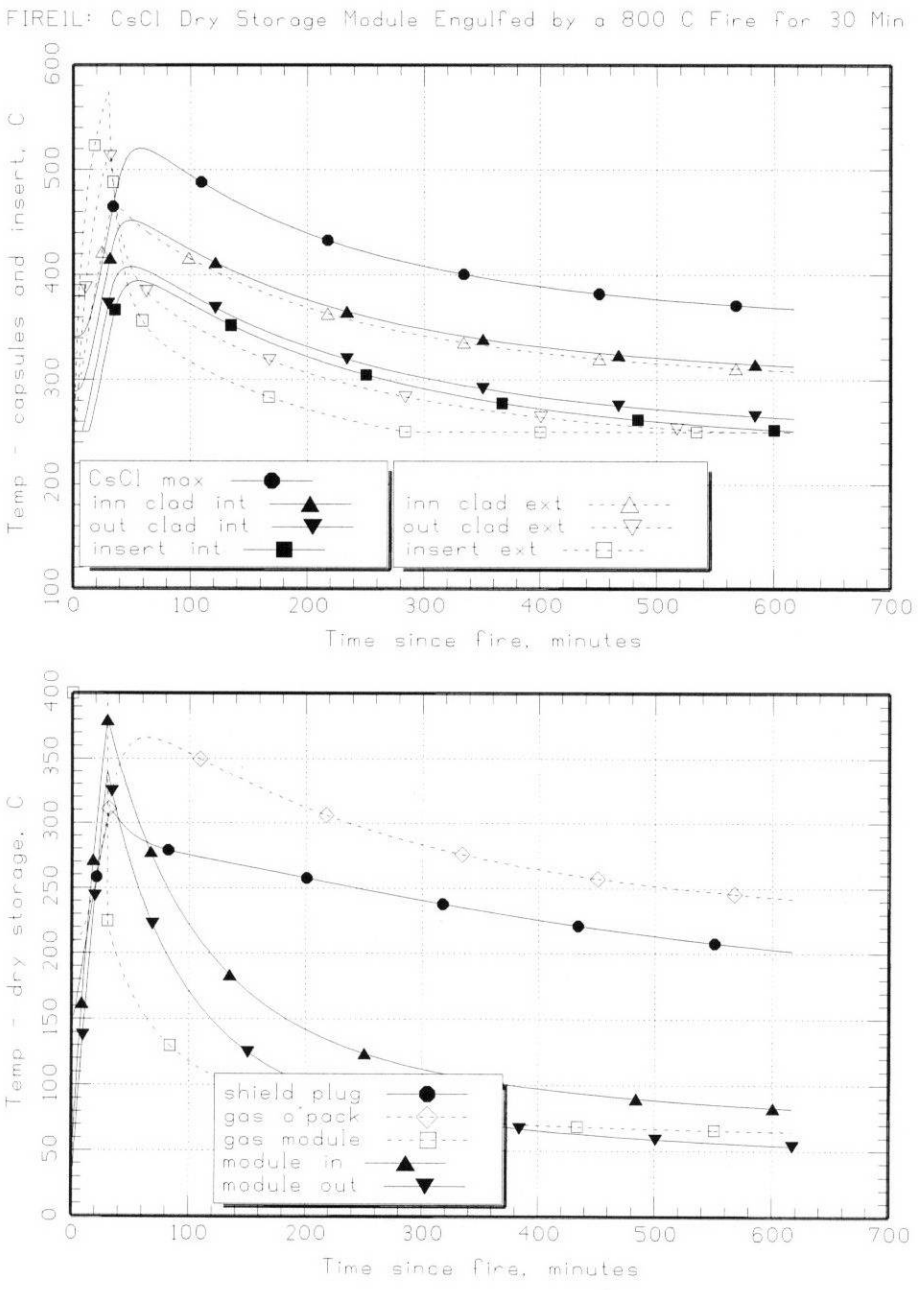

Figure 6-4a. Results of Dry Storage External Fire.

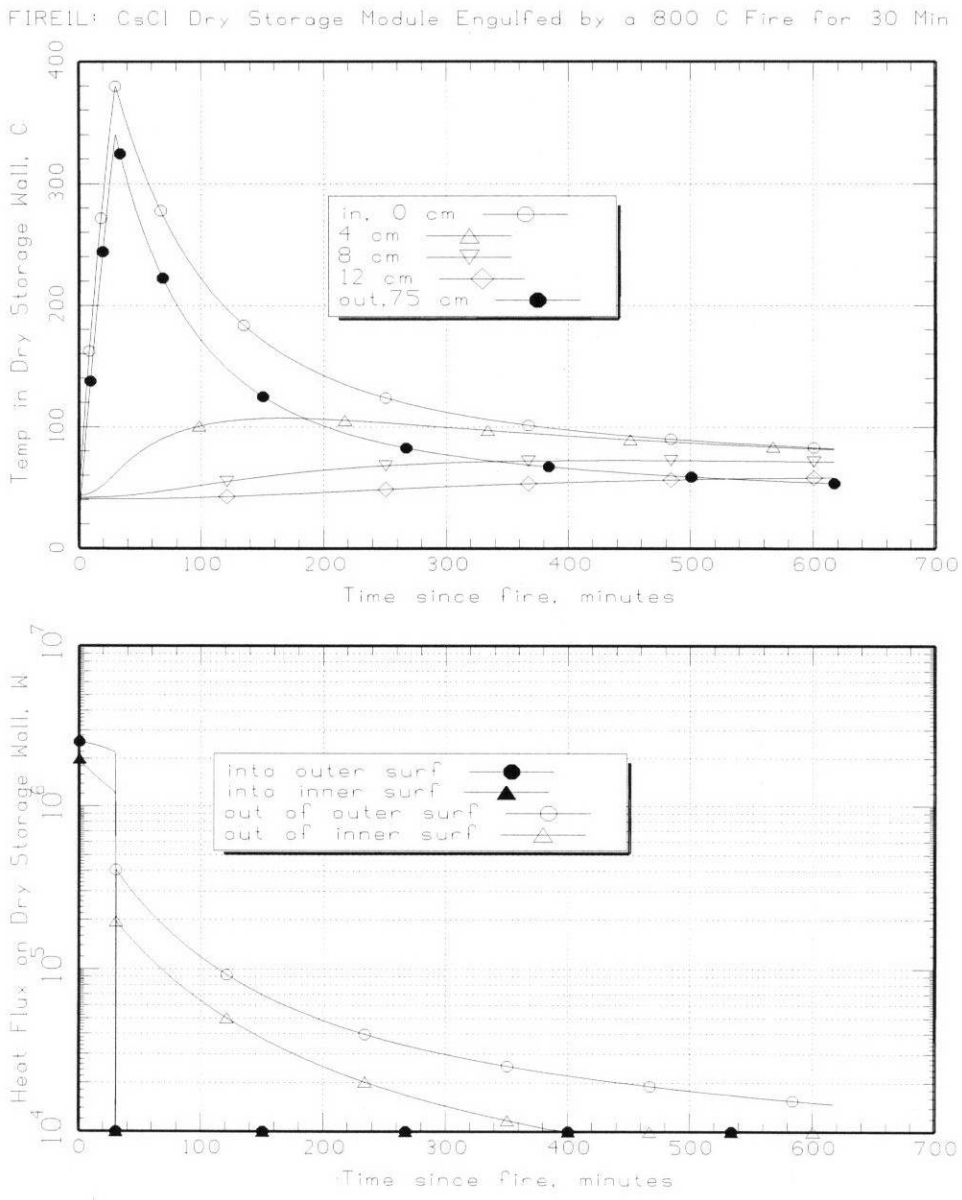

Figure 6-4b. Results of Dry Storage External Fire.

7.0 REFERENCES

BNFL, Inc. and FAI (Fauske & Associates, Inc.), 1999, *Topical Report on the Management of Risks Posed by Explosive Hazards Present at the RPP-WTP*, RPT-W375-SA00002, Rev. A. Richland, Washington.

Bird, R. B., W. E. Stewart, and E. N. Lightfoot, 1960, *Transport Phenomena,* John Wiley and Sons, Inc., New York, New York.

Churchill, S. W. and H. H. S. Chu, 1975, "Correlating Equations for Laminar and Turbulent Free Convection from a Vertical Plate," *Int. J. Heat Mass Transfer,* 18, 1323.

Crowe, R. D. and R. D. Lanning, 2002a, *Analysis of a HLW Process Vessel Hydrogen Deflagration Using HADCRT Computer Code,* 24590-HLW-U0C-30-00004, Rev. A, Bechtel National Inc., Richland, Washington.

Crowe, R. D. and R. D. Lanning, 2002b, *Analysis of HLW Melter Unplanned Pour Using HADCRT Computer Code*, 24590-HLW-U0C-30-00003, Rev. D, Bechtel National Inc., Richland, Washington.

Crowe, R. D. and R. D. Lanning, 2003, *Beyond Design Basis Event - LAW Melter Offgas Release Event Using HADCRT Computer Code*, 24590-LAW-U0C-20-00002, Rev. A, Bechtel National Inc., Richland, Washington.

Epstein, M., and J. C. Williams, 2003, *Hanford Waste Tank Bump Accident and Consequence Analysis*, RPP-6213, Rev. 2A, CH2M Hill Hanford Group, Inc., Richland, Washington.

Fuller, E. L, 2003, *Accident and Thermal Analysis for Storing K East Basin Sludge at T Plant*, Rev. 1, Fluor Hanford, Inc., Richland, Washington.

HNF-16138, 2003, *Performance Specification for Capsule Dry Storage Project Design and Fabrication*, Rev. 1, Fluor Hanford, Inc., Richland, Washington.

Heard, F. J., 2003, *Transmittal of Thermal Analyses in Support of the Cs/Sr Project*, FJH-03-2800 (internal letter to D. W. Bergmann, July 31), Duratek Federal Services, Inc., Northwest Operations, Richland, Washington.

Irwin, J. J., 2000, *Thermal Analysis Methods for Safety Analysis Reports for Packaging*, WHC SD-TP-RPT-005, Rev. 1, Fluor Hanford, Inc., Richland, Washington.

Kenna, B. T. and F. J. Schultz, 1983, *Characterization of an Aged WESF Capsule*, SAND83-0928, Sandia National Laboratory, Albuquerque, New Mexico, and Livermore, California.

Piepho, M. G., 2000, *Thermal Analysis of Cold Vacuum Drying of Spent Nuclear Fuel*, HNF-SD-SNF-CN-023, Revision 2, Fluor Federal Services Inc., Richland, Washington.

Plys, M. G., et al., 1998, *Simulation of Normal and Off-Normal Multi-Canister Overpack Behavior*, HNF-2256, Rev. 2, DE&S Hanford Inc., Richland, Washington.

Plys, M. G., et al., 2000, "Best-Estimate Facility Source Term Analysis," International Meeting on "Best Estimate" Methods in Nuclear Installation Safety Analysis (BE-2000), November, Washington D.C.

Plys, M. G., 2002, *Independent Calculation for Hanford Sludge Transportation and Storage (FAI/02-11)*, HNF-10439, Rev. 0, Fluor Hanford Company, Richland, Washington.

Plys, M. G., B. Malinovic, M. Epstein, and S. J. Lee, 2002a, *Fuel Cycle Facility Source Term Model HADCRT 1.4: User's Manual (FAI/02-50)*, SNF-10607, Rev. 0, Fluor Hanford, Richland, Washington.

Plys, M. G., S. J. Lee, and B. Malinovic, 2002b, *HANSF/SLUDGE Computer Program User's Manual, FAI/02-13*, SNF-13042, Rev.0, Fluor Hanford, Richland, Washington.

Plys, M. G., S. J. Lee, B. Malinovic, M. Epstein, and D. R. Duncan, 2002c, *Hanford Spent Nuclear Fuel Process and Safety Analysis Model HANSF/MCO 1.4: User's Manual (HADCRT 1.4B)*, SNF-3650, Rev. 3, Fluor Hanford Company, Richland, Washington.

Sasmor, D. J., Pierce, J. D., G. L. Tingey, H. E. Kjarmo, J. Tills, and D. C. McKeon, 1988, *Characterization of Two WESF Capsules After Five years of Service*, SAND86-2808, Sandia National Laboratory, Albuquerque, New Mexico, and Livermore, California.

Siciliano, E., and Puigh, R., 1999, *Combustion Accident Analysis for Double-Contained Receiver Tanks (DCRT) 244-S and 244-TX*, HNF-4526, Flour Daniel Northwest, Inc., Richland, Washington.

WMP-16878, 2003, *WESF Capsule Databook*, DRAFT, Fluor Hanford, Inc., Richland, Washington.

WMP-16837, 2003, *Corrosion Report for Capsule Dry Storage Project*, Rev. 0, Fluor Hanford, Richland, Washington.

WMP-16938, 2003, *Capsule Characterization Report for Capsule Dry Storage Project*, Rev. 0, Fluor Hanford, Richland, Washington.

WMP-16939, 2003, *Capsule Integrity Report for Capsule Dry Storage Project*, Rev. 0, Fluor Hanford, Inc., Richland, Washington.

WMP-17265, 2003, *Capsule Advisory Panel Topical Summary Report*, Rev. 0, Fluor Hanford, Inc., Richland, Washington.

APPENDIX A. DESCRIPTION OF THE HADCRT COMPUTER CODE

HADCRT is the name of the computer code containing all generic models and capable of invoking Hanford Spent Nuclear Fuel Project (SNFP) multi-canister overpack (MCO) and sludge specific models. The most recent quality assurance (QA) versions with the common platform were created in the order HADCRT 1.4 for generic models (*Fuel Cycle Facility Source Term Model HADCRT 1.4: User's Manual (FAI/02-50)*, [Plys et al. 2002a]); HADCRT 1.4A for sludge models (*HANSF/SLUDGE Computer Program User's Manual, FAI/02-13* [Plys et al. 2002b]; and HADCRT 1.4B for MCO models (*Hanford Spent Nuclear Fuel Process and Safety Analysis Model HANSF/MCO 1.4: User's Manual (HADCRT 1.4B)* [Plys et al. 2002c]). Depending on whether MCO-specific models or sludge-specific models are activated, the computer program is also called HANSF, HANSF/MCO, or HANSF/SLUDGE. If neither model is invoked (i.e., only generic models are used), the computer program is called HADCRT; this name will be used here.

HADCRT top-level generic capabilities include heat and mass transfer, fluid behavior, and aerosol behavior in a fuel cycle or chemical processing facility, described in a recent American Nuclear Society (ANS) paper ("Best-Estimate Facility Source Term Analysis," International Meeting on "Best Estimate" [Plys et al. 2000]. Phenomenological capabilities include:

- Multiple-compartment representation with arbitrary topology
- Combined pressure-driven, counter-current, and diffusion gas flow rates
- Transport of gases and aerosols between compartments
- Entrainment of aerosol from liquid and deposited particulate
- Vapor-aerosol equilibrium
- Deposition of aerosols via gravitational sedimentation, impaction, etc.
- Combustion
- Heat transfer and condensation on structures
- Liquid pools exchanging heat and mass with gas and structures.

Generic models may be used to model normal processes, operational transients, and accidents at fuel cycle facilities such as Hanford K basins, the Canister Storage Building (CSB), tank farm facilities including underground waste tanks, pits, and multi-room vaults, the future Waste Treatment Plant (WTP), and other facilities such as T-Plant, Waste Encapsulation and Storage Facility (WESF), Waste Receiving and Processing (WRAP) plant, and Plutonium Finishing Plant (PFP). A typical use is to predict radiological consequences of an accident involving combustion, including attenuation of radionuclides within the facility (the so-called leak path factor). Example analyses include double-shell tank gas release (tank bump) analysis (*Hanford Waste Tank Bump Accident and Consequence Analysis* [Epstein et al. 2000]); combustion in double-contained receiver tanks (*Combustion Accident Analysis for Double-Contained Receiver Tanks (DCRT) 244-S and 244-TX* [Siciliano and Puigh 1999]); and combustion in the WTP

(*Topical Report on the Management of Risks Posed by Explosive Hazards Present at the RPP-WTP* [BNFL and FAI 1999]).

Recent large-scale analyses have been conducted with HADCRT for the Hanford WTP (*Analysis of a HLW Process Vessel Hydrogen Deflagration Using HADCRT Computer Code*; *Analysis of HLW Melter Unplanned Pour Using HADCRT Computer Code*; *Beyond Design Basis Event - LAW Melter Offgas Release Event Using HADCRT Computer Code* [Crowe and Lanning, 2002a; 2002b; and 2003]). The first analysis considered a sudden leak of low-activity waste (LAW) melter offgas into the melter facility, tracked hazardous gases and radioactive aerosols throughout the facility including the heating, ventilation, and air conditioning (HVAC) system, and was used to predict leakage into occupied areas and the environment. The second predicted temperatures, pressures, and flows resulting from hydrogen combustion in process vessels, including the vessel vent system and HVAC systems for the high-level waste (HLW) facility. The third analyzed the impacts of an unplanned pour from the HLW melter, which include local heating of concrete walls and floor by radiation and convection, local gas temperatures and pressurization, and maximum temperatures seen by downstream high-efficiency particulate air (HEPA) filters.

HADCRT's MCO models were developed to include specific models for fuel behavior inside an MCO container for shipping, processing, and storage of Hanford Site spent nuclear fuel . These include models for fuel oxidation, hydrogen production, hydrate decomposition, ice formation, and numerous other phenomena pertinent to MCO process analyses. Together with the generic capability, the code is also capable of estimating the aerosol source term from accidents such as depressurization of an MCO or from hydrogen combustion. Example analyses conducted with the MCO models are *Simulation of Normal and Off-Normal Multi-Canister Overpack Behavior* (Plys et al. 1998) and *Thermal Analysis of Cold Vacuum Drying of Spent Nuclear Fuel* (Piepho 2000). In Plys et al. (1998), a "cradle to grave" analysis of MCO behavior from vacuum drying through dry storage was conducted. Analyses from Piepho (2000) form the basis for the SNFP safety analysis report.

HADCRT's sludge models were created to model thermal and chemical properties of Hanford Site spent nuclear fuel sludge within the integral model framework. This allows a complete analysis of behavior internal to sludge, such as oxidation, heat generation, hydrogen generation, and prediction of the sludge temperature profile, coupled with behavior external to sludge, such as calculation of pressures and gas concentrations in a sludge container, exchange flows between a sludge container and a facility, and gas concentrations throughout a facility. Using the same nodalization, the calculations can include accident analysis such as combustion and depressurization, with creation, transport, and deposition of aerosols, providing estimates of the aerosol source term, facility leak path factor, and source to the environment. Analyses of sludge container behavior in transport and at T Plant are described in *Independent Calculation for Hanford Sludge Transportation and Storage (FAI/02-11)* (Plys 2002).

HADCRT can be used for design and scoping evaluations as well as accident analyses, and indeed, it is common to first create a design via scoping and then, via straightforward new inputs, specify an accident scenario. An example of this range of capability is found in *Accident and Thermal Analysis for Storing K East Basin Sludge at T Plant* (Fuller 2003), where the sludge model was used to simulate various open port arrangements for a sludge container placed in a

cell at T Plant. A design was found which would prevent the accumulation of a flammable composition in the container, considering simultaneously the buildup of flammable gases in the cell; it was also able to predict the annual water loss rate. This input file was then extended to consider consequences of hydrogen combustion and entrainment from the container, and exposure of the container in a transfer cask to an external fire.

This page intentionally left blank.

APPENDIX B. ENERGY ABSORBED BY A SALT LOG FROM AN ADJACENT LOG

D. R.Olander July 4, 2003

The salt logs on either side of a capsule emit gamma rays, a fraction of which are absorbed in the log in the center. Absorption of these photons increases the heat generation rate of the central log.

Calculation of this effect is based on the following geometrical simplifications:

1. Only one adjacent log is considered; the effect of the other adjacent log is taken into account by multiplying by two.
2. The emitting (adjacent) log is modeled as a line source with the same length as the salt log and the same gamma emission rate.
3. The central (absorbing) salt log and the intervening section of insert steel are simplified into sections of cylindrical annuli:
    - The width of the annular section is equal to the diameter of the salt log
    - The thickness of the annular section is that which gives the same volume as the cylindrical log
    - The insert steel between the two logs is similarly modeled

The actual geometry is shown in Figure B1.1:

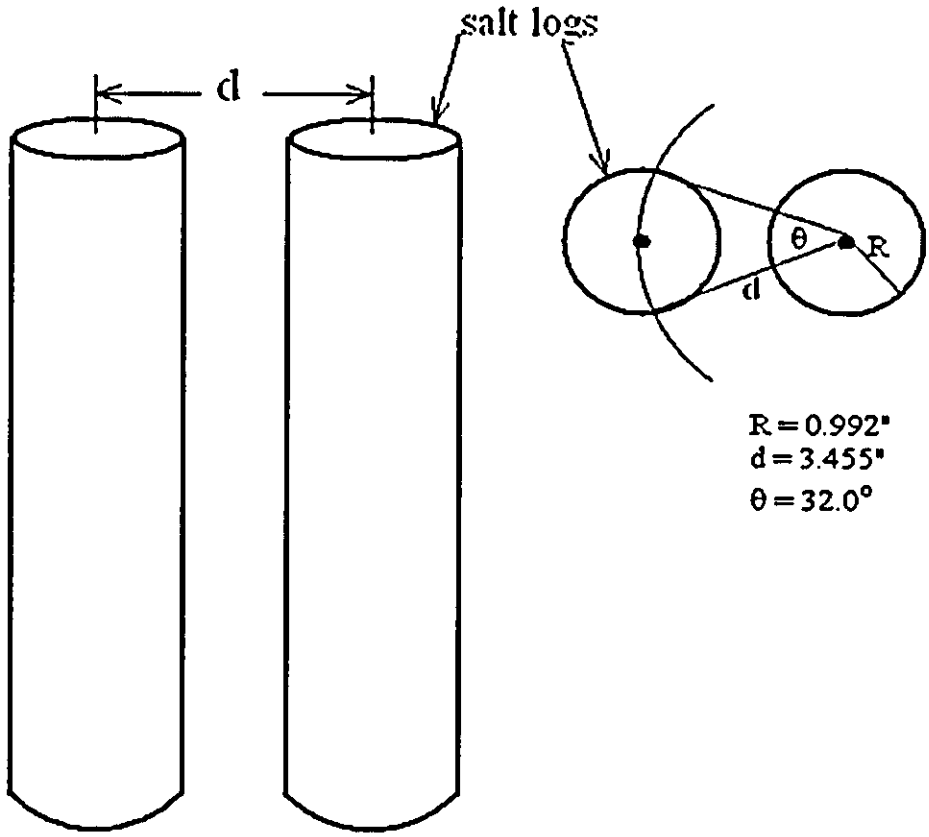

Figure B1.1. Actual Geometry.

The reconstituted geometry used for the calculation is shown in Figure B1.2:

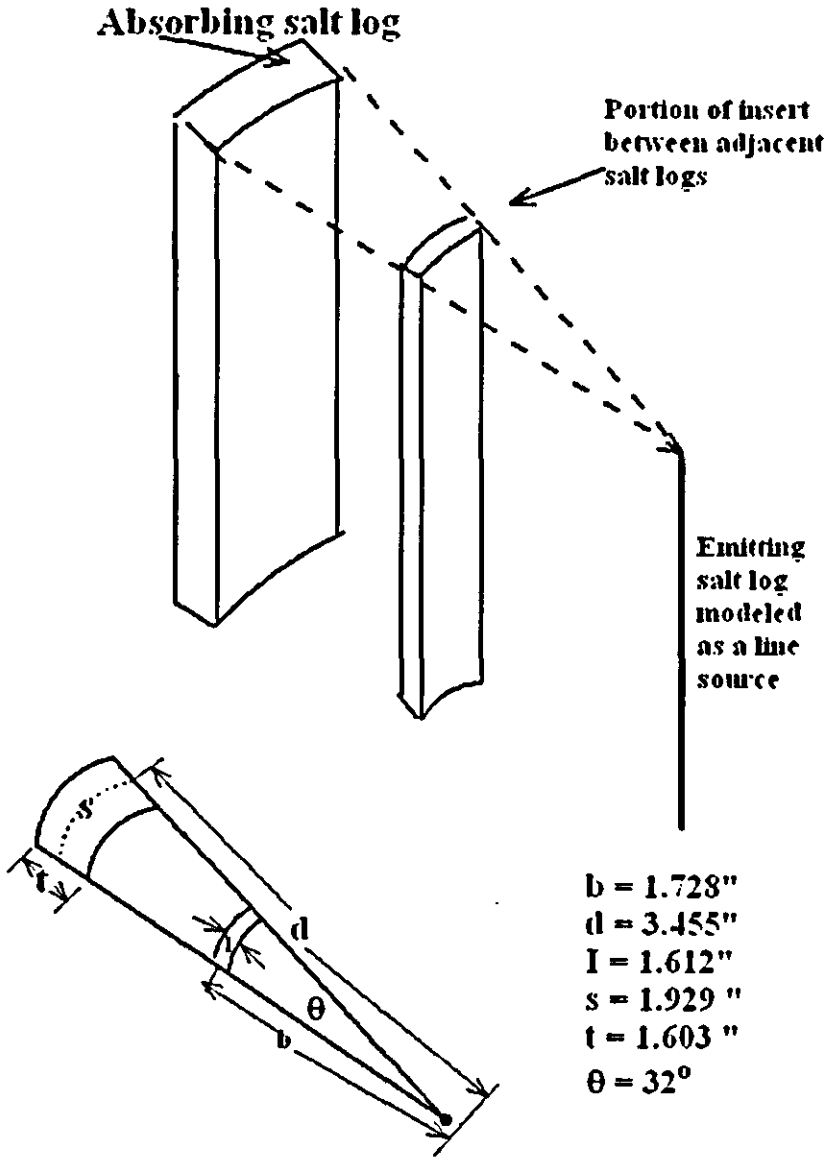

Figure B1.2. Reconstituted Geometry.

A vertical cross section of the model geometry is shown in the Figure B1.3.

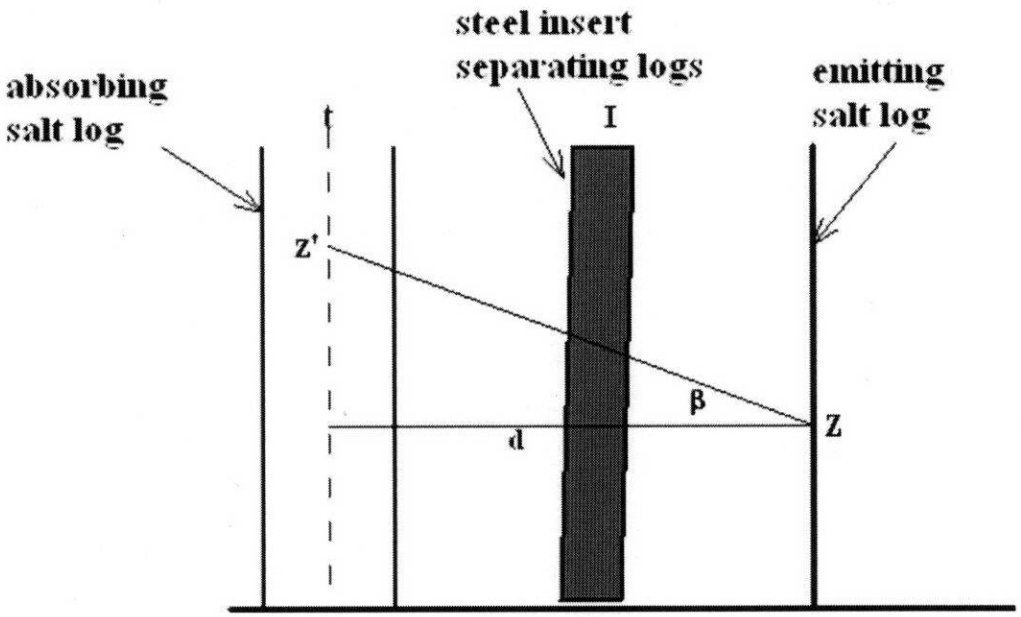

Figure B1.3. Vertical Cross Section of the Model Geometry

Consider a photon emitted from elevation z the right hand log (represented as a line source) at an angle β. The chance that the photon emitted from the right hand log will exit the salt is:

$$P_0 = 0.525 \qquad \text{Equation B1-1}$$

The shaded object in Figure B1.3 represents all of the steel in between the two logs, including the inner and outer capsule wall of both capsule and the intervening portion of the insert. The gaps have been assumed to be filled with steel. The photon will strike the absorbing log at an elevation z'.

The angle β is given by Equation B1-2:

$$\tan\beta = \frac{z'-z}{d} \qquad \text{Equation B1-2}$$

The probability of exiting the steel insert is:

$$P_1 = \exp\left(-\frac{\mu_{ss} \times I}{\cos\beta}\right) \qquad \text{Equation B1-3}$$

where μ_{ss} is the absorption coefficient of stainless steel for 661 kdV photons and I is the equivalent thickness of the steel separating the two salt logs (see Figure B1.2).

The probability that the photon passes through the absorbing salt log is:

$$P_2 = \exp\left(-\frac{\mu_{salt} \times t}{\cos\beta}\right) \qquad \text{Equation B1-4}$$

where μ_{salt} is the absorption coefficient of cesium chloride (CsCl) for 661 keV photons and t is the equivalent thickness of the salt log (see Figure B1.2). The probability of absorption of the photon in the salt log is $1 - P_2$.

Let $P_e dz'$ be the probability that the photon from the emitting log intercepts the absorbing log between heights z' and $z' + dz'$. The area of the absorbing element is sdz', where s is the arc length of the absorbing log (see Figure B1.2). Imagine a sphere of radius equal to the distance between the point at z' and the point at z. The area of this sphere is $4\pi(d/\cos\beta)^2$. The area element sdz' is foreshortened because of the angle it makes with the radius of the sphere between z' and z. The area of the absorbing element as seen from point z is $sdz'\cos\beta$. Since photon emission is isotropic, the probability that it is aimed in the correct direction is:

$$P_e dz' = \frac{s \times \cos\beta \, dz'}{4\pi(d/\cos\beta)^2} \qquad \text{Equation B1-5}$$

Multiplying Equations B1-1, -3, -4, and -5, and integrating over z' gives the probability that a photon emitted at z is absorbed anywhere in the left hand log:

$$P(z) = \frac{0.525 \times s}{4\pi d^2} \int_0^L \cos^3\beta \exp\left(-\frac{\mu_{ss} \times l}{\cos\beta}\right)\left[1 - \exp\left(-\frac{\mu_{salt} \times t}{\cos\beta}\right)\right] dz'$$

or, with all lengths made dimensionless by dividing by d:

$$P(Z) = \frac{0.525 \times S}{4\pi} \int_0^L \cos^3\beta \exp\left(-\frac{\Sigma_{ss} \times l}{\cos\beta}\right)\left[1 - \exp\left(-\frac{\Sigma_{salt} \times T}{\cos\beta}\right)\right] dZ' \qquad \text{Equation B1-6}$$

and, from Equation B1-2:

$$\beta = \tan^{-1}(Z' - Z) \qquad \text{Equation B1-7}$$

The average probability of photon absorption by the salt log is:

$$P_{avg} = \int_0^L P(Z) dZ \qquad \text{Equation B1-8}$$

For numerical work, the following values are adopted:

$S = 0.56$; $l = 0.47$; $T = 0.46$ $\Sigma_{SS} = \mu_{SS} d = 5.2$ $\Sigma_{salt} = \mu_{salt} d = 2.6$

The resulting value of P_{avg} is 1.06×10^{-3}.

The added power (in watts) in the salt in a capsule due to radiation from the adjacent two 50 kCi capsules is:

$$Q_{extra} = 2 \times 5 \times 10^{4}\ \text{Ci} \times 3.7 \times 10^{10}\ \frac{\text{dis/s}}{\text{Ci}} \times 6.61 \times 10^{5}\ \frac{\text{eV}}{\text{dis}} \times 1.6 \times 10^{-19}\ \frac{\text{J}}{\text{eV}} \times 1.06 \times 10^{-3}\ \frac{\text{photon abs. in central log}}{\text{photon emitted by adjacent log}} = 0.4\ \text{W}$$

The additional power due to the adjacent capsules is negligible compared to the power deposited by the salt log proper for a capsule activity of 5×10^{4} Ci.

APPENDIX C. RADIAL DISTRIBUTION OF THE GAMMA HEAT SOURCE IN CSCL

D. R. Olander June 24, 2003

Although the gamma generation rate is uniform in a salt log, the absorption rate (which is the rate of heat generation) is not. The following analysis calculates the rate absorption of first-collision Compton electrons. These are absorbed very close to the point of the Compton collision. The scattered photon, however, has a greater penetration distance, although not as large as the original 661 keV gamma ray. The major assumption of the analysis is that the entire energy of the latter is absorbed at the point of the Compton event.

The diagram is a two-dimensional (2-D) representation of the process, in which the emitting element and the absorbing element lie on the same plane of the cylindrical salt log of radius *R*. The absorbing elements lie along a radius at distance *y*. The emitting element is at radial position r and angle α with respect to *y*. The distance traveled by the 661 keV ray before

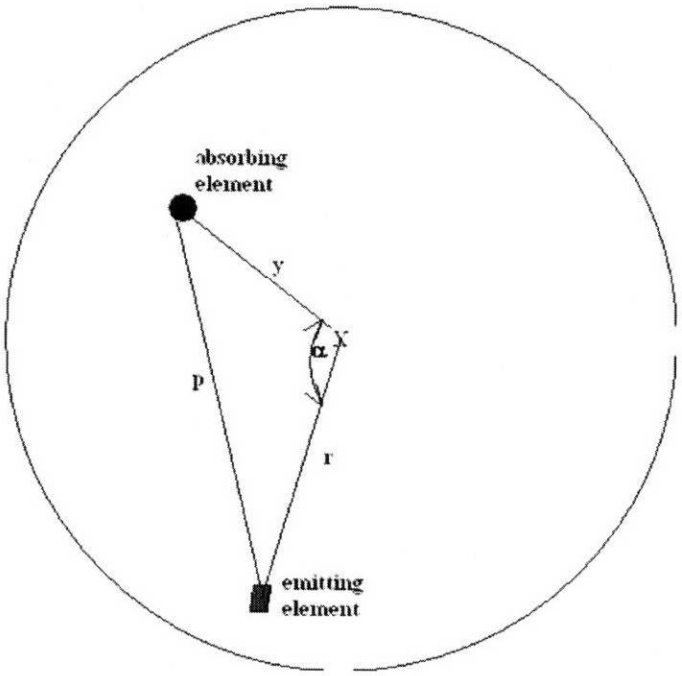

the Compton collision occurs is denoted by *p*. Using the law of cosines,

$$p^2 = r^2 + y^2 - 2rycos\alpha \qquad \text{Equation C1-1}$$

Accounting for emission from a depth *z* above or below the plane on which the absorbing element resides modifies Equation C1-1 to Equation C1-2:

$$q^2 = z^2 + r^2 + y^2 - 2rycos\alpha \qquad \text{Equation C1-2}$$

where *q* is the distance from an emitting element at coordinates *r*, α, and *z*, and an absorbing element at radial position *y* on the plane at $z = 0$.

The probability of a Compton event in the distance interval between q and $q + dq$ is $\mu e^{-\alpha q}$. The absorbing element is a unit sphere (unit projected area).

The emitting element is a volume element $rdrd\alpha dz$ in 3-D cylindrical coordinates. The photons are emitted isotropically, so the probability that the photon will intercept the unit sphere just the projected area of the unit sphere divided by the surface area of the sphere centered on the emitting element and of radius q. This probability is $1/4\pi q$. The emission rate of 661 keV photons per unit volume (S) is uniform in the salt log. The rate of absorption of the energy of the gamma rays emitted from the entire log is given by:

$$H = \frac{S\mu}{4\pi} I(y) \qquad \text{Equation C1-3}$$

where $I(y)$ is the heat production radial shape function:

$$I(y) = \int_0^R r dr \int_0^\pi d\alpha \int_0^\infty dz \frac{e^{-\mu q}}{q^2} \qquad \text{Equation C1-4}$$

Making all distances dimensionless with respect to the log radius R gives the shape function shown below in Figure C1.1:

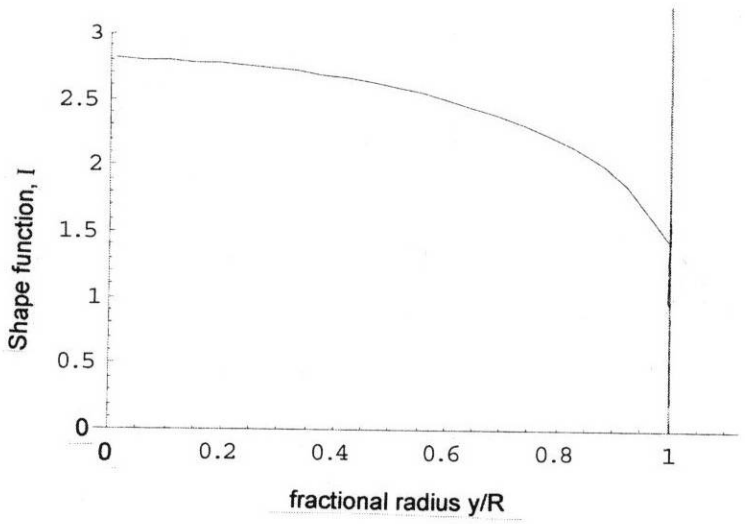

Figure C1.1. Shape Function/Fractional Radius Diagram.

Despite the spatial uniformity of the photon emission rate, the radial heat production profile varies by a factor of approximately two. This gives a higher centerline temperature than the assumed uniform heat generation rate for the same power.

APPENDIX D. MULTIPLIER TO DETERMINE PEAK CENTERLINE TEMPERATURE FOR NON-UNIFORM HEAT GENERATION

INTRODUCTION

The previous discussion (Appendix C) can be adapted to determine the peak centerline temperature when the radial heat generation profile is known.

The radial heat generation profile varies by a factor of approximately 2.

Assumptions

1. Ignore k(T) behavior—but it's real so if the multiplier is large the non-linearity will need to be simulated.

2. Source functional form: $Q(r) = A_{MAX} - a\,r^2$

   where $0 \le r \le 1$ (normalized)

3. Symmetry @ $r = 0$ implies $\frac{dT}{dr}\Big|_{r=0} = 0$

4. $Q_c\,(r = 1) = \frac{Q(r=0)}{2}$

5. Average Q (Q_0) is equal to previous constant Q (Q_c) (total heat production in salt is same).

$Q(0) = Q_{MAX}$

$Q(1) = Q_{MAX} - a(1)^2 = -\frac{Q_{MAX}}{2} \Rightarrow a = \frac{Q_{MAX}}{2}$,

So:

$Q(r) = QMAX\,(1 - \frac{1}{2}\,r^2)$ by assumptions 2 and 4

Average $Q = Q_0 = \frac{1}{A}\int_A Q\,dA = \frac{1}{\pi(1)^2}\int_0^1 2\pi\, rQ(r)dr$

$= 2\,Q_{MAX}\int_0^1 r(1-\frac{1}{2}r2)\,dr = 2Q_{MAX}\int_0^1 rdr - Q_{MAX}\int_0^1 r^3 dr$

$= Q_{MAX}\,\frac{r^2}{2}\Big|_0^1 - \frac{Q_{MAX}}{4}\,r4\Big|_0^1$

$= Q_{MAX}\left(1-0-\frac{1}{4}+0\right) = \frac{3}{4}Q_{MAX}$

by assumption 5, $\frac{3}{4}Q_{MAX} = Q_c \Rightarrow Q(r) = \frac{4}{3}Q_c\,(1-\frac{1}{2}r^2)$

by assumption 1, the heat equation is:

$$\frac{1}{r}\frac{d}{dr}\left(r\frac{dT}{dr}\right) = \frac{-Q(r)}{k}$$

$$\frac{d}{dr}\left(r\frac{dT}{dr}\right) = -\frac{1}{k}\frac{4}{3}Q_c\,r\left(1-\frac{1}{2}r^2\right)$$ Integration:

$$r\frac{dT}{dr} = -\frac{1}{k}\frac{4}{3}Q_c\left(\frac{r^2}{2}-\frac{r^4}{8}\right)+A$$

A is zero by assumption 3, so:

$$r\frac{dT}{dr} = -\frac{1}{k}\frac{4}{3}Q_c\left(\frac{r^2}{2}-\frac{r^4}{8}\right)$$

$$\frac{dT}{dr} = -\frac{1}{k}\frac{4}{3}Qc\left(\frac{r}{2}-\frac{r^3}{8}\right)$$

$$T = -\frac{1}{k}\frac{4}{3}Q_c\left(\frac{r^2}{4}-\frac{r^4}{32}\right)+A$$

$T(0) = T_{cl} = A \Rightarrow A = T_{cl}$

$$T(r) = T_{cl} - \frac{\frac{1}{k}\frac{4}{3}Q_c r^2\left(1-\frac{r^2}{8}\right)}{4} = T_{cl} - \frac{Q_c r^2\left(1-\frac{r^2}{8}\right)}{3k}$$

$$\Delta T = T(0) - T(1) = T_{cl} - T_{cl} + \frac{Q_c\left(1-\frac{1}{8}\right)}{3k} = \frac{Q_c\frac{7}{8}}{3k} = \frac{Q_c}{k}\frac{7}{24}$$

$$\text{when } Q(r) = Q_c \Rightarrow \frac{d}{dr}\left(r\frac{dT_c}{dr}\right) = -\frac{Q_c r}{k} \Rightarrow r\frac{dT_c}{dr} = -\frac{Q_c r^2}{2k} + A = -\frac{Q_c r^2}{2k}$$

$$\frac{dT_c}{dr} = -\frac{Q_c r}{2k} \Rightarrow Tc = -\frac{Q_c r^2}{4k} + T_{ccl} \Rightarrow$$

$$\Delta T_c = T_{ccl} - T_{ccl} + \frac{Q_c(1)^2}{4k} = \frac{Q_c}{4k}$$

so the multiplier is:

$$\frac{\Delta T}{\Delta T_c} = \frac{\frac{7}{24}\frac{Q_c}{k}}{\frac{Q_c}{4k}} = \frac{28}{24} = \frac{7}{6}$$

Therefore, to find the peak centerline temperature when the radial heat generation profile varies by a factor of two, simply multiply the previously calculated ΔT across the salt by $\frac{7}{6}$ and add to the salt-metal interface temperature.

See Section 4.4.5 of the main report for the resulting salt-metal and peak centerline temperatures for a revised radial power distribution across the cesium (Cs) salt.

This page intentionally left blank.

APPENDIX E. EFFECTIVE EMISSIVITY OF A FINNED SURFACE DUE TO SHADOWING

INTRODUCTION

The outside of the capsule carrier is finned and raises a question: "What does that do to the total emissivity?" To simplify our approach, we can look at the cylinder as if it were flat. We also assume that the cylinder is infinite in either direction relative to the spot we are looking at.

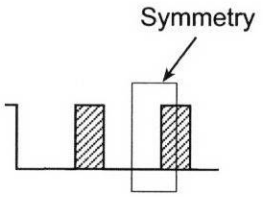

Besides the symmetry shown, there is also symmetry in and out of the paper plane.

A point s is located along the surface:

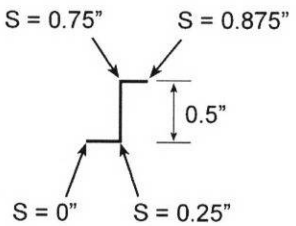

At each point there is a hemisphere of possible lines of sight from the surface to space.

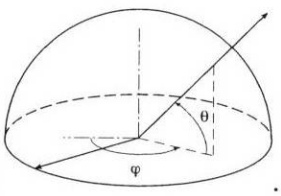

φ is the angle in the surface plane and θ is the elevation.

By equation 3-6b in Ref. 1 the total hemispherical emissivity is

$$\varepsilon(T_A) = \frac{1}{\pi} \int_{\varphi=0}^{2\pi} \int_{\theta=0}^{\pi/2} \varepsilon' \cos\theta \sin\theta \, d\theta \, d\phi$$

where ε' is the directional emissivity.

The directional effect is assumed to be just the blocked line of sight due to the fin. Thus $\varepsilon' = 0$ when $0 \le \theta < \theta_{min}$, and $\varepsilon' = \varepsilon'$ a constant when $\theta_{min} \le \theta \le \pi/2$. The inner integral can be done implicitly or directly:

$$\int_{\theta_{min}}^{\pi/2} \varepsilon' \cos\theta \sin\theta d\theta = \frac{-\varepsilon'}{z}(\cos\theta)^2 \Big|_{\theta_{min}}^{\pi/2} = \frac{-\varepsilon'}{2}(\cos \pi/2)^2 + \frac{\varepsilon'}{2}(\cos\theta_{min})^2 = \frac{\varepsilon'}{2}(\cos\theta_{min})^2$$

where

$$\int_{\theta+0}^{\theta-} \varepsilon' \cos\theta \sin\theta \, d\theta = 0, \text{and } \varepsilon' = \text{constant, and } \cos \pi/2 = 0$$

So we now have:

$$\varepsilon(T_A) = \frac{1}{\pi}\int_{\phi=0}^{2\pi} \frac{\varepsilon'}{2}\cos^2\theta_{min} \, d\varphi$$

ε' is now the material ε and is considered constant. The dependence on φ is rolled into the θ_{min} value.

By symmetry: (in-out of paper plane)

$$\varepsilon(T_A) = \frac{2}{\pi}\int_0^{\pi} \frac{\varepsilon'}{2}\cos^2\theta_{min} d\varphi$$

$$= \frac{\varepsilon'}{\pi}\int_0^{\pi} \cos^2\theta_{min} \, d\varphi$$

This integral is done numerically. θ_{min} is a function of φ.

The remaining task is to determine θ_{min} as a function of φ.

The situation at s = 0 is: S = 0"

The minimum angle on the right is θ_0 and the minimum on the left is θ_1 at φ = 0. The rise is ½" and the run is ¼" so $\theta_1 = \tan\frac{1/2}{1/4} = \tan(2) = 63.43°$. Now as φ increases (rotating into the plane of the paper), the rise stays the same and the run increases unboundedly. When the angle is at π/4 (45°), for example, the run is $\sqrt{(1/4)^2 + (1/4)^2} = 0.3535$ instead of 0.25 so the minimum θ is 54.74° instead of 63.43°. If the distance along the line is s, then if $0 \le s < 0.25$

$\theta_{min} = \text{atan}(\tan\theta_0 \cos\varphi)$ toward the right for φ = 0 to π/2

where $\theta_0 = \text{atan}\left(\frac{1/2}{1/4 - S}\right)$ i.e.., the φ = 0 line

and

θ_{min} = atan (-tan θ_1 cos φ) toward the left for $\varphi = \pi/2$ to π

where $\theta_1 = \text{atan}\left(\frac{1/2}{1/4+s}\right)$

We could use the above from $\varphi = 0$ to π, but we will, instead, use it from $\varphi = 0$ to $\pi/2$ and not change the sign on cos φ:

$$\varepsilon(T_A) = \frac{\varepsilon'}{\pi}\left(\int_0^{\pi/2} \{\cos[\text{atan}(\tan\theta_0 \cos\varphi)]\}^2 \, d\varphi + \int_0^{\pi/2} \{\cos[\text{atan}(\tan\theta, \cos\varphi)]\}^2 \, d\varphi \right)$$

Using this symmetric form, we can define the rest of the function: when $0.25 \le s < 0.75$ only the left side is visible. Here the rise changes and the run stays the same.

$$\theta_1 = \text{atan}\left(\frac{3/4 - s}{1/2}\right) \quad \text{and}$$

$$\varepsilon(T_A) = \frac{\varepsilon'}{\pi} \int_0^{\pi/2} \{\cos[\text{atan}(\tan\theta_1 \cos\varphi)]\}^2 d\varphi$$

For $0.75 \le s \le 0.875$ $\varepsilon(T_A) = \varepsilon'$ because there is no blocking of any line of sight.

We are interested in the mean value for $\varepsilon(T_A)$ along the line s:

$$\bar{\varepsilon} = \frac{1}{0.875} \int_0^{0.875} \varepsilon(T_A) \, ds$$

When we do this numerically, we get $\bar{\varepsilon} = 0.513\,\varepsilon'$. So if $\varepsilon' = 0.7$ for stainless steel, then $\bar{\varepsilon}$ = 0.359

This page intentionally left blank.

APPENDIX F. THERMO-PHYSICAL MATERIAL PROPERTIES

Table F-1. CsCl Density.

Temperature (K)	Density* (kg/m^3)	Structure
293.2	4.003 E+03	NaCl
298.2	3.999 E+03	
373.2	3.952 E+03	
423.2	3.926 E+03	
473.2	3.897 E+03	
533.2	3.857 E+03	
573.2	3.827 E+03	
643.2	3.778 E+03	
673.2	3.758 E+03	
742.2	3.709 E+03	
743.2	3.153 E+03	CsCl
753.2	3.150 E+03	
773.2	3.141 E+03	
873.2	3.095 E+03	
918.2	3.072 E+03	
919.2	2.792 E+03	Liquid

*Reagent grade CsCl.

Table F-2. CsCl Specific Heat.

Temperature (K)	Specific Heat* (J/kg-K)
273.2	304.8
423.2	311.1
533.2	314.0
643.2	315.3
753.2	315.3
873.2	397.7

*Reagent grade CsCl.

Table F-3. CsCl Thermal Conductivity.

Temperature (K)	Thermal Conductivity* (J/s-m-K)
273.2	0.830
423.2	0.574
533.2	0.450
643.2	0.370
753.2	0.315
873.2	0.373

*Reagent grade CsCl.

Table F-4. SrF_2 Density.

Temperature (K)	Density* (kg/m^3)
298.2	2.968 E+03
373.2	2.953 E+03
473.2	2.934 E+03
573.2	2.915 E+03
673.2	2.896 E+03
773.2	2.877 E+03
873.2	2.859 E+03
973.2	2.840 E+03

*Multiplied by 0.7 to account for the nominal packing efficiency during the WESF process.

Table F-5. SrF_2 Specific Heat.

Temperature (K)	Specific Heat* (J/kg-K)
298.2	398.9
320.2	408.8
360.2	422.6
400.2	432.9
440.2	440.8
480.2	447.2
520.2	450.5
560.2	450.5
600.2	450.5
700.2	450.5

*Multiplied by 0.7 to account for the nominal packing efficiency during the WESF process.

Table F-6. SrF2 Thermal Conductivity.*

Temperature (K)	Thermal Conductivity (J/s-m-K)
298.2	4.220
323.2	3.986
423.2	3.195
523.2	2.550
623.2	2.110
723.2	1.817
823.2	1.612
923.2	1.436
1023.2	1.319
1123.2	1.231

*Multiplied by 0.7 to account for the nominal packing efficiency during the WESF process.

Table F-7. Properties* of Stainless Steel 316L.

Temperature (K)	Specific Heat (J/kg-K))	Thermal Conductivity (J/s-m-K)
294.3	465.6	13.36
310.9	472.3	13.64
366.5	492.4	14.58
422.1	509.7	15.51
477.6	524.3	16.41
533.2	536.6	17.31
588.7	547.1	18.18
644.3	556.1	19.04
699.8	563.9	19.88
810.9	577.6	21.51
922.1	590.9	23.06
1033.2	606.9	24.55
1144.3	628.4	25.96

*Density (ρ) = 7,962 kg/m^3

Table F-8. Properties of Hastelloy C-276 at 293 K (20 °C).

Density, kg/m^3	8,890.0
Specific Heat, J/kg-K	427.0
Thermal conductivity, J/s-m-K	9.8

Table F-9. Properties* of Air at Atmospheric Pressure.

Temperature (K)	Density (kg/m^3)	Specific Heat (J/kg-K)	Viscosity x10^5 (kg/m-s)	Thermal Conductivity (J/s-m-K)	Pr
100	3.6010	1026.6	0.6924	0.009246	0.770
150	2.3675	1009.9	1.0283	0.013735	0.753
200	1.7684	1006.1	1.3289	0.01809	0.739
250	1.4128	1005.3	1.5990	0.02227	0.722
300	1.1774	1005.7	1.8462	0.02624	0.708
350	0.9980	1009.0	2.075	0.03003	0.697
400	0.8826	1014.0	2.286	0.03365	0.689
450	0.7833	1020.7	2.484	0.03707	0.683
500	0.7048	1029.5	2.671	0.04038	0.680
550	0.6423	1039.2	2.848	0.04360	0.680
600	0.5879	1055.1	3.018	0.04659	0.680
650	0.5430	1063.5	3.177	0.04953	0.682
700	0.5030	1075.2	3.332	0.05230	0.684
750	0.4709	1085.6	3.481	0.05509	0.686
800	0.4405	1097.8	3.625	0.05779	0.689
850	0.4149	1109.5	3.765	0.06028	0.692
900	0.3925	1121.2	3.899	0.06279	0.696
950	0.3716	1132.1	4.023	0.06525	0.699
1000	0.3524	1141.7	4.152	0.06752	0.702
1100	0.3204	1160.0	4.440	0.07320	0.704

*Molecular weight (MW) = 28.97

Table F-10. Properties* of Helium at Atmospheric Pressure.

Temperature (K)	Viscosity x10^5 (kg/m-s)	Thermal Conductivity (J/s-m-K)
100	0.9630	0.0730
200	1.4970	0.1151
250	1.7495	0.1338
300	1.9890	0.1499
350	2.2140	0.1649
400	2.4280	0.1795
500	2.8270	0.2114
600	3.1990	0.2470
700	3.5490	0.2780
800	3.8840	0.3070
900	4.2010	0.3350
1000	4.5040	0.3630

*Specific heat = 5193.07 J/kg-K

Molecular weight (MW) = 4.003 kg/kg Mole

Density (kg/m^3) = $\frac{P \cdot MW}{R \cdot T}$; where P = 101325 Pa, R = 8314.34 J/kgMole-K, and T is in Kelvin.

Table F-11. Properties* of Argon at Atmospheric Pressure.

Temperature (K)	Specific Heat (J/kg-K)	Viscosity x10^5 (kg/m-s)	Thermal Conductivity (J/s-m-K)
200	523.6	1.601	0.01244
250	522.2	1.949	0.01515
300	521.5	2.272	0.01772
350	521.5	2.571	0.02013
400	521.0	2.852	0.02233
500	520.8	3.360	0.02638
600	520.6	3.830	0.03010
700	520.5	4.250	0.03360
800	520.5	4.640	0.03690
900	520.5	5.010	0.03980
1000	520.5	5.350	0.04270

Molecular weight (MW) = 39.944

Table F-12. Properties* of Nitrogen at Atmospheric Pressure.

Temperature (K)	Specific Heat (J/kg-K)	Viscosity x10^5 (kg/m-s)	Thermal Conductivity (J/s-m-K)
200	1042.9	1.2947	0.01824
300	1040.8	1.7840	0.02620
400	1045.9	2.1980	0.03335
500	1055.5	2.5700	0.03984
600	1075.6	2.9110	0.04580
700	1096.9	3.2130	0.05123
800	1122.5	3.4840	0.05609
900	1146.4	3.7490	0.06070
1000	1167.7	4.0000	0.06475
1100	1185.7	4.2280	0.06850
1200	1203.7	4.4500	0.07184

Molecular weight (MW) = 28.016

Table F-13. Properties* of Hydrogen at Atmospheric Pressure.

Temperature (K)	Specific Heat (J/kg-K)	Viscosity x10^5 (kg/m-s)	Thermal Conductivity (J/s-m-K)
200	13540.0	0.6813	0.1282
300	14314.0	0.8963	0.182
350	14436.0	0.9954	0.206
400	14491.0	1.0864	0.228
450	14499.0	1.1779	0.251
500	14507.0	1.2636	0.272
550	14532.0	1.3475	0.292
600	14537.0	1.4285	0.315
700	14574.0	1.5890	0.351
800	14675.0	1.7400	0.384
900	14821.0	1.8780	0.412

Molecular weight (MW) = 2.016

This page intentionally left blank.

APPENDIX G. PEER REVIEW RECORD

Note: This appendix provides a record of the peer reviews performed by Dr. Joe H. Payer of Case Western Reserve University and Dr. Donald R Olander of the University of California, Berkeley.

CAPSULE ADVISORY PANEL REVIEW COMMENT RECORD (RCR) Complete highlighted areas		
	1. Date 7/20/03	2. Page

3. Choose Document Number/Title (Only 1 Document Review per RCR Form)	4. Reviewer	4. Reviewer	4. Reviewer	5. CLOSED
[]WMP-16937 Corrosion Report Draft B []WMP-16938 Capsule Characterization Draft B []WMP-16939 Capsule Integrity Draft B [x]WMP-16940 Thermal Analysis Draft B []WMP-16878 Data Book Draft B []WMP-17265 Summary Report Rev. A	[]Bath, Singh []Bryan, Garry []Cannell, Gary []Covey, Lori []Heard, Fred []Josephson, Walt	[]Kraemer, Laurie []Miller, Bill [x]Olander, Don []Payer, Joe []Plys, Marty []Robbins, Dewey	[]Swenson, Joe []Thomson, Jim []Tingey, Garth []Tingey, Joel [] [] []	September 1, 2003 DATE Signature on File REVIEWER Signature on File AUTHOR/ORIGINATOR

6. Item	7. Comment(s)/Discrepancy(s) (Provide technical justification for the comment and detailed recommendation of the action required to correct/resolve the discrepancy/problem indicated.)	8. Reviewer Concurrence Required (Reviewer should 'X' this box if wants to concur with the closure of comment)	9. Disposition (Provide justification if NOT accepted.)	10. Status
1	The limitations on p. iii should include: Contact resistance associated with a salt- metal gap is neglected		Will revise limitations to address neglecting contact resistance when a salt-metal gap is NOT present.	Accpt'd
2	p. 7, 5th paragraph:: Modify to include use of the material in my memos: " Radial Distribution of the Gamma Heat source in CsCl" "Energy Absorbed by a Salt log from an Adjacent Log"		Will refer reader to Appendix B (new) "Radial Distribution of the Gamma Heat Source in CsCl" and Appendix C (new) "Energy Absorbed by a Salt Log from an Adjacent Log."	Accpt'd
3	Sect. 3.1.1: Eq 3.1.1 is an oversimplified heat balance. See Item 11 in my memo " Comments on the Thermal Analysis"	X	This section is revised to explain the heat balance on the dry storage module. The revised Section 3.1.1 was reviewed with you at last CAP meeting.	Accpt'd
4	Eqs (3.1.2) and (3.1.3): Why not do away with the mythical H entirely? Just substitute Eq (3.1.3) into (3.1.2) and H disappears from the analysis.		Derivation revised to use actual height, and text now explains why the effective H is useful and is always less than actual H.	Accpt'd

CAPSULE ADVISORY PANEL REVIEW COMMENT RECORD (RCR) Complete highlighted areas	1. Date 7/20/03	2. Page

3. Choose Document Number/Title (Only 1 Document Review per RCR Form)	4. Reviewer	4. Reviewer	4. Reviewer	5. CLOSED
[]WMP-16937 Corrosion Report Draft B []WMP-16938 Capsule Characterization Draft B []WMP-16939 Capsule Integrity Draft B [x]WMP-16940 Thermal Analysis Draft B []WMP-16878 Data Book Draft B []WMP-17265 Summary Report Rev. A	[]Bath, Singh []Bryan, Garry []Cannell, Gary []Covey, Lori []Heard, Fred []Josephson, Walt	[]Kraemer, Laurie []Miller, Bill [x]Olander, Don []Payer, Joe []Plys, Marty []Robbins, Dewey	[]Swenson, Joe []Thomson, Jim []Tingey, Garth []Tingey, Joel [] [] []	September 1, 2003 DATE Signature on File REVIEWER Signature on File AUTHOR/ORIGINATOR

6. Item	7. Comment(s)/Discrepancy(s) (Provide technical justification for the comment and detailed recommendation of the action required to correct/resolve the discrepancy/problem indicated.)	8. Reviewer Concurrence Required (Reviewer should 'X' this box if wants to concur with the closure of comment)	9. Disposition (Provide justification if NOT accepted.)	10. Status
5	Eq (3.1.3): The units don't match. H has the units of length, and the RHS has the units of moles/cm^2. Something is missing		Equation deleted	Accpt'd
6	E q (3.1.4): why not just use the ideal gas law and write: $\rho(z) - \rho_{□‡} = \frac{p}{R}\left(1/T(z) - 1/T_{□‡}\right)$		Can be done but linearized approach using beta is appropriate, and beta is derived from the ideal gas law	Accpt'd
7	Eq (3.1.5) should be replaced by the temperature profile derived from the analysis cited in Item No. 3		Satisfied by the revised analysis	Accpt'd
8	Eq (3.1.6): this is $T(z) = T_G$. It should be replaced by the solution of Eq (1) in the memo cited in Item No. 3 with $T_{over} - T_g$ taken from Eq (4) of that memo with $q = 0$		Satisfied by the revised analysis	Accpt'd

CAPSULE ADVISORY PANEL REVIEW COMMENT RECORD (RCR) *Complete highlighted areas*		
	1. Date 7/20/03	2. Page

3. Choose Document Number/Title (Only 1 Document Review per RCR Form)	4. Reviewer	4. Reviewer	4. Reviewer	5. CLOSED
[]WMP-16937 Corrosion Report Draft B []WMP-16938 Capsule Characterization Draft B []WMP-16939 Capsule Integrity Draft B [x]WMP-16940 Thermal Analysis Draft B []WMP-16878 Data Book Draft B []WMP-17265 Summary Report Rev. A	[]Bath, Singh []Bryan, Garry []Cannell, Gary []Covey, Lori []Heard, Fred []Josephson, Walt	[]Kraemer, Laurie []Miller, Bill [x]Olander, Don []Payer, Joe []Plys, Marty []Robbins, Dewey	[]Swenson, Joe []Thomson, Jim []Tingey, Garth []Tingey, Joel [] [] []	September 1, 2003 DATE Signature on File REVIEWER Signature on File AUTHOR/ORIGINATOR

6. Item	7. Comment(s)/Discrepancy(s) (Provide technical justification for the comment and detailed recommendation of the action required to correct/resolve the discrepancy/problem indicated.)	8. Reviewer Concurrence Required (Reviewer should 'X' this box if wants to concur with the closure of comment)	9. Disposition (Provide justification if NOT accepted.)	10. Status
9	The assumption $H_Q = H/2$ is not justifiable. H_Q is a physical dimension, as is H_{act}. Furthermore, H can be eliminated as described in Item No. 4		Satisfied by the revised analysis	Accpt'd
10	The line below Eq (3.1.6) refers to "the integral yields...". What integral?		Satisfied by the revised analysis	Accpt'd
11	The result $H = ¾ H_{act}$ is not necessary if H is removed from the analysis as indicated in Item No. 4		Satisfied by the revised analysis	Accpt'd
12	Eq (3.1.7): the numerator ¾ is physically unreal and should not be there.		Satisfied by the revised analysis	Accpt'd

CAPSULE ADVISORY PANEL REVIEW COMMENT RECORD (RCR) Complete highlighted areas	1. Date 7/20/03	2. Page

3. Choose Document Number/Title (Only 1 Document Review per RCR Form)	4. Reviewer	4. Reviewer	4. Reviewer	5. CLOSED
[]WMP-16937 Corrosion Report Draft B []WMP-16938 Capsule Characterization Draft B []WMP-16939 Capsule Integrity Draft B [x]WMP-16940 Thermal Analysis Draft B []WMP-16878 Data Book Draft B []WMP-17265 Summary Report Rev. A	[]Bath, Singh []Bryan, Garry []Cannell, Gary []Covey, Lori []Heard, Fred []Josephson, Walt	[]Kraemer, Laurie []Miller, Bill [x]Olander, Don []Payer, Joe []Plys, Marty []Robbins, Dewey	[]Swenson, Joe []Thomson, Jim []Tingey, Garth []Tingey, Joel [] [] []	September 1, 2003 DATE Signature on File REVIEWER Signature on File AUTHOR/ORIGINATOR

6. Item	7. Comment(s)/Discrepancy(s) (Provide technical justification for the comment and detailed recommendation of the action required to correct/resolve the discrepancy/problem indicated)	8. Reviewer *Concurrence Required* (Reviewer should 'X' this box if wants to concur with the closure of comment)	9. Disposition (Provide justification if NOT accepted)	10. Status
13	p. 29: The three variables (T_g, T_i and T_o) and the three equations can be reduced to a single equation. T_o can be eliminated between Eqs (3.1.8) and (3.1.9) (without the factor of ¾ in the former), but where is another equation that contains T_i? If Eq (3.1.1) is supposed to be the third equation, it doesn't contain T_i (unless it's buried in the Rayleigh number). In fact, couldn't Eqs (3.1.1) and (3.1.2) be solved *directly for* T_g?		Satisfied by the revised analysis	Accpt'd
14	Eqs (3.1.10-12). Don't these equations apply to a vertical plate *in an infinite medium*? I'm not sure whether they can be used for the convective heat transfer coefficients for the overpack outer wall and the module inner surface.		Applicable since scale large enough that well-defined boundary layers will exist	Accpt'd
15	ΔT in Eq (3.1.11) should be defined.		Will insert "where delta-T is from surface to bulk gas"	Accpt'd

CAPSULE ADVISORY PANEL REVIEW COMMENT RECORD (RCR) Complete highlighted areas	1. Date 7/20/03	2. Page

3. Choose Document Number/Title (Only 1 Document Review per RCR Form)	4. Reviewer	4. Reviewer	4. Reviewer	5. CLOSED
[]WMP-16937 Corrosion Report Draft B []WMP-16938 Capsule Characterization Draft B []WMP-16939 Capsule Integrity Draft B [x]WMP-16940 Thermal Analysis Draft B []WMP-16878 Data Book Draft B []WMP-17265 Summary Report Rev. A	[]Bath, Singh []Bryan, Garry []Cannell, Gary []Covey, Lori []Heard, Fred []Josephson, Walt	[]Kraemer, Laurie []Miller, Bill [x]Olander, Don []Payer, Joe []Plys, Marty []Robbins, Dewey	[]Swenson, Joe []Thomson, Jim []Tingey, Garth []Tingey, Joel [] [] []	September 1, 2003 DATE Signature on File REVIEWER Signature on File AUTHOR/ORIGINATOR

6. Item	7. Comment(s)/Discrepancy(s) (Provide technical justification for the comment and detailed recommendation of the action required to correct/resolve the discrepancy/problem indicated.)	8. Reviewer *Concurrence Required* (Reviewer should 'X' this box if wants to concur with the closure of comment)	9. Disposition (Provide justification if NOT accepted.)	10. Status
16	Eq (3.1.14) applies to radiation between concentric cylinders. Is it applicable to radiation to an infinite medium in which air absorbs the radiation? What do you use for T_W?		Applicable because short air distance is effectively transparent	Accpt'd
17	p. 33, 2nd paragraph: after "Node point number 1...", add "in Fig. 3-4"		Revised sentence to refer to both Figures 3-4 and 3-5.	Accpt'd
18	p. 36 et seq: the "one over one over something" form of equations should be changed to just plain "something"		No change. Followed existing MathCAD construction from "Principles of Heat Transfer" by Frank Kreith and Mark Bohn. Note equations are developed first for resistances then overall heat transfer coefficients.	Accpt'd
19	p. 40 3rd paragraph, 4th line: Is there any quantitative justification for the 4% increase in the salt radius to account for the asymmetry of the problem?		No quantitative justification. Just knowledge that a one-dimensional analysis (for this configuration) will miss the peak temperature without a slight adjustment. Not necessary to dwell on the adjustment for salt centerline. Current performance spec is for salt-metal interface temperature.	Accpt'd

CAPSULE ADVISORY PANEL REVIEW COMMENT RECORD (RCR) Complete highlighted areas	1. Date 7/20/03	2. Page

3. Choose Document Number/Title (Only 1 Document Review per RCR Form)	4. Reviewer	4. Reviewer	4. Reviewer	5. CLOSED
[]WMP-16937 Corrosion Report Draft B []WMP-16938 Capsule Characterization Draft B []WMP-16939 Capsule Integrity Draft B [x]WMP-16940 Thermal Analysis Draft B []WMP-16878 Data Book Draft B []WMP-17265 Summary Report Rev. A	[]Bath, Singh []Bryan, Garry []Cannell, Gary []Covey, Lori []Heard, Fred []Josephson, Walt	[]Kraemer, Laurie []Miller, Bill [x]Olander, Don []Payer, Joe []Plys, Marty []Robbins, Dewey	[]Swenson, Joe []Thomson, Jim []Tingey, Garth []Tingey, Joel [] [] []	September 1, 2003 DATE Signature on File REVIEWER Signature on File AUTHOR/ORIGINATOR

6. Item	7. Comment(s)/Discrepancy(s) (Provide technical justification for the comment and detailed recommendation of the action required to correct/resolve the discrepancy/problem indicated.)	8. Reviewer Concurrence Required (Reviewer should 'X' this box if wants to concur with the closure of comment)	9. Disposition (Provide justification if NOT accepted.)	10. Status
20	p. 40 3rd paragraph: Is an iterative solution necessary? Why can't you add Eqs (3.2.2-15) and (3.2.2-16) to give: $Q_5 + U89x(T8 - T9) = Q_{total}$ And solve immediately for T8 since T9 (ambient air temperature) is known?		Text changed to reflect equations are solved by successive substitution with a check of the overall energy balance and iteration, if necessary.	Accpt'd
21	Some coordination of nomenclature between sections 3.1 and 3.2 is in order. For example, is Q_{total} the same as Q_{load}? Is T9 the same as T_{oo}?		These examples are true. Will check for any others.	Accpt'd
22	Eq(3.2.2-28): how can U9A be specified numerically in advance since h_c depends on T9 according to Eq(3.2.2-11)?		Script uses an initial guess. Followed by several iterations to obtain convergence. Final energy balance across external surface is OK.	Accpt'd
23	p. 41 The geometry of fins is such that the entire area of the finned surface does not radiate to the surroundings; there is considerable viewing of adjacent fins at a higher temperature than T_W. Some sort of view factor is needed		Recent calculations show a view factor on the order of 0.513 for the assumed longitudinal rectangular fins used for the preliminary design. A parametric analysis will be added to Table 3-9 presenting the results of reducing the overall heat transfer by thermal radiation from the external surface by 50%.	Accpt'd

CAPSULE ADVISORY PANEL REVIEW COMMENT RECORD (RCR) Complete highlighted areas	1. Date 7/20/03	2. Page

3. Choose Document Number/Title (Only 1 Document Review per RCR Form)	4. Reviewer	4. Reviewer	4. Reviewer	5. CLOSED
[]WMP-16937 Corrosion Report Draft B []WMP-16938 Capsule Characterization Draft B []WMP-16939 Capsule Integrity Draft B [x]WMP-16940 Thermal Analysis Draft B []WMP-16878 Data Book Draft B []WMP-17265 Summary Report Rev. A	[]Bath, Singh []Bryan, Garry []Cannell, Gary []Covey, Lori []Heard, Fred []Josephson, Walt	[]Kraemer, Laurie []Miller, Bill [x]Olander, Don []Payer, Joe []Plys, Marty []Robbins, Dewey	[]Swenson, Joe []Thomson, Jim []Tingey, Garth []Tingey, Joel [] [] []	September 1, 2003 DATE Signature on File REVIEWER Signature on File AUTHOR/ORIGINATOR

6. Item	7. Comment(s)/Discrepancy(s) (Provide technical justification for the comment and detailed recommendation of the action required to correct/resolve the discrepancy/problem indicated)	8. Reviewer Concurrence Required (Reviewer should 'X' this box if wants to concur with the closure of comment)	9. Disposition (Provide justification if NOT accepted.)	10. Status
24	How many adjustable parameters are in the model in addition to the off-center position of the maximum temperature of the salt log and the ratio AR,. All adjustable parameters should be clearly brought out so that the reader does not suspect foul play in the excellent agreement between the 1D model and the 2D models. Sect. 3.6 is an appropriate place for the listing of adjustable parameters.		Only one adjustable factor: the off-center location of the peak salt temperature. Not necessary to dwell on the adjustment for salt centerline, since the current performance spec is for salt-metal interface temperature. AR is based on geometry and is calculated for the given number of capsules per insert. Concept of AR works based on comparison to a series of independent checks with HADCRT and FlexPDE.	Accpt'd
25	Question. A sensitivity analysis should be made for each adjustable parameter in the 1D model. Table 3-6 and Fig. 3-17 are not sensitivity analyses; they give the output temperatures as functions of log power.		Changed text to discuss parametric analyses and results of Table 3-8. Added new Section 3.4.	Accpt'd

CAPSULE ADVISORY PANEL REVIEW COMMENT RECORD (RCR) Complete highlighted areas	REV C PEER REVIEW	
	1. Date 8-17-03	2. Page

3. Choose Document Number/Title (Only 1 Document Review per RCR Form)	4. Reviewer	4. Reviewer	4. Reviewer	5. CLOSED
[]WMP-16937 Corrosion Report Draft C []WMP-16938 Capsule Characterization Draft C []WMP-16939 Capsule Integrity Draft C [X]WMP-16940 Thermal Analysis Draft C []WMP-16878 Data Book Draft C []WMP-17265 Summary Report Rev. C	[]Bath, Singh []Bryan, Garry []Cannell, Gary []Covey, Lori []Heard, Fred []Josephson, Walt	[]Kraemer, Laurie []Miller, Bill []Olander, Don [X]Payer, Joe []Plys, Marty []Robbins, Dewey	[]Swenson, Joe []Thomson, Jim []Tingey, Garth []Tingey, Joel [] [] []	September 1, 2003 DATE Signature on File REVIEWER Signature on File AUTHOR/ORIGINATOR

6. Item	7. Comment(s)/Discrepancy(s) (Provide technical justification for the comment and detailed recommendation of the action required to correct/resolve the discrepancy/problem indicated.)	8. Reviewer Concurrence Required (Reviewer should 'X' this box if wants to concur with the closure of comment)	9. Disposition (Provide justification if NOT accepted.)	10. Status
1	Exec Smmry and body: Purpose is "to ensure design requirements for the project are conservative and defensible". *Thermal analysis has some non-conservative items, e.g. no insert/overpack gap; uniform capsules-no heterogeneities. Recd clear statement in text that these assumptions are justified for conceptual design, but they would not be justifiable (without technical support) for final design.*		Added following sentence to first paragraph Executive Summary and third paragraph section 1.1: "All assumptions and related design features, while appropriate for conceptual design, must be technically justified for the final design."	Accpt'd
2	1.1 Purpose: *The pertinent thermal design requirements ...(describing organization of report.)* Add a section for data used in analysis and Recommend that table of data used for thermal analysis be included in this report body or appendices. All data necessary to reproduce the calculations should be included. These should be included (repeated) in Data Book along with other data not required in this analysis.		Data will be added as new appendix to the document.	Accpt'd

CAPSULE ADVISORY PANEL REVIEW COMMENT RECORD (RCR) Complete highlighted areas	REV C PEER REVIEW	
	1. Date 8-17-03	2. Page

3. Choose Document Number/Title (Only 1 Document Review per RCR Form)	4. Reviewer	4. Reviewer	4. Reviewer	5. CLOSED
[]WMP-16937 Corrosion Report Draft C []WMP-16938 Capsule Characterization Draft C []WMP-16939 Capsule Integrity Draft C [X]WMP-16940 Thermal Analysis Draft C []WMP-16878 Data Book Draft C []WMP-17265 Summary Report Rev. C	[]Bath, Singh []Bryan, Garry []Cannell, Gary []Covey, Lori []Heard, Fred []Josephson, Walt	[]Kraemer, Laurie []Miller, Bill []Olander, Don [X]Payer, Joe []Plys, Marty []Robbins, Dewey	[]Swenson, Joe []Thomson, Jim []Tingey, Garth []Tingey, Joel [] [] []	September 1, 2003 DATE Signature on File REVIEWER Signature on File AUTHOR/ORIGINATOR

6. Item	7. Comment(s)/Discrepancy(s) (Provide technical justification for the comment and detailed recommendation of the action required to correct/resolve the discrepancy/problem indicated.)	8. Reviewer Concurrence Required (Reviewer should 'X' this box if wants to concur with the closure of comment)	9. Disposition (Provide justification if NOT accepted.)	10. Status
3	1.3 Design Criteria The design criteria include requirements that will facilitate acceptance at the repository. Recommend change to "... some requirements, e.g. size of overpacks and maximum thermal load per overpack ..."		Replaced second sentence in Section 1.3 with the following sentence: "The design criteria includes some requirements, e.g. size of the overpacks and maximum thermal load per overpack, that will facilitate repository acceptance."	Accpt'd
4	1.3 Design criteria #1 To ensure eventual transfer of the capsules to the national repository ... Replace "ensure" with anticipate or not preclude ...		Deleted the following phrase from item #1 in Section 1.3: "To ensure eventual transfer of the capsules to the national repository,....". This sentence now reads as: "The overpack shall be limited to an outer diameter no greater than 22 inches."	Accpt'd
5	2.4 other recommendations • *Variations in capsule type (except Type W) are only worth about 10 °C centerline temperature.* Clarify "worth", i.e. does it increase or decrease the predicted centerline temp.		This sentence has been revised to read: "Variations in capsule type (except Type W) increase the salt-metal and centerline temperatures about 10°C."	Accpt'd
6	4.4.8 External Overpack Temp over 50-year design life The temperature distribution within a capsule overpack within a dry storage module was determined vs. time for long-term storage conditions. Time was varied from 0 to 100		Added the following sentence to the end of Section 4.4.8: "It is recommended that this type of long-term thermal analysis be performed with more detail in support of the final design. This analysis will support	Accpt'd

CAPSULE ADVISORY PANEL REVIEW COMMENT RECORD (RCR) Complete highlighted areas	REV C PEER REVIEW	
	1. Date 8-17-03	2. Page

3. Choose Document Number/Title (Only 1 Document Review per RCR Form)	4. Reviewer	4. Reviewer	4. Reviewer	5. CLOSED
[]WMP-16937 Corrosion Report Draft C []WMP-16938 Capsule Characterization Draft C []WMP-16939 Capsule Integrity Draft C [X]WMP-16940 Thermal Analysis Draft C []WMP-16878 Data Book Draft C []WMP-17265 Summary Report Rev. C	[]Bath, Singh []Bryan, Garry []Cannell, Gary []Covey, Lori []Heard, Fred []Josephson, Walt	[]Kraemer, Laurie []Miller, Bill []Olander, Don [X]Payer, Joe []Plys, Marty []Robbins, Dewey	[]Swenson, Joe []Thomson, Jim []Tingey, Garth []Tingey, Joel [] [] []	September 1, 2003 DATE Signature on File REVIEWER Signature on File AUTHOR/ORIGINATOR

6. Item	7. Comment(s)/Discrepancy(s) (Provide technical justification for the comment and detailed recommendation of the action required to correct/resolve the discrepancy/problem indicated.)	8. Reviewer Concurrence Required (Reviewer should 'X' this box if wants to concur with the closure of comment)	9. Disposition (Provide justification if NOT accepted.)	10. Status
	years. Recommend specification that this screening analysis be completed in more detail as part of final design analysis. This analysis will support the confidence in overpack durability from both corrosion and thermal aging of the 316L overpack material.		confidence in overpack durability from both corrosion and thermal aging of the 316L overpack material."	
7	4.5 Summary and Conclusions • *Care must be exercised when employing fins in a low-flow natural circulation environment where radiative heat transfer provides a significant fraction of the energy rejected from the system.* Clarify "care". Reason for care and consequence of insufficient care.		Deleted last sentence in Section 4.4.7 and added new paragraph added to the end of Section 4.4.7: "Self-shadowing of fins has a significant effect on the salt-metal and centerline temperatures, especially for natural circulation systems where radiative heat transfer provides a large fraction of the energy rejected from the system. The correct view-factor or effective emissivity must be determined for a given fin design. Under prediction of the peak salt-metal and salt centerline temperatures can result, if the appropriate view-factor is not applied for fin-based systems. Deleted text associated last bullet in Section 4.5.	Accpt'd

CAPSULE ADVISORY PANEL REVIEW COMMENT RECORD (RCR) Complete highlighted areas	REV C PEER REVIEW	
	1. Date 8-17-03	2. Page

3. Choose Document Number/Title (Only 1 Document Review per RCR Form)	4. Reviewer	4. Reviewer	4. Reviewer	5. CLOSED
[]WMP-16937 Corrosion Report Draft C []WMP-16938 Capsule Characterization Draft C []WMP-16939 Capsule Integrity Draft C [X]WMP-16940 Thermal Analysis Draft C []WMP-16878 Data Book Draft C []WMP-17265 Summary Report Rev. C	[]Bath, Singh []Bryan, Garry []Cannell, Gary []Covey, Lori []Heard, Fred []Josephson, Walt	[]Kraemer, Laurie []Miller, Bill []Olander, Don [X]Payer, Joe []Plys, Marty []Robbins, Dewey	[]Swenson, Joe []Thomson, Jim []Tingey, Garth []Tingey, Joel [] [] []	September 1, 2003 DATE Signature on File REVIEWER Signature on File AUTHOR/ORIGINATOR

6. Item	7. Comment(s)/Discrepancy(s) (Provide technical justification for the comment and detailed recommendation of the action required to correct/resolve the discrepancy/problem indicated.)	8. Reviewer Concurrence Required (Reviewer should 'X' this box if wants to concur with the closure of comment)	9. Disposition (Provide justification if NOT accepted.)	10. Status
			Replaced bullet text with above sentence.	
8	6.5 Summary and Conclusions last para. However, with a process/process upset limit of 450 °C at the salt-metal interface, centerline temperatures in the CsCl capsules could potentially exceed 500 °C. In addition, during the fire simulation the salt centerline temperature exceeded the conservative 430 °C melting point for a period of a few hours, with a maximum temperature predicted to be approximately 520 °C. Here and elsewhere, high temperatures are determined for accident and upset scenarios. Recommend add statement that these crucial issues be revisited in more depth for final design.		Added new second sentence to Section 6.5, as follows: "It is recommended that the final design include an in-depth thermal analysis of all process, process upset, and postulated accident conditions."	Accpt'd
9	6.5 Summary and Conclusions last para. However, with a process/process upset limit of 450 °C at the salt-metal interface, centerline temperatures in the CsCl capsules could potentially exceed 500 °C. In addition, during		Added new paragraph to the end of Section 6.5: "In addition to corrosion and salt thermal expansion issues, the effects of elevated metal temperatures on the fracture toughness of metal and welds must be	Accpt'd

CAPSULE ADVISORY PANEL REVIEW COMMENT RECORD (RCR) Complete highlighted areas	REV C PEER REVIEW	
	1. Date 8-17-03	2. Page

3. Choose Document Number/Title (Only 1 Document Review per RCR Form)	4. Reviewer	4. Reviewer	4. Reviewer	5. CLOSED
[]WMP-16937 Corrosion Report Draft C []WMP-16938 Capsule Characterization Draft C []WMP-16939 Capsule Integrity Draft C [X]WMP-16940 Thermal Analysis Draft C []WMP-16878 Data Book Draft C []WMP-17265 Summary Report Rev. C	[]Bath, Singh []Bryan, Garry []Cannell, Gary []Covey, Lori []Heard, Fred []Josephson, Walt	[]Kraemer, Laurie []Miller, Bill []Olander, Don [X]Payer, Joe []Plys, Marty []Robbins, Dewey	[]Swenson, Joe []Thomson, Jim []Tingey, Garth []Tingey, Joel [] [] []	September 1, 2003 DATE Signature on File REVIEWER Signature on File AUTHOR/ORIGINATOR

6. Item	7. Comment(s)/Discrepancy(s) (Provide technical justification for the comment and detailed recommendation of the action required to correct/resolve the discrepancy/problem indicated.)	8. Reviewer Concurrence Required (Reviewer should 'X' this box if wants to concur with the closure of comment)	9. Disposition (Provide justification if NOT accepted.)	10. Status
	the fire simulation the salt centerline temperature exceeded the conservative 430 °C melting point for a period of a few hours, with a maximum temperature predicted to be approximately 520 °C. Recommend add statement: In addition to corrosion and thermal expansion of salt issues, it is necessary to consider the effects of elevated metal temperatures on fracture toughness of the metal and welds. Temperatures above 540C during processing, upset or accident will degrade the fracture toughness of metal and welds.		considered. Refer to WMP-16938, "*Capsule Characterization Report for Capsule Dry Storage Project,*" and WMP-16939, "Capsule *Integrity Report for Capsule Dry Storage Project*" for additional discussion."	